# Chapter 2. 1D Wave Mechanics

*Even the simplest, 1D version of wave mechanics enables quantitative analysis of many important quantum-mechanical effects. The order of their discussion in this chapter is dictated mostly by mathematical convenience – going from the simplest potential profiles to more complex ones, so that we may build upon the previous results. However, the reader is advised to focus not on the math, but rather on the physics of the non-classical phenomena it describes, ranging from particle penetration into classically-forbidden regions, to quantum-mechanical tunneling, to the metastable state decay, to covalent bonding, to quantum oscillations, to energy bands and gaps.*

## 2.1. Basic relations

In many important cases, the wavefunction may be represented in the form $\Psi(x, t)\chi(y, z)$, where $\Psi(x, t)$ satisfies the 1D version of the Schrödinger equation,[1]

Schrödinger equation

$$i\hbar\frac{\partial\Psi(x,t)}{\partial t} = -\frac{\hbar^2}{2m}\frac{\partial^2\Psi(x,t)}{\partial x^2} + U(x,t)\Psi(x,t)\,. \tag{2.1}$$

If the transverse factor $\chi(y, z)$ is normalized:

$$\int |\chi(y,z)|^2\, dydz = 1\,, \tag{2.2}$$

then the similar integration of Eq. (1.22b) over the $[y, z]$ plane gives the following probability of finding the particle on a segment $[x_1, x_2]$:

Probability

$$W(t) \equiv \int_{x_1}^{x_2} \Psi(x,t)\Psi^*(x,t)dx\,. \tag{2.3a}$$

In particular, if the particle under analysis is definitely somewhere inside the system, the normalization of its 1D wavefunction $\Psi(x, t)$ may be provided by extending this integral to the whole axis $x$:

Normalization

$$\int_{-\infty}^{+\infty} w(x,t)dx = 1, \quad \text{where } w(x,t) \equiv \Psi(x,t)\Psi^*(x,t)\,. \tag{2.3b}$$

Similarly, the $[y, z]$-integration of Eq. (1.23) shows that in this case, the expectation value of any observable depending only on the coordinate $x$ (and possibly time), may be expressed as

Expectation value

$$\langle A\rangle(t) = \int_{-\infty}^{+\infty} \Psi^*(x,t)\hat{A}\Psi(x,t)dx\,, \tag{2.4}$$

and that of Eq. (1.47) makes it valid for the whole *probability current* along the $x$-axis (a *scalar*):

[1] Note that for this reduction, it is *not* sufficient for the potential energy $U(\mathbf{r}, t)$ to depend on just one spatial coordinate ($x$). Actually, Eq. (1) is a more robust model for the description of the opposite situations when the potential energy changes within the $[y, z]$ much *faster* than in the $x$-direction, so that the transverse factor $\chi(y, z)$ is confined in space much more than $\Psi$, if the confining potential profile is independent of $x$ and $t$. Let me leave a semi-quantitative analysis of this issue for the reader's exercise. (See also Sec. 3.1.)

$$I(x,t) \equiv \int j_x dydz = \frac{\hbar}{m}\mathrm{Im}\left(\Psi^* \frac{\partial}{\partial x}\Psi\right) = \frac{\hbar}{m}|\Psi(x,t)|^2 \frac{\partial \varphi}{\partial x}. \quad (2.5)$$

Probability current

Then the continuity equation (1.48) for any segment $[x_1, x_2]$ takes the form

$$\frac{dW}{dt} + I(x_2) - I(x_1) = 0. \quad (2.6)$$

Continuity equation

The above formulas are sufficient for the analysis of 1D problems of wave mechanics, but before proceeding to particular cases, let me deliver on my earlier promise to prove that Heisenberg's uncertainty relation (1.35) is indeed valid for any wavefunction $\Psi(x, t)$. For that, let us consider the following positive (or at least non-negative) integral:

$$J(\lambda) \equiv \int_{-\infty}^{+\infty} \left| x\Psi + \lambda \frac{\partial \Psi}{\partial x} \right|^2 dx \geq 0, \quad (2.7)$$

where $\lambda$ is an arbitrary real constant, and assume that at $x \to \pm\infty$ the wavefunction vanishes, together with its first derivative – as we will see below, a very common case. Then the left-hand side of Eq. (7) may be recast as

$$\begin{aligned} J(\lambda) &\equiv \int_{-\infty}^{+\infty} \left| x\Psi + \lambda \frac{\partial \Psi}{\partial x} \right|^2 dx = \int_{-\infty}^{+\infty} \left( x\Psi + \lambda \frac{\partial \Psi}{\partial x} \right)\left( x\Psi + \lambda \frac{\partial \Psi}{\partial x} \right)^* dx \\ &= \int_{-\infty}^{+\infty} x^2 \Psi\Psi^* dx + \lambda \int_{-\infty}^{+\infty} x\left( \Psi \frac{\partial \Psi^*}{\partial x} + \frac{\partial \Psi}{\partial x}\Psi^* \right) dx + \lambda^2 \int_{-\infty}^{+\infty} \frac{\partial \Psi}{\partial x}\frac{\partial \Psi^*}{\partial x} dx. \end{aligned} \quad (2.8)$$

According to Eq. (4), the first term in the last form of Eq. (8) is just $\langle x^2 \rangle$, while the second and the third integrals may be worked out by parts:

$$\int_{-\infty}^{+\infty} x\left( \Psi \frac{\partial \Psi^*}{\partial x} + \frac{\partial \Psi}{\partial x}\Psi^* \right) dx \equiv \int_{-\infty}^{+\infty} x \frac{\partial}{\partial x}\left(\Psi\Psi^*\right) dx = \int_{x=-\infty}^{x=+\infty} x d\left(\Psi\Psi^*\right) = \Psi\Psi^* x \Big|_{x=-\infty}^{x=+\infty} - \int_{-\infty}^{+\infty} \Psi\Psi^* dx = -1, \quad (2.9)$$

$$\int_{-\infty}^{+\infty} \frac{\partial \Psi}{\partial x}\frac{\partial \Psi^*}{\partial x} dx = \int_{x=-\infty}^{x=+\infty} \frac{\partial \Psi}{\partial x} d\Psi^* = \frac{\partial \Psi}{\partial x}\Psi^* \Big|_{x=-\infty}^{x=+\infty} - \int_{-\infty}^{+\infty} \Psi^* \frac{\partial^2 \Psi}{\partial x^2} dx = \frac{1}{\hbar^2}\int_{-\infty}^{+\infty} \Psi^* \hat{p}_x^2 \Psi dx = \frac{\langle p_x^2 \rangle}{\hbar^2}. \quad (2.10)$$

As a result, Eq. (7) takes the following form:

$$J(\lambda) = \langle x^2 \rangle - \lambda + \lambda^2 \frac{\langle p_x^2 \rangle}{\hbar^2} \geq 0, \quad \text{i.e. } \lambda^2 + a\lambda + b \geq 0, \quad \text{with } a \equiv -\frac{\hbar^2}{\langle p_x^2 \rangle},\ b \equiv \frac{\hbar^2 \langle x^2 \rangle}{\langle p_x^2 \rangle}. \quad (2.11)$$

This inequality should be valid for any real $\lambda$, so the corresponding quadratic equation, $\lambda^2 + a\lambda + b = 0$, can have either one (degenerate) real root or no real roots at all. This is only possible if its discriminant $a^2 - 4b$, is non-positive, leading to the following requirement:

$$\langle x^2 \rangle \langle p_x^2 \rangle \geq \frac{\hbar^2}{4}. \quad (2.12)$$

In particular, if $\langle x \rangle = 0$ and $\langle p_x \rangle = 0$, then according to Eq. (1.33), Eq. (12) takes the form

$$\langle \tilde{x}^2 \rangle \langle \tilde{p}_x^2 \rangle \geq \frac{\hbar^2}{4}, \quad (2.13)$$

Heisenberg's uncertainty relation

which, according to the definition (1.34) of the r.m.s. uncertainties, is equivalent to Eq. (1.35).[2]

Now let us notice that Heisenberg's uncertainty relation looks very similar to the *commutation relation* between the corresponding operators:

$$[\hat{x}, \hat{p}_x]\Psi \equiv (\hat{x}\hat{p}_x - \hat{p}_x\hat{x})\Psi = x\left(-i\hbar\frac{\partial\Psi}{\partial x}\right) - \left(-i\hbar\frac{\partial}{\partial x}\right)(x\Psi) = i\hbar\Psi\,. \tag{2.14a}$$

Coordinate/ momentum operators' commutator

Since this relation is valid for any wavefunction $\Psi(x, t)$, it may be represented as operator equality:

$$\boxed{[\hat{x}, \hat{p}_x] = i\hbar \neq 0\,.} \tag{2.14b}$$

In Sec. 4.5 we will see that the relation between Eqs. (13) and (14) is just a particular case of a general relation between the expectation values of non-commuting operators and their commutators.

## 2.2. Free particle: Wave packets

Let us start our discussion of particular problems with the free 1D motion, i.e. with $U(x, t) = 0$. From Eq. (1.29), it is evident that in the 1D case, a similar "fundamental" (i.e. a particular but the most important) solution of the Schrödinger equation (1) is a sinusoidal ("monochromatic") wave

$$\Psi_0(x,t) = \text{const} \times \exp\{i(k_0 x - \omega_0 t)\}. \tag{2.15}$$

According to Eqs. (1.32), it describes a particle with a definite momentum[3] $p_0 = \hbar k_0$ and energy $E_0 = \hbar\omega_0 = \hbar^2 k_0^2/2m$. However, for this wavefunction, the product $\Psi^*\Psi$ does not depend on either $x$ or $t$, so the particle is completely delocalized, i.e. the probability to find it the same along all axis $x$, at all times.

In order to describe a space-localized state, let us form, at the initial moment of time ($t = 0$), a wave packet of the type shown in Fig. 1.6, by multiplying the sinusoidal waveform (15) by some smooth *envelope function* $A(x)$. As the most important particular example, consider the *Gaussian wave packet*

Gaussian wave packet: $t = 0$

$$\boxed{\Psi(x,0) = A(x)e^{ik_0 x}, \qquad \text{with } A(x) = \frac{1}{(2\pi)^{1/4}(\delta x)^{1/2}}\exp\left\{-\frac{x^2}{(2\delta x)^2}\right\}.} \tag{2.16}$$

(By the way, Fig. 1.6a shows exactly such a packet.) The pre-exponential factor in this envelope function has been selected to have the initial probability density,

$$w(x,0) \equiv \Psi^*(x,0)\Psi(x,0) = A^*(x)A(x) = \frac{1}{(2\pi)^{1/2}\delta x}\exp\left\{-\frac{x^2}{2(\delta x)^2}\right\}, \tag{2.17}$$

normalized as in Eq. (3b), for any parameters $\delta x$ and $k_0$.[4]

---

[2] Eq. (13) may be proved even if $\langle x\rangle$ and $\langle p_x\rangle$ are not equal to zero, by making the replacements $x \to x - \langle x\rangle$ and $\partial/\partial x \to \partial/\partial x + i\langle p\rangle/\hbar$ in Eq. (7), and then repeating all the calculations – which in this case become somewhat bulky. In Chapter 4, equipped with the bra-ket formalism, we will derive a more general uncertainty relation, which includes Heisenberg's relation (13) as a particular case, in a more efficient way.

[3] From this point on to the end of this chapter, I will drop index $x$ in the $x$-components of the vectors **k** and **p**.

[4] This fact may be readily proved using the well-known integral of the Gaussian function (17), in infinite limits – see, e.g., MA Eq. (6.9b). It is also straightforward to use MA Eq. (6.9c) to prove that for the wave packet (16), the parameter $\delta x$ is indeed the r.m.s. uncertainty (1.34) of the coordinate $x$, thus justifying its notation.

To explore the evolution of this wave packet in time, we could try to solve Eq. (1) with the initial condition (16) directly, but in the spirit of the discussion in Sec. 1.5, it is easier to proceed differently. Let us first represent the initial wavefunction (16) as a sum (1.67) of the eigenfunctions $\psi_k(x)$ of the corresponding stationary 1D Schrödinger equation (1.60), in our current case

$$-\frac{\hbar^2}{2m}\frac{d^2\psi_k}{dx^2} = E_k\psi_k, \qquad \text{with } E_k \equiv \frac{\hbar^2 k^2}{2m}, \tag{2.18}$$

which are simply monochromatic waves,

$$\psi_k = a_k e^{ikx}. \tag{2.19}$$

Since (as was discussed in Sec. 1.7) at the unconstrained motion the spectrum of possible wave numbers $k$ is continuous, the sum (1.67) should be replaced with an integral:[5]

$$\Psi(x,0) = \int a_k e^{ikx}\,dk. \tag{2.20}$$

Now let us notice that from the point of view of mathematics, Eq. (20) is just the usual Fourier transform from the variable $k$ to the "conjugate" variable $x$, and we can use the well-known formula of the reciprocal Fourier transform to write

$$a_k = \frac{1}{2\pi}\int \Psi(x,0)e^{-ikx}dx = \frac{1}{2\pi}\frac{1}{(2\pi)^{1/4}(\delta x)^{1/2}}\int \exp\left\{-\frac{x^2}{(2\delta x)^2} - i\tilde{k}x\right\}dx, \quad \text{where } \tilde{k} \equiv k - k_0. \tag{2.21}$$

This *Gaussian integral* may be worked out by the following standard method, which will be used many times in this course. Let us complement the exponent to the full square of a linear combination of $x$ and $k$, adding a compensating term independent of $x$:

$$-\frac{x^2}{(2\delta x)^2} - i\tilde{k}x \equiv -\frac{1}{(2\delta x)^2}\left[x + 2i(\delta x)^2\tilde{k}\right]^2 - \tilde{k}^2(\delta x)^2. \tag{2.22}$$

Since the integration in the right-hand side of Eq. (21) should be performed at constant $\tilde{k}$, in the infinite limits of $x$, its result would not change if we replace $dx$ with $d\boldsymbol{x} \equiv d[x + 2i(\delta x)^2\tilde{k}]$. As a result, we get:[6]

$$\begin{aligned} a_k &= \frac{1}{2\pi}\frac{1}{(2\pi)^{1/4}(\delta x)^{1/2}}\exp\left\{-\tilde{k}^2(\delta x)^2\right\}\int \exp\left\{-\frac{\boldsymbol{x}^2}{(2\delta x)^2}\right\}d\boldsymbol{x} \\ &= \left(\frac{1}{2\pi}\right)^{1/2}\frac{1}{(2\pi)^{1/4}(\delta k)^{1/2}}\exp\left\{-\frac{\tilde{k}^2}{(2\delta k)^2}\right\}, \end{aligned} \tag{2.23}$$

so $a_k$ also has a Gaussian distribution, now along the $k$-axis, centered to the value $k_0$ (Fig. 1.6b), with the constant $\delta k$ defined as

$$\delta k \equiv 1/2\delta x. \tag{2.24}$$

Thus we may represent the initial wave packet (16) as

[5] For the notation brevity, from this point on the infinite limit signs will be dropped in all 1D integrals.

[6] The fact that the argument's shift is imaginary is not important. (Let me leave proof of this fact for the reader's exercise.)

$$\Psi(x,0)=\left(\frac{1}{2\pi}\right)^{1/2}\frac{1}{(2\pi)^{1/4}(\delta k)^{1/2}}\int\exp\left\{-\frac{(k-k_0)^2}{(2\delta k)^2}\right\}e^{ikx}dk\,. \tag{2.25}$$

From the comparison of this formula with Eq. (16), it is evident that the r.m.s. uncertainty of the wave number $k$ in this packet is indeed equal to $\delta k$ defined by Eq. (24), thus justifying the notation. The comparison of the last relation with Eq. (1.35) shows that the Gaussian packet represents the ultimate case in which the product $\delta x\delta p = \delta x(\hbar\delta k)$ has the lowest possible value ($\hbar/2$); for any other envelope's shape, the uncertainty product may only be larger.

We could of course get the same result for $\delta k$ from Eq. (16) using the definitions (1.23), (1.33), and (1.34); the real advantage of Eq. (25) is that it can be readily generalized to $t > 0$. Indeed, we already know that the time evolution of the wavefunction is always given by Eq. (1.69), for our current case[7]

Gaussian wave packet: arbitrary time

$$\Psi(x,t)=\left(\frac{1}{2\pi}\right)^{1/2}\frac{1}{(2\pi)^{1/4}(\delta k)^{1/2}}\int\exp\left\{-\frac{(k-k_0)^2}{(2\delta k)^2}\right\}e^{ikx}\exp\left\{-i\frac{\hbar k^2}{2m}t\right\}dk\,. \tag{2.26}$$

Fig. 1 shows several snapshots of the real part of the wavefunction (26), for a particular case $\delta k = 0.1\,k_0$.

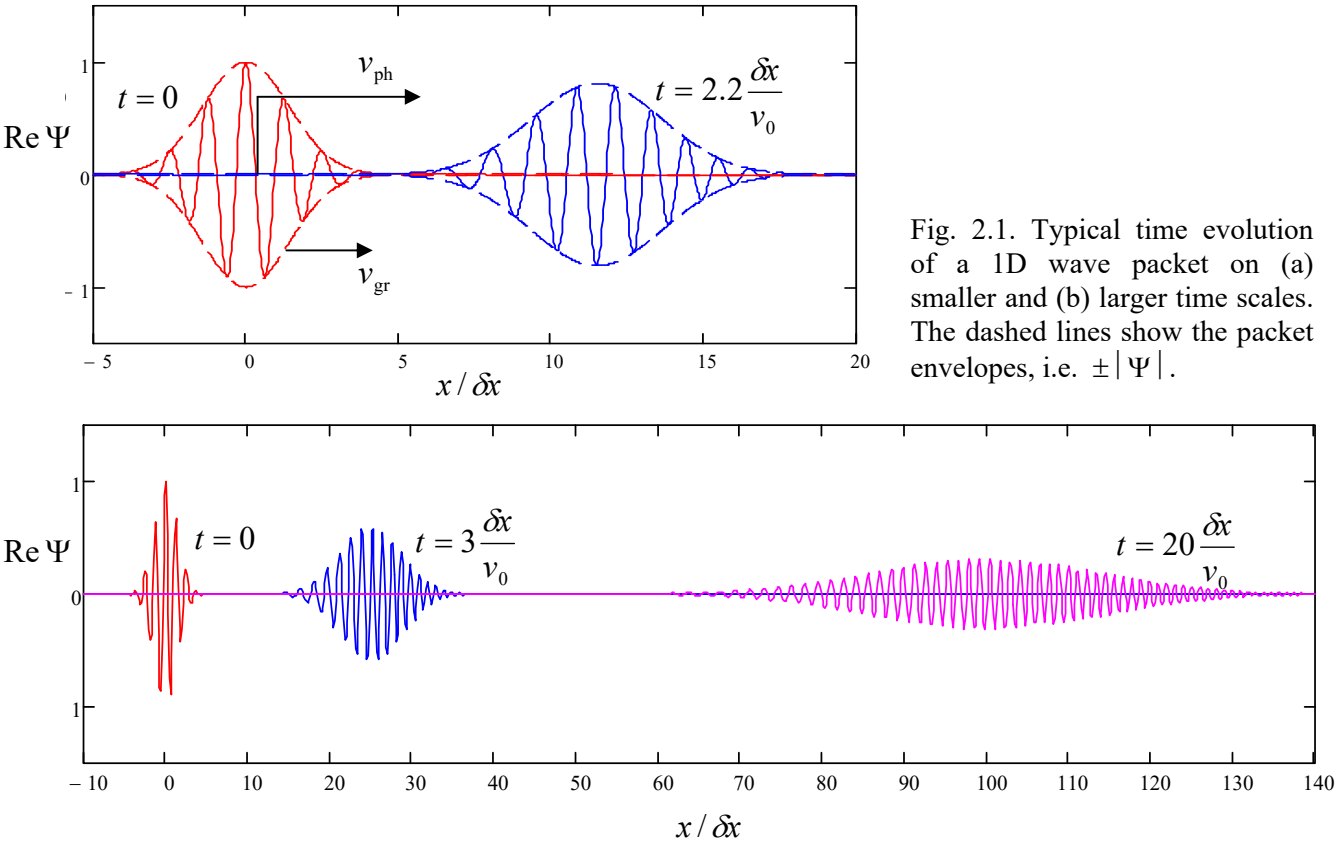


Fig. 2.1. Typical time evolution of a 1D wave packet on (a) smaller and (b) larger time scales. The dashed lines show the packet envelopes, i.e. $\pm|\Psi|$.

The plots clearly show the following effects:

[7] Note that Eq. (26) differs from Eq. (16) only by an exponent of a purely imaginary number, and hence this wavefunction is also properly normalized to 1 – see Eq. (3). Hence the wave packet introduction offers a natural solution to the problem of traveling de Broglie wave's normalization, which was mentioned in Sec. 1.2.

(i) the wave packet as a whole (as characterized by its envelope) moves along the $x$-axis with a certain *group velocity* $v_{gr}$,

(ii) the "carrier" quasi-sinusoidal wave inside the packet moves with a different, *phase velocity* $v_{ph}$ that may be defined as the velocity of the spatial points where the wave's phase $\varphi(x, t) \equiv \arg\Psi$ takes a certain fixed value (say, $\varphi = \pi/2$ where $\mathrm{Re}\Psi$ vanishes), and

(iii) the wave packet's spatial width gradually increases with time – the packet *spreads*.

All these effects are common for waves of any physical nature.[8] Indeed, let us consider a 1D wave packet of the type (26) but a more general one:

$$\Psi(x,t) = \int a_k e^{i(kx-\omega t)} dk, \tag{2.27}$$

Arbitrary 1D wave packet

propagating in a medium with an arbitrary (but smooth!) dispersion relation $\omega(k)$, and assume that the wave number distribution $a_k$ is narrow: $\delta k << \langle k \rangle \equiv k_0$ – see Fig. 1.6b. Then we may expand the function $\omega(k)$ into the Taylor series near the central wave number $k_0$, and keep only three of its leading terms:

$$\omega(k) \approx \omega_0 + \frac{d\omega}{dk}\tilde{k} + \frac{1}{2}\frac{d^2\omega}{dk^2}\tilde{k}^2, \qquad \text{where } \tilde{k} \equiv k - k_0,\ \omega_0 \equiv \omega(k_0), \tag{2.28}$$

where the derivatives have to be evaluated at the point $k = k_0$. In this approximation,[9] the expression in the parentheses on the right-hand side of Eq. (27) may be rewritten as

$$\begin{aligned} kx - \omega(k)t &\approx k_0 x + \tilde{k}x - \left(\omega_0 + \frac{d\omega}{dk}\tilde{k} + \frac{1}{2}\frac{d^2\omega}{dk^2}\tilde{k}^2\right)t \\ &\equiv (k_0 x - \omega_0 t) + \tilde{k}\left(x - \frac{d\omega}{dk}t\right) - \frac{1}{2}\frac{d^2\omega}{dk^2}\tilde{k}^2 t, \end{aligned} \tag{2.29}$$

and Eq. (27) becomes

$$\Psi(x,t) \approx e^{i(k_0 x - \omega_0 t)} \int a_k \exp\left\{i\left[\tilde{k}\left(x - \frac{d\omega}{dk}t\right) - \frac{1}{2}\frac{d^2\omega}{dk^2}\tilde{k}^2 t\right]\right\} d\tilde{k}\,. \tag{2.30}$$

First, let us neglect the last term in the square brackets (which is much smaller than the first term if the dispersion relation is smooth enough), and compare the result with the initial form of the wave packet (27):

$$\Psi(x,0) = \int a_k e^{ikx} dk = A(x) e^{ik_0 x}, \quad \text{with } A(x) \equiv \int a_k e^{i\tilde{k}x} d\tilde{k}\,. \tag{2.31}$$

The comparison shows that in this approximation, Eq. (30) is reduced to

$$\Psi(x,t) = A(x - v_{gr}t) e^{ik_0(x - v_{ph}t)}, \tag{2.32}$$

where $v_{gr}$ and $v_{ph}$ are two constants with the dimension of velocity:

$$v_{gr} \equiv \left.\frac{d\omega}{dk}\right|_{k=k_0}, \qquad v_{ph} \equiv \left.\frac{\omega}{k}\right|_{k=k_0}. \tag{2.33a}$$

Group and phase velocities

[8] See, e.g., brief discussions in CM Sec. 6.3 and EM Sec. 7.2.

[9] By the way, in the particular case of de Broglie waves described by the dispersion relation (1.30), Eq. (28) is exact, because $\omega = E/\hbar$ is a quadratic function of $k = p/\hbar$, and all higher derivatives of $\omega$ over $k$ vanish for any $k_0$.

Clearly, Eq. (32) describes the effects (i) and (ii) listed above. For the particular case of the de Broglie waves, whose dispersion law is given by Eq. (1.30),

$$v_{\rm gr} \equiv \frac{d\omega}{dk}\Big|_{k=k_0} = \frac{\hbar k_0}{m} \equiv v_0, \qquad v_{\rm ph} \equiv \frac{\omega}{k}\Big|_{k=k_0} = \frac{\hbar k_0}{2m} = \frac{v_{\rm gr}}{2}. \tag{2.33b}$$

We see that (very fortunately for the correspondence principle :-) the velocity of the wave packet's envelope is equal to $v_0$ – the classical velocity of the same particle.

Next, the last term in the square brackets of Eq. (30) describes the effect (iii), the wave packet's spread. It may be readily evaluated if the packet (27) is initially Gaussian, as in our example (25):

$$a_k = \text{const} \times \exp\left\{-\frac{\tilde{k}^2}{(2\delta k)^2}\right\}. \tag{2.34}$$

In this case, the integral (30) is Gaussian, and may be worked out exactly as the integral (21), i.e. by representing the merged exponents under the integral as a full square of a linear combination of $x$ and $k$:

$$\begin{aligned} &-\frac{\tilde{k}^2}{(2\delta k)^2} + i\tilde{k}(x - v_{\rm gr}t) - \frac{i}{2}\frac{d^2\omega}{dk^2}\tilde{k}^2 t \\ &\equiv -\Delta(t)\left(\tilde{k} + i\frac{x - v_{\rm gr}t}{2\Delta(t)}\right)^2 - \frac{(x - v_{\rm gr}t)^2}{4\Delta(t)} + ik_0 x - \frac{i}{2}\frac{d^2\omega}{dk^2}k_0^2 t, \end{aligned} \tag{2.35}$$

where I have introduced the following complex function of time:

$$\Delta(t) \equiv \frac{1}{4(\delta k)^2} + \frac{i}{2}\frac{d^2\omega}{dk^2}t = (\delta x)^2 + \frac{i}{2}\frac{d^2\omega}{dk^2}t, \tag{2.36}$$

and used Eq. (24). Now integrating over $\tilde{k}$, we get

$$\Psi(x,t) \propto \exp\left\{-\frac{(x - v_{\rm gr}t)^2}{4\Delta(t)} + i\left(k_0 x - \frac{1}{2}\frac{d^2\omega}{dk^2}k_0^2 t\right)\right\}. \tag{2.37}$$

The imaginary part of the ratio $1/\Delta(t)$ in this exponent gives just an additional contribution to the wave's phase and does not affect the resulting probability distribution

$$w(x,t) = \Psi^*\Psi \propto \exp\left\{-\frac{(x - v_{\rm gr}t)^2}{2}\,\mathrm{Re}\frac{1}{\Delta(t)}\right\}. \tag{2.38}$$

This is again a Gaussian distribution over the $x$-axis, centered to point $\langle x\rangle = v_{\rm gr}t$, with the variance

$$(\delta x')^2 \equiv \left\{\mathrm{Re}\left[\frac{1}{\Delta(t)}\right]\right\}^{-1} = (\delta x)^2 + \left(\frac{1}{2}\frac{d^2\omega}{dk^2}t\right)^2 \frac{1}{(\delta x)^2}. \tag{2.39a}$$

In the particular case of de Broglie waves, $d^2\omega/dk^2 = \hbar/m$, so

Wave packet's spread

$$(\delta x')^2 = (\delta x)^2 + \left(\frac{\hbar t}{2m}\right)^2 \frac{1}{(\delta x)^2}. \tag{2.39b}$$

The physics of the packet spreading is very simple: if $d^2\omega/dk^2 \neq 0$, the group velocity $d\omega/dk$ of each small group $dk$ of the monochromatic components of the wave is different, resulting in the gradual (eventually, linear) accumulation of the differences of the distances traveled by the groups. The most curious feature of Eq. (39) is that the packet width at $t > 0$ depends on its initial width $\delta x'(0) = \delta x$ in a non-monotonic way, tending to infinity at both $\delta x \to 0$ and $\delta x \to \infty$. Because of that, for a given time interval $t$, there is an optimal value of $\delta x$ that minimizes $\delta x'$:

$$(\delta x')_{\min} = \sqrt{2}\,(\delta x)_{\text{opt}} = \left(\frac{\hbar t}{m}\right)^{1/2}. \tag{2.40}$$

This expression may be used to estimate the spreading effect's magnitude. Due to the smallness of the Planck constant $\hbar$ on the human scale of things, for macroscopic bodies the spreading is extremely small even for very long time intervals; however, for light particles, it may be very noticeable: for an electron ($m = m_e \approx 10^{-30}$ kg), and $t = 1$ s, Eq. (40) yields $(\delta x')_{\min} \sim 1$ cm.

Note also that for any $t \neq 0$, the wave packet retains its Gaussian envelope, but the ultimate relation (24) is *not* satisfied, $\delta x' \delta p > \hbar/2$, due to a gradually accumulated phase shift between the component monochromatic waves.

The last remark on this topic: in quantum mechanics, the wave packet spreading is *not* a ubiquitous effect! For example, in Chapter 5 we will see that in a quantum oscillator, the spatial width of a Gaussian packet (for that system, called the *Glauber state* of the oscillator) does not grow monotonically but rather either stays constant or oscillates in time.

Now let us briefly discuss the case when the initial wave packet is not Gaussian but is described by an arbitrary initial wavefunction. To make the forthcoming result more aesthetically pleasing, it is beneficial to generalize our calculations to an arbitrary initial time $t_0$; it is evident that if $U$ does not depend on time explicitly, it is sufficient to replace $t$ with $(t - t_0)$ in the above formulas. With this replacement, Eq. (27) becomes

$$\Psi(x,t) = \int a_k e^{i\left[kx - \omega(t - t_0)\right]} dk\,, \tag{2.41}$$

and the reciprocal transform (21) reads

$$a_k = \frac{1}{2\pi}\int \Psi(x,t_0)\, e^{-ikx} dx\,. \tag{2.42}$$

If we want to express these two formulas with one relation, i.e. plug Eq. (42) into Eq. (41), we should give the integration variable $x$ some other name, e.g., $x_0$. (Such notation is appropriate because this variable describes the coordinate argument in the initial wave packet.) The result is

$$\Psi(x,t) = \frac{1}{2\pi}\int dk \int dx_0\, \Psi(x_0,t_0)\, e^{i\left[k(x - x_0) - \omega(t - t_0)\right]}\,. \tag{2.43}$$

Changing the order of integration, this expression may be represented in the following general form:

$$\boxed{\Psi(x,t) = \int G(x,t;x_0,t_0)\,\Psi(x_0,t_0)\,dx_0\,,} \tag{2.44}$$

1D propagator: definition

where the function $G$, usually called *kernel* in mathematics, in quantum mechanics is called the *propagator*.[10] Its physical sense may be understood by considering the following special initial condition:[11]

$$\Psi(x_0,t_0)=\delta(x_0-x'), \tag{2.45}$$

where $x'$ is a certain point within the particle's motion domain. In this particular case, Eq. (44) gives

$$\Psi(x,t)=G(x,t;x',t_0). \tag{2.46}$$

Hence, the propagator, considered as a function of its arguments $x$ and $t$ only, is just the wavefunction of the particle, at the $\delta$-functional initial conditions (45). Thus, just as Eq. (41) may be understood as a mathematical expression of the linear superposition principle in the momentum (i.e., reciprocal) space domain, Eq. (44) is an expression of this principle in the direct space domain: the system's "response" $\Psi(x,t)$ to an arbitrary initial condition $\Psi(x_0,t_0)$ is just a sum of its responses to elementary spatial "slices" of this initial function, with the propagator $G(x,\ t;\ x_0,\ t_0)$ representing the weight of each slice in the final sum.

According to Eqs. (43) and (44), in the case of a free particle, the propagator is equal to

$$G(x,t;x_0,t_0)=\frac{1}{2\pi}\int e^{i\left[k(x-x_0)-\omega(t-t_0)\right]}dk\,, \tag{2.47}$$

Calculating this integral, one should remember that here $\omega$ is not a constant but a function of $k$, given by the dispersion relation for the partial waves. In particular, for the de Broglie waves, with $\hbar\omega=\hbar^2k^2/2m$,

$$G(x,t;x_0,t_0)\equiv\frac{1}{2\pi}\int\exp\left\{i\left[k(x-x_0)-\frac{\hbar k^2}{2m}(t-t_0)\right]\right\}dk\,. \tag{2.48}$$

This is a Gaussian integral again, and it may be readily calculated just it was done (twice) above, by completing the exponent to the full square. The result is

Free particle's propagator

$$G(x,t;x_0,t_0)=\left[\frac{m}{2\pi i\hbar(t-t_0)}\right]^{1/2}\exp\left\{-\frac{m(x-x_0)^2}{2i\hbar(t-t_0)}\right\}. \tag{2.49}$$

Please note the following features of this complex function:

(i) It depends only on the differences $(x-x_0)$ and $(t-t_0)$. This is natural because the free-particle propagation problem is *translation-invariant* both in space and time.

(ii) The function's shape (Fig. 2) does not depend on its arguments – they just rescale the same function: as a function of $x$, it just becomes broader and lower with time. It is curious that the spatial broadening scales as $(t-t_0)^{1/2}$ – just as at the classical diffusion, indicating a deep mathematical analogy between quantum mechanics and classical statistics – to be discussed further in Chapter 7.

[10] Its standard notation by letter $G$ stems from the fact that the propagator is essentially the spatial-temporal *Green's function* of the Schrödinger equation (1), defined very similarly to Green's functions of other ordinary and partial differential equations describing various physics systems – see, e.g., CM Sec. 5.1 and/or EM Sec. 2.7 and 7.3.

[11] Note that this initial condition is mathematically *not* equivalent to a $\delta$-functional initial probability density (3).

(iii) In accordance with the uncertainty relation, the ultimately compressed wave packet (45) has an infinite width of momentum distribution, and the quasi-sinusoidal tails of the free-particle's propagator, clearly visible in Fig. 2, are the results of the free propagation of the fastest (highest-momentum) components of that distribution, in both directions from the packet's center.

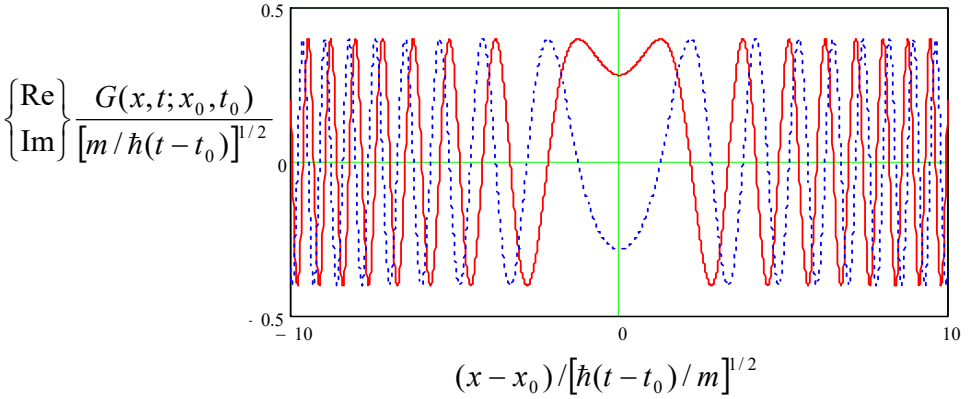


Fig. 2.2. The real (solid line) and imaginary (dotted line) parts of the 1D free particle's propagator (49).

In the following sections, I will mostly focus on monochromatic wavefunctions (which, for unconfined motion, may be interpreted as wave packets of a very large spatial width $\delta x$), and only rarely discuss wave packets. My best excuse is the linear superposition principle, i.e. our conceptual ability to restore the general solution from that of monochromatic waves of all possible energies. However, the reader should not forget that, as the above discussion has illustrated, mathematically such restoration is not always trivial.

## 2.3. Particle reflection and tunneling

Now, let us proceed to the cases when a 1D particle moves in various potential profiles $U(x)$ that are constant in time. Conceptually, the simplest of such profiles is a potential step – see Fig. 3.

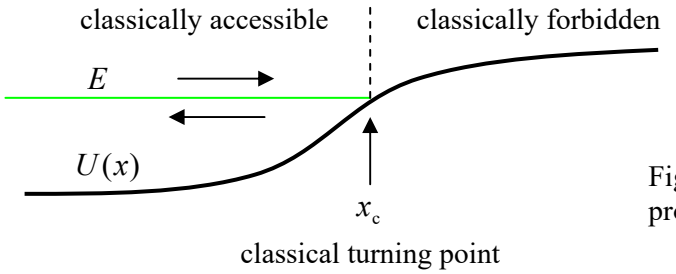


Fig. 2.3. Classical 1D motion in a potential profile $U(x)$.

As I am sure the reader knows, in classical mechanics the particle's kinetic energy $p^2/2m$ cannot be negative, so if the particle is incident on such a step (in Fig. 3, from the left), it can only move within the *classically accessible* region where its (conserved) full energy,

$$E = \frac{p^2}{2m} + U(x), \tag{2.50}$$

is larger than the local value $U(x)$. Let, for example, the initial velocity $v = p/m$ be positive, i.e. directed toward the step. Before it has reached the *classical turning point* $x_c$, defined by equality

$$U(x_c) = E\,, \tag{2.51}$$

the particle's kinetic energy $p^2/2m$ is positive, so it continues to move in the initial direction. On the other hand, a classical particle cannot penetrate that *classically forbidden region* $x > x_c$, because there, its kinetic energy would be negative. Hence when the particle reaches the point $x = x_c$, its velocity has to change its sign, i.e. the particle is reflected back from the classical turning point.

In order to see what the wave mechanics says about this situation, let us start from the simplest, sharp potential step shown with the bold black line in Fig. 4:

$$U(x) = U_0\theta(x) \equiv \begin{cases} 0, & \text{at } x < 0, \\ U_0, & \text{at } 0 < x. \end{cases} \tag{2.52}$$

For this choice, and any energy within the interval $0 < E < U_0$, the classical turning point is $x_c = 0$.

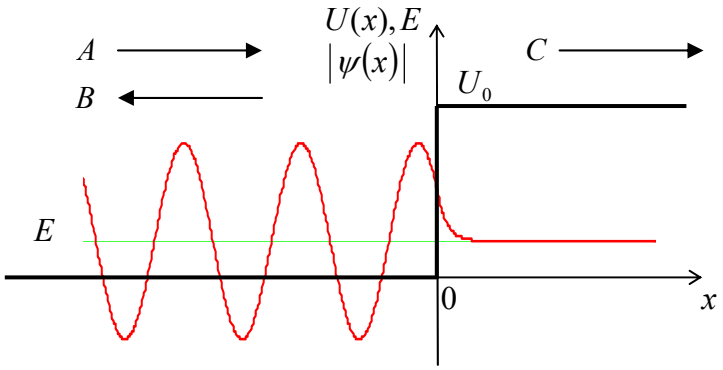


Fig. 2.4. Reflection of a monochromatic de Broglie wave from a potential step $U_0 > E$. (This particular wavefunction's shape is for $U_0 = 5E$.) The wavefunction is plotted with the same schematic vertical offset by $E$ as those in Fig. 1.8.

Let us represent the incident particle with a wave packet so long that the spread $\delta k \sim 1/\delta x$ of its wave-number spectrum is sufficiently small to make the energy uncertainty $\delta E = \hbar\delta\omega = \hbar(d\omega/dk)\delta k$ negligible in comparison with its average value $E < U_0$, as well as with $(U_0 - E)$. In this case, $E$ may be considered as a given constant, the time dependence of the wavefunction is given by Eq. (1.62), and we can calculate its spatial factor $\psi(x)$ from the 1D version of the stationary Schrödinger equation (1.65):[12]

$$-\frac{\hbar^2}{2m}\frac{d^2\psi}{dx^2} + U(x)\psi = E\psi\,. \tag{2.53}$$

At $x < 0$, i.e. at $U = 0$, the equation is reduced to the Helmholtz equation (1.78), and may be satisfied with either of two traveling waves, proportional to, respectively, $\exp\{+ikx\}$ and $\exp\{-ikx\}$, with $k$ satisfying the dispersion equation (1.30):

$$k^2 \equiv \frac{2mE}{\hbar^2}. \tag{2.54}$$

Thus the general solution of Eq. (53) in this region may be represented as

Incident and reflected waves

$$\boxed{\psi_-(x) = Ae^{+ikx} + Be^{-ikx}, \qquad \text{for } x < 0\,.} \tag{2.55}$$

[12] Note that this is *not* an eigenproblem like the one we have solved in Sec. 1.4 for a potential well. Indeed, now the energy $E$ is considered given – e.g., by the initial conditions that launch a long wave packet upon the potential step – in Fig. 4, from the left side.

The second term on the right-hand side of Eq. (55) evidently describes a (formally, infinitely long) wave packet traveling to the left, arising because of the particle's reflection from the potential step. If $B = -A$, Eq. (55) is reduced to Eq. (1.84) for a potential well with infinitely high walls, but for our current case of a finite step height $U_0$, the relation between the coefficients $B$ and $A$ may be different.

To show this, let us solve Eq. (53) for $x > 0$, where $U = U_0 > E$. In this region, the equation may be rewritten as

$$\frac{d^2\psi_+}{dx^2} = \kappa^2 \psi_+ , \tag{2.56}$$

where $\kappa$ is a real and positive constant defined by a formula similar in structure to Eq. (54):

$$\kappa^2 \equiv \frac{2m(U_0 - E)}{\hbar^2} > 0. \tag{2.57}$$

Decay in classically forbidden region

The general solution of Eq. (56) is the sum of $\exp\{+\kappa x\}$ and $\exp\{-\kappa x\}$, with arbitrary pre-exponential coefficients. However, in our particular case the wavefunction should be finite at $x \to +\infty$, so only the latter exponent is acceptable:

$$\psi_+(x) = Ce^{-\kappa x}, \qquad \text{for } x > 0 . \tag{2.58}$$

Such penetration of the wavefunction into the classically forbidden region, and hence a non-zero probability to find the particle there, is one of the most fascinating predictions of quantum mechanics, which has been repeatedly observed in experiment – for example, via tunneling experiments, to be discussed in the next section.[13] From Eq. (58), it is evident that the constant $\kappa$, defined by Eqs. (57), may be interpreted as the reciprocal penetration depth. Even for the lightest particles, this depth is usually very small. Indeed, for any $E << U_0$ that relation yields

$$\delta \equiv \frac{1}{\kappa}\Big|_{E\to 0} = \frac{\hbar}{(2mU_0)^{1/2}} . \tag{2.59}$$

For example, let us consider a conduction electron in a typical metal, which runs, at the metal's surface, into a sharp potential step whose height is equal to the metal's workfunction $U_0 \approx 5$ eV – see the discussion of the photoelectric effect in Sec. 1.1. In this case, according to Eq. (59), $\delta$ is close to 0.1 nm, i.e. is close to a typical size of an atom. For heavier elementary particles (e.g., protons) the penetration depth is correspondingly lower, and for macroscopic bodies, it is hardly measurable.

Returning to Eqs. (55) and (58), we still should relate the coefficients $B$ and $C$ to the amplitude $A$ of the incident wave, using the boundary conditions at $x = 0$. Since $E$ is a finite constant, and $U(x)$ is a finite function, Eq. (53) says that $d^2\psi/dx^2$ should be finite as well. This means that the first derivative should be continuous:

$$\lim_{\varepsilon\to 0}\left(\frac{d\psi}{dx}\Big|_{x=+\varepsilon} - \frac{d\psi}{dx}\Big|_{x=-\varepsilon}\right) = \lim_{\varepsilon\to 0}\int_{-\varepsilon}^{+\varepsilon}\frac{d^2\psi}{dx^2}dx = \frac{2m}{\hbar^2}\lim_{\varepsilon\to 0}\int_{-\varepsilon}^{+\varepsilon}[U(x) - E]\psi\, dx = 0 . \tag{2.60}$$

Repeating such calculation for the wavefunction $\psi(x)$ itself, we see that it also should be continuous at all points, including the border point $x = 0$, so the boundary conditions in our problem are

[13] Note that this effect is also pertinent to *classical waves* of any type, including mechanical waves (see, e.g., CM Secs. 6.4 and 7.7) and electromagnetic waves (see, e.g., EM Secs. 7.3-7.7), but not *classical particles*.

$$\psi_-(0) = \psi_+(0), \qquad \frac{d\psi_-}{dx}(0) = \frac{d\psi_+}{dx}(0). \tag{2.61}$$

Plugging Eqs. (55) and (58) into Eqs. (61), we get a system of two linear equations

$$A + B = C, \qquad ikA - ikB = -\kappa C, \tag{2.62}$$

whose (easy :-) solution allows us to express $B$ and $C$ via $A$ :

$$B = A\frac{k - i\kappa}{k + i\kappa}, \qquad C = A\frac{2k}{k + i\kappa}. \tag{2.63}$$

We immediately see that the numerator and denominator in the first of these fractions have equal moduli, so $|B| = |A|$. This means that, as we could expect, a particle with energy $E < U_0$ is totally reflected from the step – just as in classical mechanics. As a result, our solution (55) for $x < 0$ may be represented as a standing wave:

$$\psi_- = 2iAe^{i\theta}\sin(kx - \theta), \qquad \text{with } \theta \equiv \tan^{-1}\frac{k}{\kappa}. \tag{2.64}$$

Note that the shift $\Delta x \equiv \theta/k = (\tan^{-1}k/\kappa)/k$ of the standing wave to the right, due to the partial penetration of the wavefunction under the potential step, is commensurate with, but generally not equal to the penetration depth $\delta \equiv 1/\kappa$. The red line in Fig. 4 shows the exact behavior of the wavefunction, for a particular case $E = U_0/5$, at which $k/\kappa \equiv [E/(U_0 - E)]^{1/2} = 1/2$.

According to Eq. (59), as the particle's energy $E$ is increased to approach $U_0$, the penetration depth $1/\kappa$ diverges. This raises an important question: what happens at $E > U_0$, i.e. if there is no classically forbidden region in the problem? In classical mechanics, the incident particle would continue to move to the right, though with a reduced velocity corresponding to the new kinetic energy $E - U_0$, so there would be no reflection. In quantum mechanics, however, the situation is different. To analyze it, it is not necessary to the whole problem again; it is sufficient to note that all our calculations, and hence Eqs. (63) are still valid if we take[14]

$$\kappa = -ik', \qquad \text{with} \qquad k'^2 \equiv \frac{2m(E - U_0)}{\hbar^2} > 0. \tag{2.65}$$

With this replacement, Eq. (63) becomes[15]

$$B = A\frac{k - k'}{k + k'}, \quad C = A\frac{2k}{k + k'}. \tag{2.66}$$

The most important result of this change is that now the particle's reflection is *not* total: $|B| < |A|$. To evaluate this effect quantitatively, it is fairer to use not the $B/A$ or $C/A$ ratios, but rather that of the probability currents (5) carried by the de Broglie waves traveling to the right, with amplitudes $C$ and $A$, in the corresponding regions (respectively, for $x > 0$ and $x < 0$):

[14] Our earlier discarding of the particular solution $\exp\{\kappa x\}$, now becoming $\exp\{-ik'x\}$, is still valid, but now on different grounds: this term would describe a wave packet incident on the potential step from the right, and this is not the problem under our current consideration.

[15] These formulas are completely similar to those describing the partial reflection of classical waves from a sharp interface between two uniform media, at normal incidence (see, e.g., CM Sec. 6.4 and EM Sec. 7.4), with the effective impedance $Z$ of de Broglie waves being proportional to their wave number $k$.

$$\mathcal{T} \equiv \frac{I_C}{I_A} = \frac{k'|C|^2}{k|A|^2} = \frac{4kk'}{(k+k')^2} \equiv \frac{4[E(E-U_0)]^{1/2}}{\left[E^{1/2}+(E-U_0)^{1/2}\right]^2}. \quad (2.67)$$

Potential step's transparency

(The parameter $\mathcal{T}$ so defined is called the *transparency* of the system, in our current case of the potential step of height $U_0$, at particle's energy $E$.) The result given by Eq. (67) is plotted in Fig. 5a as a function of the $U_0/E$ ratio. Note its most important features:

(i) At $U_0 = 0$, the transparency is full, $\mathcal{T} = 1$ – naturally, because there is no step at all.

(ii) At $U_0 \to E$, the transparency drops to zero, giving a proper connection to the case $E < U_0$.

(iii) Nothing in our solution's procedure prevents us from using Eq. (67) even for $U_0 < 0$, i.e. for the *step-down* (or "cliff") potential profile – see Fig. 5b. Very counter-intuitively, the particle is (partly) reflected even from such a cliff, and the transmission diminishes (though rather slowly) at $U_0 \to -\infty$.

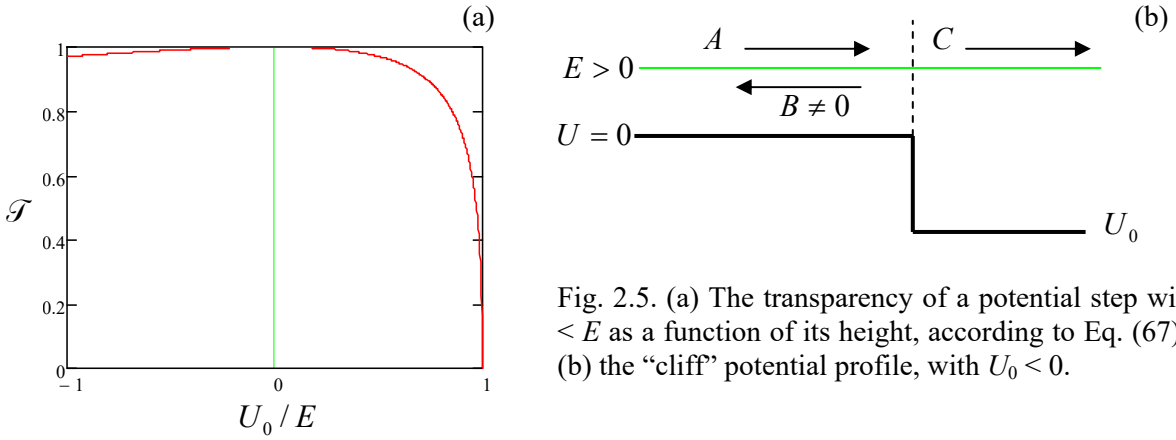


Fig. 2.5. (a) The transparency of a potential step with $U_0 < E$ as a function of its height, according to Eq. (67), and (b) the "cliff" potential profile, with $U_0 < 0$.

The most important conceptual conclusion of this analysis is that the quantum particle is *partly reflected* from a potential step with $U_0 < E$, in the sense that there is a non-zero probability $\mathcal{T} < 1$ to find it passed over the step, while there is also some probability, $(1 - \mathcal{T}) > 0$, to have it reflected.

The last property is exhibited, but for *any* relation between $E$ and $U_0$, by another simple potential profile $U(x)$, the famous *potential* (or "tunnel") *barrier*. Fig. 6 shows its simple flat-top ("rectangular") version:

$$U(x) = \begin{cases} 0, & \text{for } x < -d/2, \\ U_0, & \text{for } -d/2 < x < +d/2, \\ 0, & \text{for } +d/2 < x. \end{cases} \quad (2.68)$$

To analyze this problem, it is sufficient to look for the solution to the Schrödinger equation in the form (55) at $x \le -d/2$. At $x > +d/2$, i.e., behind the barrier, we may use the arguments presented above (no wave source on the right!) to keep just one traveling wave, now with the same wave number:

$$\psi_+(x) = Fe^{ikx}. \quad (2.69)$$

However, under the barrier, i.e. at $-d/2 \le x \le +d/2$, we should generally keep both exponential terms,

$$\psi_b(x) = Ce^{-\kappa x} + De^{+\kappa x}, \quad (2.70)$$

because our previous argument used in the potential step problem's solution is no longer valid. (Here $k$ and $\kappa$ are still defined, respectively, by Eqs. (54) and (57).) In order to express the coefficients $B$, $C$, $D$, and $F$ via the amplitude $A$ of the incident wave, we need to plug these solutions into the boundary conditions similar to Eqs. (61), but now at two boundary points, $x = \pm d/2$.

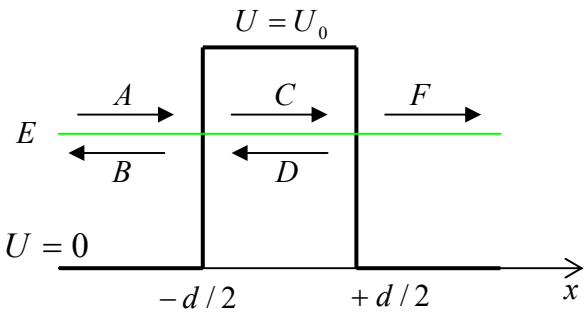


Fig. 2.6. A rectangular potential barrier, and the de Broglie waves taken into account in its analysis.

Solving the resulting system of 4 linear equations, we get 4 ratios $B/A$, $C/A$, etc.; in particular,

$$\frac{F}{A} = \left[\cosh \kappa d + \frac{i}{2}\left(\frac{\kappa}{k} - \frac{k}{\kappa}\right)\sinh \kappa d\right]^{-1} e^{-ikd}, \tag{2.71a}$$

and hence the barrier's transparency

Rectangular tunnel barrier's transparency

$$\mathcal{T} \equiv \left|\frac{F}{A}\right|^2 = \left[\cosh^2 \kappa d + \left(\frac{\kappa^2 - k^2}{2\kappa k}\right)^2 \sinh^2 \kappa d\right]^{-1} \equiv \left[1 + \left(\frac{\kappa^2 + k^2}{2\kappa k}\right)^2 \sinh^2 \kappa d\right]^{-1}. \tag{2.71b}$$

So, quantum mechanics indeed allows particles with energies $E < U_0$ to pass "through" the potential barrier – see Fig. 6 again. This is the famous effect of *quantum-mechanical tunneling*. Fig. 7a shows the barrier transparency as a function of the particle energy $E$, for several characteristic values of its thickness $d$, or rather of the ratio $d/\delta$, with $\delta$ defined by Eq. (59).[16]

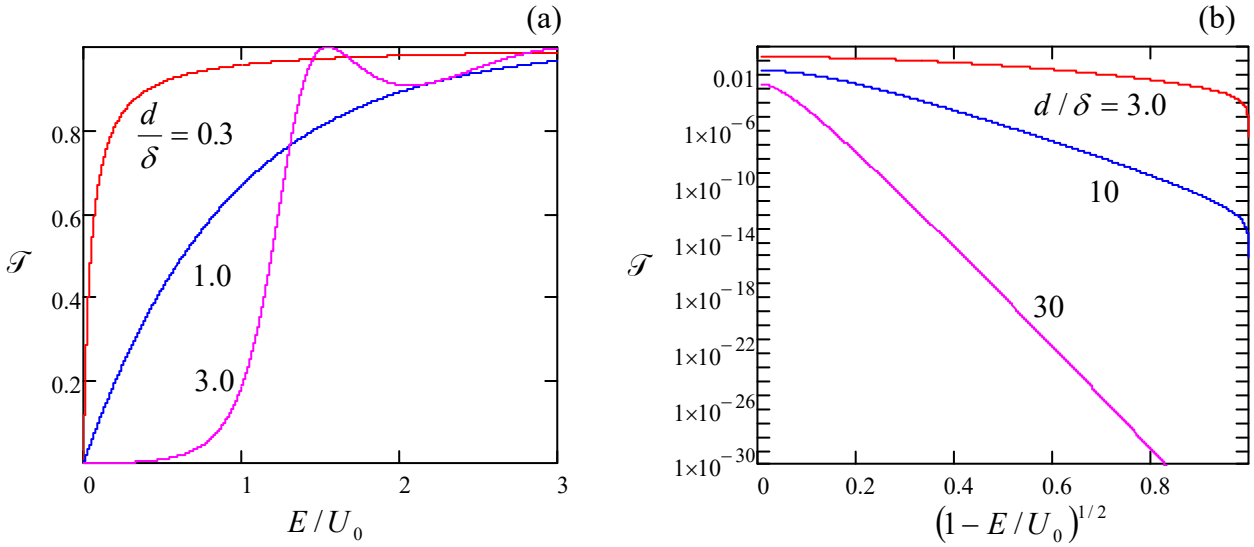


Fig. 2.7. The transparency of a rectangular potential barrier as a function of the particle's energy $E$.

[16] The branches with $E > U_0$ have been computed from Eq. (71b) by using the replacement (65).

The plots show that generally, the transparency grows with the particle's energy. This growth is natural because the penetration constant $\kappa$ decreases with the growth of $E$, i.e., the wavefunction penetrates more and more into the barrier, so more and more of it is "picked up" at the second interface ($x = +d/2$) and transferred into the wave $F\exp\{ikx\}$ propagating behind the barrier.

Now let us consider the important limit of a very thin and high rectangular barrier with $d << \delta$, $E << U_0$, giving $k << \kappa << 1/d$. In this limit, the second form of Eq. (71b) yields

$$\mathcal{T} \to \frac{1}{1+\alpha^2}, \qquad \text{where } \alpha \equiv \left(\frac{\kappa^2+k^2}{2\kappa k}\right)\kappa d \approx \frac{\kappa^2 d}{2k} \approx \frac{m}{\hbar^2 k}U_0 d\,, \tag{2.72}$$

The last product, $U_0 d$, is just the *weight* (or the "energy area")

$$\mathcal{W} \equiv \int_{U(x)>E} U(x)dx \tag{2.73}$$

of the barrier for our particular case (68). This fact implies that the very simple result (72) may be correct for a barrier of any shape, provided that it is sufficiently thin and high.

To examine this guess, let us consider the tunneling problem for a very thin barrier with $\kappa d$, $kd << 1$, by approximating it with the Dirac's $\delta$-function (Fig. 8):

$$U(x) = \mathcal{W}\delta(x)\,, \tag{2.74}$$

so that the parameter $\mathcal{W}$ satisfies Eq. (73).

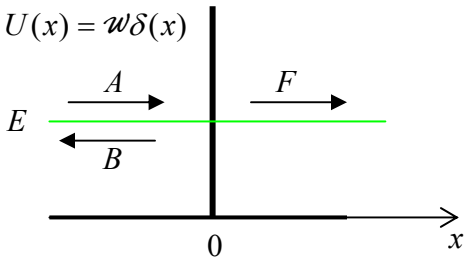


Fig. 2.8. A delta-functional potential barrier.

The solutions of the tunneling problem at all points but $x = 0$ still may be taken in the form of Eqs. (55) and (69), so we only need to analyze the boundary conditions at that point. However, due to the special character of the $\delta$-function, we should be careful here. Indeed, instead of Eq. (60) we now get

$$\begin{aligned}\lim_{\varepsilon\to 0}\left(\frac{d\psi}{dx}\Big|_{x=+\varepsilon} - \frac{d\psi}{dx}\Big|_{x=-\varepsilon}\right) &= \lim_{\varepsilon\to 0}\int_{-\varepsilon}^{+\varepsilon}\frac{d^2\psi}{dx^2}dx = \lim_{\varepsilon\to 0}\frac{2m}{\hbar^2}\int_{-\varepsilon}^{+\varepsilon}[U(x)-E]\psi\,dx \\ &= \frac{2m}{\hbar^2}\mathcal{W}\psi(0).\end{aligned} \tag{2.75}$$

According to this relation, at a finite $\mathcal{W}$, the derivatives $d\psi/dx$ are also finite, so the wavefunction itself is still continuous:

$$\lim_{\varepsilon\to 0}\left(\psi\big|_{x=+\varepsilon} - \psi\big|_{x=+\varepsilon}\right) = \lim_{\varepsilon\to 0}\int_{-\varepsilon}^{+\varepsilon}\frac{d\psi}{dx}dx = 0. \tag{2.76}$$

Using these two boundary conditions, we readily get the following system of two linear equations,

$$A + B = F, \qquad ikF - (ikA - ikB) = \frac{2m\mathcal{W}}{\hbar^2} F, \tag{2.77}$$

whose solution yields

$$\frac{B}{A} = \frac{-i\alpha}{1+i\alpha}, \quad \frac{F}{A} = \frac{1}{1+i\alpha}, \qquad \text{where } \alpha \equiv \frac{m\mathcal{W}}{\hbar^2 k}. \tag{2.78}$$

(Taking Eq. (73) into account, this definition of $\alpha$ coincides with that in Eq. (72).) For the barrier transparency $\mathscr{T} \equiv |F/A|^2$, this result again gives the first of Eqs. (72), which is therefore general for such thin barriers. That formula may be recast to give the following simple expression (valid only for $E << U_{max}$):

Transparency: thin barrier

$$\mathscr{T} = \frac{1}{1+\alpha^2} \equiv \frac{E}{E+E_0}, \qquad \text{where } E_0 \equiv \frac{m\mathcal{W}^2}{2\hbar^2}, \tag{2.79}$$

which shows that as energy becomes larger than the constant $E_0$, the transparency approaches 1 – as it eventually does for *any* tunnel barrier. Another general behavior of Eq. (79) is that at $E \to 0$ (i.e. $k \to 0$), $\mathscr{T} \propto E$. Indeed, at $ka << 1$, *any* barrier of a finite width $a$ may be well approximated with Eq. (74).

As Eq. (71) shows, in the opposite limit of relatively thick barriers ($d >> \delta$), the transparency is dominated by what is called the *tunnel exponent*:

Transparency: thick barrier

$$\mathscr{T} = \left( \frac{4k\kappa}{k^2+\kappa^2} \right)^2 e^{-2\kappa d} \tag{2.80}$$

– the behavior which may be clearly seen as the straight-line segments in semi-log plots (Fig. 7b) of $\mathscr{T}$ as a function of the combination $(1 - E/U_0)^{1/2}$ which is proportional to $\kappa$ – see Eq. (57).

The exponential dependence of the barrier's transparency on its thickness is the most important factor for various applications of quantum-mechanical tunneling – from the field emission of electrons to vacuum[17] to the scanning tunneling microscopy.[18] Note also substantial negative implications of the effect on the electronic technology progress. Most importantly, it imposes limits on the so-called *Dennard scaling* of field-effect transistors in semiconductor integrated circuits (which was the technological basis of the well-known *Moore's law*), due to the increase of tunneling both through the gate oxide and along the channel of the transistors, from source to drain.[19]

Finally, one more feature visible in Fig. 7a (for case $d = 3\delta$) are the oscillations of the transparency as a function of energy, at $E > U_0$, with $\mathscr{T} = 1$, i.e. the reflection completely vanishing, at some points.[20] This is our first glimpse at one more interesting quantum effect: *resonant tunneling*. This

[17] See, e.g., G. Fursey, *Field Emission in Vacuum Microelectronics*, Kluwer, New York, 2005.

[18] See, e.g., G. Binning and H. Rohrer, *Helv. Phys. Acta* **55**, 726 (1982).

[19] See, e.g., V. Sverdlov *et al.*, *IEEE Trans. on Electron Devices* **50**, 1926 (2003), and references therein. (A brief discussion of the field-effect transistors, and literature for further reading, may be found in SM Sec. 6.4.)

[20] Let me mention in passing the curious case of the potential well $U(x) = -(\hbar^2/2m)\nu(\nu+1)/\cosh^2(x/a)$, with any positive integer $\nu$ and any real $a$, which is reflection-free ($\mathscr{T} = 1$) for the incident de Broglie wave of *any* energy $E$, and hence for any incident wave packet. (The well is called the *Pöschl-Teller potential*, though it was first described in a 1930 paper by P. Epstein, before the 1933 publication by G. Pöschl and E. Teller.)

effect will be discussed in more detail in Sec. 5 below, by using another potential profile where it is more clearly pronounced.

## 2.4. Motion in soft potentials[21]

Before moving on to explore other quantum-mechanical effects, let us examine how the results discussed in the previous section are modified in the opposite limit of the so-called *soft* (or "smooth") potential profiles, like the one sketched in Fig. 3.[22] The most efficient analytical tool to study this limit is the so-called *WKB* (or "JWKB", or "quasiclassical") *approximation* developed by H. Jeffrey, G. Wentzel, A. Kramers, and L. Brillouin in 1925-27. In order to derive its 1D version, let us rewrite the Schrödinger equation (53) in a simpler form

$$\frac{d^2\psi}{dx^2} + k^2(x)\psi = 0, \tag{2.81}$$

where the local wave number $k(x)$ is defined similarly to Eq. (65),

$$k^2(x) \equiv \frac{2m[E - U(x)]}{\hbar^2}, \tag{2.82}$$

Local wave number

besides that now it may be a function of $x$. We already know that for $k(x) = \text{const}$, the fundamental solutions of this equation are $A\exp\{+ikx\}$ and $B\exp\{-ikx\}$, which may be represented in a single form

$$\psi(x) = e^{i\Phi(x)}, \tag{2.83}$$

where $\Phi(x)$ is a complex function, in these two simplest cases being equal, respectively, to $(kx - i\ln A)$ and $(-kx - i\ln B)$. This is why we may try to use Eq. (83) to look for a solution of Eq. (81) even in the general case when $k(x) \neq \text{const}$. Differentiating Eq. (83) twice, we get

$$\frac{d\psi}{dx} = i\frac{d\Phi}{dx}e^{i\Phi}, \qquad \frac{d^2\psi}{dx^2} = \left[i\frac{d^2\Phi}{dx^2} - \left(\frac{d\Phi}{dx}\right)^2\right]e^{i\Phi}. \tag{2.84}$$

Plugging the last expression into Eq. (81) and canceling the common factor $\exp\{i\Phi(x)\} \neq 0$, we get

$$i\frac{d^2\Phi}{dx^2} - \left(\frac{d\Phi}{dx}\right)^2 + k^2(x) = 0. \tag{2.85}$$

This is still an exact, general equation. Superficially, it looks even harder to solve than the initial equation (81) because Eq. (85) is nonlinear. However, it is ready for simplification in the limit when the potential profile is soft, $dU/dx \to 0$. Indeed, for a uniform potential, $d^2\Phi/dx^2 = 0$. Hence, in the so-called *$0^{th}$ approximation*, $\Phi(x) \to \Phi_0(x)$, we may try to keep that equality, so Eq. (85) is reduced to

$$\left(\frac{d\Phi_0}{dx}\right)^2 = k^2(x), \qquad \text{i.e. } \frac{d\Phi_0}{dx} = \pm k(x), \qquad \Phi_0(x) = \pm i\int^x k(x')dx', \tag{2.86}$$

so its general solution is a linear superposition of the two functions (83), with $\Phi$ replaced with $\Phi_0$:

[21] Following tradition, I will frequently use this shorthand for "potential energy", returning to the full term in cases where there is any chance of confusion between this notion and another (say, electrostatic) potential.

[22] Quantitative conditions of the "softness" will be formulated later in this section.

$$\psi_0(x) = A\exp\left\{+i\int^x k(x')dx'\right\} + B\exp\left\{-i\int^x k(x')dx'\right\}, \tag{2.87}$$

where the choice of the lower limits of integration affects only the constants $A$ and $B$. The physical sense of this result is simple: it is a sum of the forward- and back-propagating de Broglie waves, with the coordinate-dependent local wave number $k(x)$ adjusted to the potential profile.

Let me emphasize the non-trivial nature of this approximation.[23] First, any attempt to address the problem with the standard perturbation approach (say, $\psi = \psi_0 + \psi_1 + \ldots$, with $\psi_n$ proportional to the $n^{\text{th}}$ power of some small parameter) would fail for most potentials, because as Eq. (86) shows, even a slight but persisting deviation of $U(x)$ from a constant leads to a gradual accumulation of the phase $\Phi_0$, impossible to describe by any small perturbation of $\psi$. Second, the dropping of the term $d^2\Phi/dx^2$ in Eq. (85) is not too easy to justify. Indeed, since we are committed to the "soft potential limit" $dU/dx \to 0$, we should be ready to assume the characteristic length $a$ of the spatial variation of $\Phi$ to be large, and neglect the terms that are the smallest ones in the limit $a \to \infty$. However, both first terms in Eq. (85) are apparently of the same order in $a$, namely $O(a^{-2})$; why have we neglected just one of them?

The price we have paid for such a "sloppy" treatment is substantial: Eq. (87) does *not* satisfy the fundamental property of solutions of the stationary Schrödinger equation, namely the probability current's conservation: $I(x)$ = const. However, this is not true for any component of Eq. (87); for example for the first, forward-propagating component on its right-hand side, Eq. (5) yields

$$I_0(x) = \frac{\hbar}{m}\left|A\right|^2 k(x), \tag{2.88}$$

evidently not a constant if $k(x) \neq$ const. The brilliance of the WKB theory is that the problem may be fixed without a full revision of the 0th approximation, just by amending it. Indeed, let us explore the next, 1st approximation:

$$\Phi(x) \to \Phi_{\text{WKB}}(x) \equiv \Phi_0(x) + \Phi_1(x), \tag{2.89}$$

where $\Phi_0$ still obeys Eq. (86), while $\Phi_1$ describes a 0th approximation's correction that is small in the following sense:[24]

$$\left|\frac{d\Phi_1}{dx}\right| << \left|\frac{d\Phi_0}{dx}\right| = k(x). \tag{2.90}$$

Plugging Eq. (89) into Eq. (85), with the account of the definition (86), we get

$$i\left(\frac{d^2\Phi_0}{dx^2} + \frac{d^2\Phi_1}{dx^2}\right) - \frac{d\Phi_1}{dx}\left(2\frac{d\Phi_0}{dx} + \frac{d\Phi_1}{dx}\right) = 0. \tag{2.91}$$

Using the condition (90), we may neglect $d^2\Phi_1/dx^2$ in comparison with $d^2\Phi_0/dx^2$ inside the first parentheses, and $d\Phi_1/dx$ in comparison with $2d\Phi_0/dx$ inside the second parentheses. As a result, we get the following (still approximate!) result:

[23] Philosophically, this space-domain method is very close to the time-domain *van der Pol method* in classical mechanics, and the very similar *rotating wave approximation* (RWA) in quantum mechanics – see, e.g., CM Secs. 5.2-5.5, and also Secs. 6.5, 7.6, 9.2, and 9.4 of this course.

[24] For certainty, I will use the discretion given by Eq. (82) to define $k(x)$ as the *positive* root of its right-hand side.

$$\frac{d\Phi_1}{dx} = \frac{i}{2}\frac{d^2\Phi_0}{dx^2}\Big/\frac{d\Phi_0}{dx} \equiv \frac{i}{2}\frac{d}{dx}\left(\ln\frac{d\Phi_0}{dx}\right) = \frac{i}{2}\frac{d}{dx}\left[\ln k(x)\right] \equiv i\frac{d}{dx}\left[\ln k^{1/2}(x)\right], \tag{2.92}$$

$$i\Phi\big|_{\text{WKB}} \equiv i\Phi_0 + i\Phi_1 = \pm i\int^x k(x')dx' + \ln\frac{1}{k^{1/2}(x)}, \tag{2.93}$$

$$\psi_{\text{WKB}}(x) = \frac{a}{k^{1/2}(x)}\exp\left\{i\int^x k(x')dx'\right\} + \frac{b}{k^{1/2}(x)}\exp\left\{-i\int^x k(x')dx'\right\}. \qquad \text{for } k^2(x) > 0. \tag{2.94}$$

WKB wave-function

(Again, the lower integration limit is arbitrary, because its choice may be incorporated into the complex constants $a$ and $b$.) This modified approximation overcomes the problem of current continuity; for example, for the forward-propagating wave, Eq. (5) gives

$$I_{\text{WKB}}(x) = \frac{\hbar}{m}|a|^2 = \text{const}. \tag{2.95}$$

WKB probability current

Physically, the factor $k^{1/2}$ in the denominator of the WKB wavefunction's pre-exponent may be easily understood. The smaller the local group velocity (32) of the wave packet, $v_{\text{gr}}(x) = \hbar k(x)/m$, the "easier" (more probable) it should be to find the particle within a certain interval $dx$. This is exactly the result that the WKB approximation gives: $w(x) = \psi\psi^* \propto 1/k(x) \propto 1/v_{\text{gr}}$. Another value of the 1st approximation is a clarification of the WKB theory's validity condition: it is given by Eq. (90). Plugging into this relation the first form of Eq. (92), and estimating $|d^2\Phi_0/dx^2|$ as $|d\Phi_0/dx|/a$, where $a$ is the spatial scale of a substantial change of $|\,d\Phi_0/dx\,| = k(x)$, we may write the condition as

$$ka >> 1. \tag{2.96}$$

WKB: first condition of validity

In plain English, this means that the region where $U(x)$, and hence $k(x)$, change substantially should contain many de Broglie wavelengths $\lambda = 2\pi/k$.

So far I have implied that $k^2(x) \propto E - U(x)$ is positive, i.e. particle moves in the classically accessible region. Now let us extend the WKB approximation to situations where the difference $E - U(x)$ may change sign, for example to the reflection problem sketched in Fig. 3. Just as we did for the sharp potential step, we first need to find the appropriate solution in the classically forbidden region, in this case for $x > x_c$. For that, there is again no need to redo our calculations, because they are still valid if we, just as in the sharp-step problem, take $k(x) = i\kappa(x)$, where

$$\kappa^2(x) \equiv \frac{2m[U(x) - E]}{\hbar^2} > 0, \qquad \text{for } x > x_c, \tag{2.97}$$

and keep just one of two possible solutions (with $\kappa > 0$), in analogy with Eq. (58). The result is

$$\psi_{\text{WKB}}(x) = \frac{c}{\kappa^{1/2}(x)}\exp\left\{-\int^x \kappa(x')dx'\right\}, \qquad \text{for } k^2 < 0, \text{ i.e. } \kappa^2 > 0, \tag{2.98}$$

with the lower limit at some point with $\kappa^2 > 0$ as well. This is a really wonderful formula! It describes the quantum-mechanical penetration of the particle into the classically forbidden region and provides a natural generalization of Eq. (58) – leaving intact our estimates of the depth $\delta \sim 1/\kappa$ of such penetration.

Now we have to do what had been done for the sharp-step problem in Sec. 2: use the boundary conditions at the classical turning point $x = x_c$ to relate the constants $a$, $b$, and $c$. However, now this operation is a tad more complex, because both WKB functions (94) and (98) diverge, albeit weakly, at the point, because here both $k(x)$ and $\kappa(x)$ tend to zero. This *connection problem* may be solved in the following way. [25]

Let us use our commitment to the potential's "softness", assuming that it allows us to keep just two leading terms in the Taylor expansion of the function $U(x)$ at the point $x_c$:

$$U(x) \approx U(x_c) + \left.\frac{dU}{dx}\right|_{x=x_c}(x - x_c) \equiv E + \left.\frac{dU}{dx}\right|_{x=x_c}(x - x_c). \tag{2.99}$$

Using this truncated expansion, and introducing the following dimensionless variable for the coordinate's deviation from the classical turning point,

$$\zeta \equiv \frac{x - x_c}{x_0}, \qquad \text{with } x_0 \equiv \left[\frac{\hbar^2}{2m\left(dU/dx\right)_{x=x_c}}\right]^{1/3}, \tag{2.100}$$

we reduce the Schrödinger equation (81) to the so-called *Airy equation*

Airy equation

$$\boxed{\frac{d^2\psi}{d\zeta^2} - \zeta\psi = 0}. \tag{2.101}$$

This simple linear, ordinary, homogenous differential equation of the second order has been very well studied. Its general solution may be represented as a linear combination of two fundamental solutions, the *Airy functions*, $\mathrm{Ai}(\zeta)$ and $\mathrm{Bi}(\zeta)$, shown in Fig. 9a.[26]

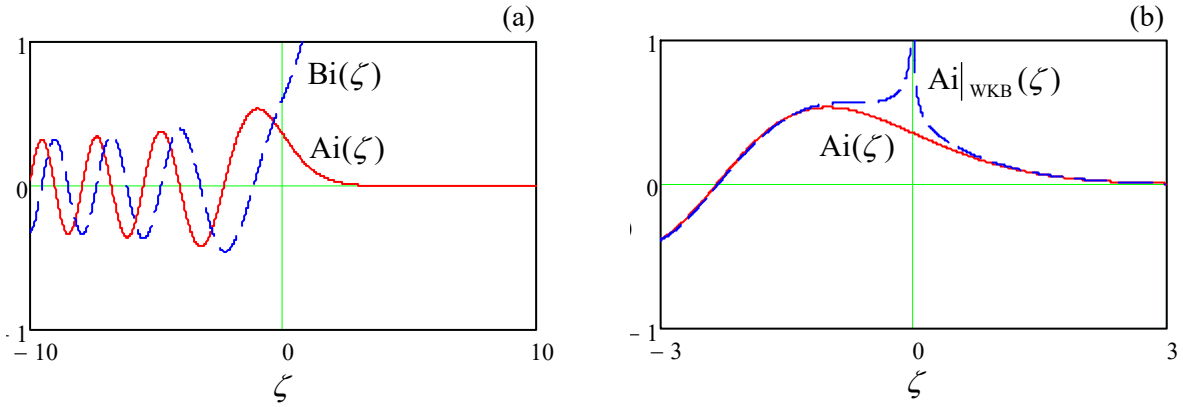


Fig. 2.9. (a) The Airy functions Ai and Bi, and (b) the WKB approximation for the function $\mathrm{Ai}(\zeta)$.

[25] An alternative way to solve the connection problem, without involving the Airy functions but using an analytical extension of WKB formulas to the complex-argument plane, may be found, e.g., in Sec. 47 of the textbook by L. Landau and E. Lifshitz, *Quantum Mechanics*, *Non-Relativistic Theory*, 3rd ed. Pergamon, 1977.

[26] Note the following (exact) integral formulas,

$$\mathrm{Ai}(\zeta) = \frac{1}{\pi}\int_0^\infty \cos\left(\frac{\xi^3}{3} + \zeta\xi\right)d\xi, \qquad \mathrm{Bi}(\zeta) = \frac{1}{\pi}\int_0^\infty \left[\exp\left\{-\frac{\xi^3}{3} + \zeta\xi\right\} + \sin\left(\frac{\xi^3}{3} + \zeta\xi\right)\right]d\xi,$$

frequently more convenient for practical calculations of the Airy functions than the differential equation (101).

The latter function diverges at $\zeta \to +\infty$, and thus is not suitable for our current problem (Fig. 3), while the former function has the following asymptotic behaviors at $|\zeta| >> 1$:

$$\mathrm{Ai}(\zeta) \to \frac{1}{\pi^{1/2}|\zeta|^{1/4}} \times \begin{cases} \frac{1}{2}\exp\left\{-\frac{2}{3}\zeta^{3/2}\right\}, & \text{for } \zeta \to +\infty, \\ \sin\left\{\frac{2}{3}(-\zeta)^{3/2} + \frac{\pi}{4}\right\}, & \text{for } \zeta \to -\infty. \end{cases} \tag{2.102}$$

Now let us apply the WKB approximation to the Airy equation (101). Taking the classical turning point ($\zeta = 0$) for the lower limit, for $\zeta > 0$ we get

$$\kappa^2(\zeta) = \zeta, \qquad \kappa(\zeta) = \zeta^{1/2}, \qquad \int_0^{\zeta} \kappa(\zeta')d\zeta' = \frac{2}{3}\zeta^{3/2}, \tag{2.103}$$

i.e. exactly the exponent in the top line of Eq. (102). Making a similar calculation for $\zeta < 0$, with the natural assumption $|b| = |a|$ (full reflection from the potential step), we arrive at the following result:

$$\mathrm{Ai}_{\mathrm{WKB}}(\zeta) = \frac{1}{|\zeta|^{1/4}} \times \begin{cases} c'\exp\left\{-\frac{2}{3}\zeta^{3/2}\right\}, & \text{for } \zeta > 0, \\ a'\sin\left\{\frac{2}{3}(-\zeta)^{3/2} + \varphi\right\}, & \text{for } \zeta < 0. \end{cases} \tag{2.104}$$

This approximation differs from the exact solution at small values of $\zeta$, i.e. close to the classical turning point – see Fig. 9b. However, at $|\zeta| >> 1$, Eqs. (104) describe the Airy function exactly, provided that

$$\varphi = \frac{\pi}{4}, \qquad c' = \frac{a'}{2}. \tag{2.105}$$

WKB: connection formulas

These *connection formulas* may be used to rewrite Eq. (104) as

$$\mathrm{Ai}_{\mathrm{WKB}}(\zeta) = \frac{a'}{2|\zeta|^{1/4}} \times \begin{cases} \exp\left\{-\frac{2}{3}\zeta^{3/2}\right\}, & \text{for } \zeta > 0, \\ \frac{1}{i}\left[\exp\left\{+i\frac{2}{3}\zeta^{3/2} + i\frac{\pi}{4}\right\} - \exp\left\{-i\frac{2}{3}\zeta^{3/2} - i\frac{\pi}{4}\right\}\right], & \text{for } \zeta < 0, \end{cases} \tag{2.106}$$

and hence may be described by the following two simple mnemonic rules:

(i) If the classical turning point is taken for the lower limit in the WKB integrals in the classically allowed and the classically forbidden regions, then the moduli of the quasi-amplitudes of the exponents are equal.

(ii) Reflecting from a "soft" potential step, the wavefunction acquires an additional phase shift $\Delta\varphi = \pi/2$, if compared with its reflection from a "hard", infinitely high potential wall located at point $x_c$ (for which, according to Eq. (63) with $\kappa = \infty$, we have $B = -A$).

In order for the connection formulas (105)-(106) to be valid, deviations from the linear approximation (99) of the potential profile should be relatively small within the region where the WKB approximation differs from the exact Airy function: $|\zeta| \sim 1$, i.e. $|x - x_c| \sim x_0$. These deviations may be estimated using the next term of the Taylor expansion, dropped in Eq. (99): $(d^2U/d^2x)(x - x_c)^2/2$. As a result, the condition of validity of the connection formulas (i.e. of the "softness" of the reflecting

potential profile) may be expressed as $\left|d^2U/d^2x\right|_{x_0} << \left|dU/dx\right|$ at $x \approx x_c$ – meaning the ~$x_0$–wide vicinity of the point $x_c$). With the account of Eq. (100) for $x_0$, this condition becomes

Connection formulas' validity

$$\left|\frac{d^2U}{dx^2}\right|^3_{x\approx x_c} << \frac{2m}{\hbar^2}\left(\frac{dU}{dx}\right)^4_{x\approx x_c}. \tag{2.107}$$

As an example of a very useful application of the WKB approximation, let us use the connection formulas to calculate the energy spectrum of a 1D particle in a soft 1D potential well (Fig. 10).

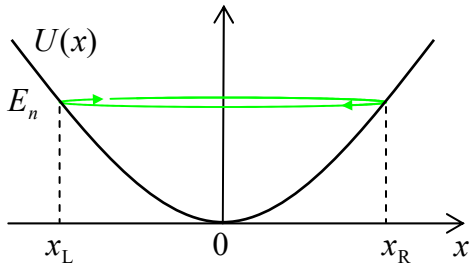


Fig. 2.10. The WKB treatment of an eigenstate of a particle in a soft 1D potential well.

As was discussed in Sec. 1.7, we may consider the standing wave describing an eigenfunction $\psi_n$ (corresponding to an eigenenergy $E_n$) as a sum of two traveling de Broglie waves going back and forth between the walls, being sequentially reflected from each of them. Let us apply the WKB approximation to such traveling waves. First, according to Eq. (94), propagating from the left classical turning point $x_L$ to the right such point $x_R$, it acquires the phase change

$$\Delta\varphi_{\rightarrow} = \int_{x_L}^{x_R} k(x)dx\,. \tag{2.108}$$

At the reflection from the soft wall at $x_R$, according to the mnemonic rule (ii), the wave acquires an additional shift $\pi/2$. Now, traveling back from $x_R$ to $x_L$, the wave gets a shift similar to one given by Eq. (108): $\Delta\varphi_{\leftarrow} = \Delta\varphi_{\rightarrow}$. Finally, at the reflection from $x_L$, it gets one more $\pi/2$-shift. Summing up all these contributions at the wave's roundtrip, we may write the self-consistency condition (that the wavefunction "catches its own tail with its teeth") in the form

$$\Delta\varphi_{\text{total}} \equiv \Delta\varphi_{\rightarrow} + \frac{\pi}{2} + \Delta\varphi_{\leftarrow} + \frac{\pi}{2} \equiv 2\int_{x_L}^{x_R} k(x)dx + \pi = 2\pi m, \quad \text{with } n = 1, 2, ... \tag{2.109}$$

Rewriting this result in terms of the particle's momentum $p(x) = \hbar k(x)$, we arrive at the so-called *Wilson-Sommerfeld* (or, less fairly, "Bohr-Sommerfeld") *quantization rule*

Wilson-Sommerfeld quantization rule

$$\oint_C p(x)dx = 2\pi\hbar\left(n - \frac{1}{2}\right), \tag{2.110}$$

where the closed path $C$ means the full period of classical motion.[27]

[27] Note that at the motion in more than one dimension, a closed classical trajectory may have no classical turning points. In this case, the constant ½, arising from the turns, should be dropped from Eqs. (110) written for the scalar product $\mathbf{p}(\mathbf{r})\cdot d\mathbf{r}$, giving the so-called *Bohr quantization* rule. It was suggested by N. Bohr as early as 1913 as an interpretation of Eq. (1.8) for the circular motion of the electron around the proton, while its 1D modification (110) is due to W. Wilson (1915) and A. Sommerfeld (1916).

Let us see what this quantization rule gives for the very important particular case of a quadratic potential profile of a harmonic oscillator of frequency $\omega_0$. In this case,

$$U(x) = \frac{m}{2}\omega_0^2 x^2, \tag{2.111}$$

and the classical turning points (where $U(x) = E$) are the roots of a simple equation

$$\frac{m}{2}\omega_0^2 x_c^2 = E_n, \qquad \text{so that } x_R = \frac{1}{\omega_0}\left(\frac{2E_n}{m}\right)^{1/2} > 0, \quad x_L = -x_R < 0. \tag{2.112}$$

Due to the potential's symmetry, the integration required by Eq. (110) is also simple:

$$\begin{aligned} \int_{x_L}^{x_R} p(x)dx &= \int_{x_L}^{x_R} \{2m[E_n - U(x)]\}^{1/2} dx \equiv (2mE_n)^{1/2} 2\int_0^{x_R}\left(1 - \frac{x^2}{x_R^2}\right)^{1/2} dx \\ &\equiv (2mE_n)^{1/2} 2x_R \int_0^1 (1-\xi^2)^{1/2} d\xi = (2mE_n)^{1/2} 2x_R \frac{\pi}{4} \equiv \frac{\pi E_n}{\omega_0}, \end{aligned} \tag{2.113}$$

so Eq. (110) yields

$$E_n = \hbar\omega_0\left(n' + \frac{1}{2}\right), \qquad \text{with } n' \equiv n - 1 = 0, 1, 2, \ldots. \tag{2.114}$$

To estimate the validity of this result, we have to check the condition (96) at all points of the classically allowed region, and Eq. (107) at the turning points. The checkup shows that both conditions are valid only for $n >> 1$. However, we will see in Sec. 9 below that Eq. (114) is actually exactly correct for *all* energy levels – thanks to the special properties of the potential profile (111).

Now let us use the mnemonic rule (i) to examine the particle's penetration into the classically forbidden region of an abrupt potential step of a height $U_0 > E$. For this case, the rule, i.e. the second of Eqs. (105), yields the following relation of the quasi-amplitudes in Eqs. (94) and (98): $|c| = |a|/2$. If we now naively applied this relation to the sharp step sketched in Fig. 4, forgetting that it does not satisfy Eq. (107), we would get the following relation of the full amplitudes defined by Eqs. (55) and (58):

$$\left|\frac{C}{\kappa}\right| = \frac{1}{2}\left|\frac{A}{k}\right|. \qquad \text{(WRONG!)} \tag{2.115}$$

This result differs from the correct Eq. (63), and hence we may expect that the WKB approximation's prediction for more complex potentials, most importantly for tunneling through a soft potential barrier (Fig. 11) should be also different from the exact result (71) for the rectangular barrier shown in Fig. 6.

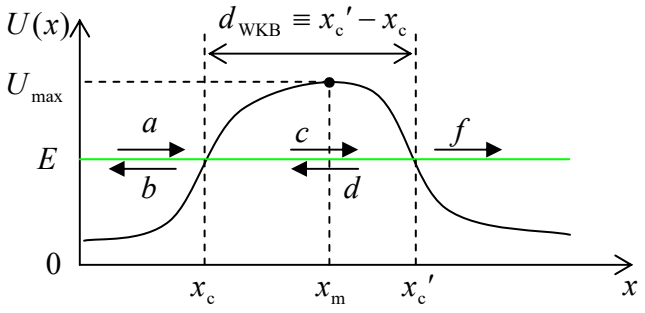


Fig. 2.11. Tunneling through a soft 1D potential barrier.

To analyze tunneling through such a soft barrier, we need (just as in the case of a rectangular barrier) to take into consideration five partial waves, but now they should be taken in the WKB form:

$$\psi_{\rm WKB} = \begin{cases} \dfrac{a}{k^{1/2}(x)}\exp\left\{i\int^{x} k(x')dx'\right\} + \dfrac{b}{k^{1/2}(x)}\exp\left\{-i\int^{x} k(x')dx'\right\}, & \text{for } x < x_{\rm c}, \\ \dfrac{c}{\kappa^{1/2}(x)}\exp\left\{-\int^{x} \kappa(x')dx'\right\} + \dfrac{d}{\kappa^{1/2}(x)}\exp\left\{\int^{x} \kappa(x')dx'\right\}, & \text{for } x_{\rm c} < x < x_{\rm c}', \\ \dfrac{f}{k^{1/2}(x)}\exp\left\{i\int^{x} k(x')dx'\right\}, & \text{for } x_{\rm c}' < x, \end{cases} \tag{2.116}$$

where the lower limits of integrals are arbitrary (each within the corresponding range of $x$). Since on the right of the left classical point, we have two exponents rather than one, and on the right of the second point, one traveling wave rather than two, the connection formulas (105) have to be generalized by using asymptotic formulas not only for Ai($\zeta$), but also for the second Airy function, Bi($\zeta$). The analysis, similar to that carried out above (though naturally a bit bulkier),[28] gives a remarkably simple result:

Soft potential barrier: transparency

$$\mathcal{T}_{\rm WKB} \equiv \left|\frac{f}{a}\right|^2 = \exp\left\{-2\int_{x_{\rm c}}^{x_{\rm c}'} \kappa(x)dx\right\} \equiv \exp\left\{-\frac{2}{\hbar}\int_{x_{\rm c}}^{x_{\rm c}'} \left(2m[U(x)-E]\right)^{1/2} dx\right\}, \tag{2.117}$$

with the pre-exponential factor equal to 1 – the fact that might be readily expected from the mnemonic rule (i) of the connection formulas.

This formula is broadly used in applied quantum mechanics, despite the approximate character of its pre-exponential coefficient for insufficiently soft barriers that do not satisfy Eq. (107). For example, Eq. (80) shows that for a rectangular barrier with thickness $d >> \delta$, the WKB approximation (117) with $d_{\rm WKB} = d$ underestimates $\mathcal{T}$ by a factor of $[4k\kappa/(k^2 + \kappa^2)]^2$ – equal, for example, 4, if $k = \kappa$, i.e. if $U_0 = 2E$. However, on the appropriate logarithmic scale (see Fig. 7b), such a factor, smaller than an order of magnitude, is just a small correction.

Note also that when $E$ approaches the barrier's top $U_{\rm max}$ (Fig. 11), the points $x_{\rm c}$ and $x_{\rm c}'$ merge, so according to Eq. (117), $\mathcal{T}_{\rm WKB} \to 1$, i.e. the particle reflection vanishes at $E = U_{\rm max}$. So, the WKB approximation does not describe the effect of the over-barrier reflection at $E > U_{\rm max}$. (This fact could be noticed already from Eq. (95): in the absence of the classical turning points, the WKB probability current is constant for any barrier profile.) This conclusion is incorrect even for apparently smooth barriers where one could naively expect the WKB approximation to work perfectly. Indeed, near the point $x = x_{\rm m}$ where the potential reaches maximum (i.e. $U(x_{\rm m}) = U_{\rm max}$), we may approximate almost any smooth function $U(x)$ with the quadratic term of the Taylor expansion, i.e. with an inverted parabola:

$$U(x) \approx U_{\rm max} - \frac{m\omega_0^2 (x - x_{\rm m})^2}{2}. \tag{2.118}$$

Calculating the derivatives $dU/dx$ and $d^2U/dx^2$ for this function and plugging the results into the condition (107), we may see that the WKB approximation is only valid if $|U_{\rm max} - E| >> \hbar\omega_0$. Just for the

[28] For the most important case $\mathcal{T}_{\rm WKB} << 1$, Eq. (117) may be simply derived from Eqs. (105)-(106) – the exercise left for the reader.

reader's reference, an exact analysis of tunneling through the barrier (118) gives the following *Kemble formula*:[29]

$$\mathcal{T} = \frac{1}{1+\exp\{-2\pi(E-U_{\max})/\hbar\omega_0\}}, \tag{2.119}$$

Kemble formula

valid for any sign of the difference $(E - U_{max})$. This formula describes a gradual approach of $\mathcal{T}$ to 1, i.e. a *gradual* reduction of reflection, at the particle energy's increase, with $\mathcal{T} = ½$ at $E = U_{max}$.

To conclude this section, one last remark: the WKB approximation opens a straight way toward an alternative formulation of quantum mechanics, based on the *Feynman path integral*. However, I will postpone its discussion until a more compact notation has been introduced in Chapter 4.

## 2.5. Resonant tunneling, and metastable states

Now let us move to other, conceptually different quantum effects taking place in more elaborate potential profiles. Neither piecewise-constant nor smooth-potential models of $U(x)$ are convenient for their quantitative description because they both require "stitching" partial de Broglie waves at each classical turning point, which may lead to cumbersome calculations. However, we may get a very good insight into the physics of quantum effects that may take place in such profiles, while avoiding overcomplicated math, by approximating them with sets of Dirac's delta functions.

Big help in this way is provided by the notions of *scattering* and *transfer matrices*, very useful for other purposes as well. Let us consider an arbitrary but finite-length potential "bump" (formally called a *scatterer*), localized somewhere between points $x_1$ and $x_2$, on a flat potential background, say $U = 0$ (Fig. 12).

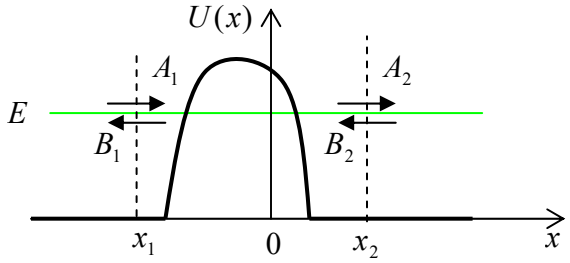


Fig. 2.12. De Broglie wave amplitudes near a single 1D scatterer.

From Sec. 2, we know that the general solutions of the stationary Schrödinger equation, with a certain energy $E$, in the regions outside the interval $[x_1, x_2]$, are sets of two sinusoidal waves, traveling in opposite directions. Let us represent them in the form

$$\psi_j = A_j e^{ik(x-x_j)} + B_j e^{-ik(x-x_j)}, \tag{2.120}$$

where the index $j$ equals either 1 or 2 (for now), and $(\hbar k)^2/2m = E$. Note that each of the two wave pairs (129) has, in this notation, its own reference point $x_j$, because this will be very convenient for what

[29] This formula was derived (in a more general form, valid for an arbitrary soft potential barrier) by E. Kemble in 1935. In some communities, it is known as the "Hill-Wheeler formula", after D. Hill and J. Wheeler's 1953 paper in that the Kemble formula was spelled out for the quadratic profile (118). Note that mathematically Eq. (119) is similar to the Fermi distribution in statistical physics, with an effective temperature $T_{ef} = \hbar\omega_0/2\pi k_B$. This coincidence has some curious implications for the Fermi particle tunneling statistics.

follows. As we have already discussed, if the de Broglie wave/particle is incident from the left (i.e. $B_2 = 0$), the solution of the *linear* Schrödinger equation within the scatterer range ($x_1 < x < x_2$) can provide only *linear* expressions of the transmitted ($A_2$) and reflected ($B_1$) wave amplitudes via the incident wave amplitude $A_1$:

$$A_2 = S_{21}A_1, \quad B_1 = S_{11}A_1, \tag{2.121}$$

where $S_{11}$ and $S_{21}$ are certain (generally, complex) coefficients. Alternatively, if a wave with amplitude $B_2$ is incident on the scatterer from the right (i.e. if $A_1 = 0$), it can induce a transmitted wave ($B_1$) and a reflected wave ($A_2$), with amplitudes

$$B_1 = S_{12}B_2, \quad A_2 = S_{22}B_2, \tag{2.122}$$

where the coefficients $S_{22}$ and $S_{12}$ are generally different from $S_{11}$ and $S_{21}$. Now we can use the linear superposition principle to argue that if the waves with amplitudes $A_1$ and $B_2$ are simultaneously incident on the scatterer (say, because the wave $B_2$ has been partly reflected back by some other scatterer located at $x > x_2$), the resulting *scattered wave* amplitudes $A_2$ and $B_1$ are just the sums of their values for separate incident waves:

$$\begin{aligned} B_1 &= S_{11}A_1 + S_{12}B_2, \\ A_2 &= S_{21}A_1 + S_{22}B_2. \end{aligned} \tag{2.123}$$

These two relations may be conveniently represented using the so-called *scattering matrix* S:

Scattering matrix: definition

$$\boxed{\begin{pmatrix} B_1 \\ A_2 \end{pmatrix} = \mathrm{S}\begin{pmatrix} A_1 \\ B_2 \end{pmatrix}, \qquad \text{with } \mathrm{S} \equiv \begin{pmatrix} S_{11} & S_{12} \\ S_{21} & S_{22} \end{pmatrix}.} \tag{2.124}$$

Scattering matrices, duly generalized, are an important tool for the analysis of wave scattering in higher dimensions than one; for 1D problems, however, another matrix is often more convenient to represent the same linear relations (123). Indeed, let us solve this system for $A_2$ and $B_2$. The result is

Transfer matrix: definition

$$\boxed{\begin{aligned} A_2 &= T_{11}A_1 + T_{12}B_1, \\ B_2 &= T_{21}A_1 + T_{22}B_1, \end{aligned} \quad \text{i.e.} \quad \begin{pmatrix} A_2 \\ B_2 \end{pmatrix} = \mathrm{T}\begin{pmatrix} A_1 \\ B_1 \end{pmatrix},} \tag{2.125}$$

where T is the *transfer matrix*, with the following elements:

$$T_{11} = S_{21} - \frac{S_{11}S_{22}}{S_{12}}, \quad T_{12} = \frac{S_{22}}{S_{12}}, \quad T_{21} = -\frac{S_{11}}{S_{21}}, \quad T_{22} = \frac{1}{S_{12}}. \tag{2.126}$$

The matrices S and T have some universal properties, valid for an arbitrary (but time-independent) scatterer; they may be readily found from the probability current conservation and the time-reversal symmetry of the Schrödinger equation. Let me leave finding these relations for the reader's exercise. The results show, in particular, that the scattering matrix may be rewritten in the following form:

$$\mathrm{S} = e^{i\theta}\begin{pmatrix} re^{i\varphi} & t \\ t & -re^{-i\varphi} \end{pmatrix}, \tag{2.127a}$$

where the four real parameters $r$, $t$, $\theta$, and $\varphi$ satisfy the following universal relation:

$$r^2 + t^2 = 1, \tag{2.127b}$$

so only three of these parameters are independent. As a result of this symmetry, $T_{11}$ may be also represented in a simpler form similar to $T_{22}$: $T_{11} = \exp\{i\theta\}/t = 1/S_{12}^{*} = 1/S_{21}^{*}$. The last form allows a ready expression of the scatterer's transparency via just one coefficient of the transfer matrix:

$$\mathscr{T} \equiv \left|\frac{A_2}{A_1}\right|^2_{B_2=0} = \left|S_{21}\right|^2 = \left|T_{11}\right|^{-2}. \tag{2.128}$$

In our current context, the most important property of the 1D transfer matrices is that to find the total transfer matrix T of a system consisting of several (say, $N$) sequential arbitrary scatterers (Fig. 13), it is sufficient to multiply their matrices.

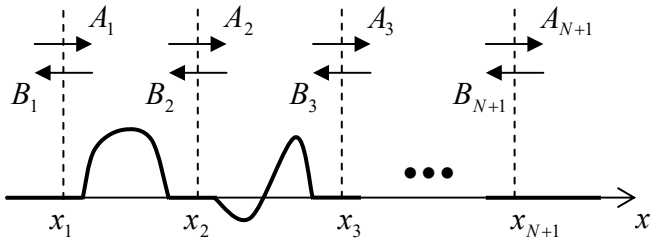


Fig. 2.13. A sequence of several 1D scatterers.

Indeed, extending the definition (125) to other points $x_j$ ($j = 1, 2, \ldots, N + 1$), we can write

$$\begin{pmatrix} A_2 \\ B_2 \end{pmatrix} = \mathrm{T}_1 \begin{pmatrix} A_1 \\ B_1 \end{pmatrix}, \qquad \begin{pmatrix} A_3 \\ B_3 \end{pmatrix} = \mathrm{T}_2 \begin{pmatrix} A_2 \\ B_2 \end{pmatrix} = \mathrm{T}_2\mathrm{T}_1 \begin{pmatrix} A_1 \\ B_1 \end{pmatrix}, \quad \text{etc.} \tag{2.129}$$

(where the matrix indices correspond to the scatterers' order on the $x$-axis), so

$$\begin{pmatrix} A_{N+1} \\ B_{N+1} \end{pmatrix} = \mathrm{T}_N \mathrm{T}_{N-1} \ldots \mathrm{T}_1 \begin{pmatrix} A_1 \\ B_1 \end{pmatrix}. \tag{2.130}$$

But we can also define a *total transfer matrix* similarly to Eq. (125), i.e. as

$$\begin{pmatrix} A_{N+1} \\ B_{N+1} \end{pmatrix} \equiv \mathrm{T} \begin{pmatrix} A_1 \\ B_1 \end{pmatrix}, \tag{2.131}$$

so comparing Eqs. (130) and (131) we get

$$\boxed{\mathrm{T} = \mathrm{T}_N \mathrm{T}_{N-1} \ldots \mathrm{T}_1 .} \tag{2.132}$$

Transfer matrix: composite scatterer

This formula is valid even if the flat-potential gaps between component scatterers are shrunk to zero, so it may be applied to a scatterer with an arbitrary profile $U(x)$, by fragmenting its length into many small segments $\Delta x = x_{j+1} - x_j$, and treating each fragment as a rectangular barrier of the average height $(U_j)_{\text{ef}} = [U(x_{j+1}) - U(x_j)]/2$ – see Fig. 14. Since very efficient numerical algorithms are readily available for fast multiplication of matrices (especially as small as 2×2 in our case), this approach is broadly used in practice for the computation of transparency of 1D potential barriers with complicated profiles $U(x)$. (This procedure is much more efficient than the direct numerical solution of the stationary Schrödinger equation.)

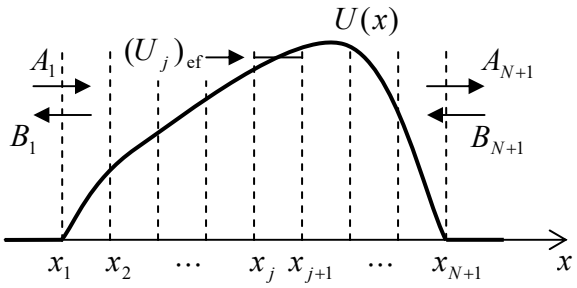


Fig. 2.14. The transfer matrix approach to a potential barrier with an arbitrary profile.

In order to apply this approach to several particular, conceptually important systems, let us calculate the transfer matrices for a few elementary scatterers, starting from the delta-functional barrier located at $x = 0$ – see Fig. 8. Taking $x_1, x_2 \to 0$, we can merely change the notation of the wave amplitudes in Eq. (78) to get

$$S_{11} = \frac{-i\alpha}{1+i\alpha}, \qquad S_{21} = \frac{1}{1+i\alpha}. \tag{2.133}$$

An absolutely similar analysis of the wave incidence from the left yields

$$S_{22} = \frac{-i\alpha}{1+i\alpha}, \qquad S_{12} = \frac{1}{1+i\alpha}, \tag{2.134}$$

and using Eqs. (126), we get

Transfer matrix: short scatterer

$$\boxed{\mathrm{T}_\alpha = \begin{pmatrix} 1-i\alpha & -i\alpha \\ i\alpha & 1+i\alpha \end{pmatrix}}. \tag{2.135}$$

As a sanity check, Eq. (128) applied to this result, immediately brings us back to Eq. (79).

The next example may seem strange at first glance: what if there is no scatterer at all between points $x_1$ and $x_2$? If the points coincide, the answer is indeed trivial and can be obtained, e.g., from Eq. (135) by taking $\alpha = 0$, i.e. $\alpha = 0$:

Identity transfer matrix

$$\boxed{\mathrm{T}_0 = \begin{pmatrix} 1 & 0 \\ 0 & 1 \end{pmatrix} \equiv \mathrm{I}} \tag{2.136}$$

– the so-called *identity matrix*. However, we are free to choose the reference points $x_{1,2}$ participating in Eq. (120) as we wish. For example, what if $x_2 - x_1 = a$? Let us first take the forward-propagating wave alone: $B_2 = 0$ (and hence $B_1 = 0$); then

$$\psi_2 = \psi_1 = A_1 e^{ik(x-x_1)} \equiv A_1 e^{ik(x_2-x_1)} e^{ik(x-x_2)}. \tag{2.137}$$

The comparison of this expression with the definition (120) for $j = 2$ shows that $A_2 = A_1 \exp\{ik(x_2 - x_1)\} = A_1 \exp\{ika\}$, i.e. $T_{11} = \exp\{ika\}$. Repeating the calculation for the back-propagating wave, we see that $T_{22} = \exp\{-ika\}$, and since the space interval provides no particle reflection, we finally get

Transfer matrix: spatial interval

$$\boxed{\mathrm{T}_a = \begin{pmatrix} e^{ika} & 0 \\ 0 & e^{-ika} \end{pmatrix}}, \tag{2.138}$$

independently of a common shift of points $x_1$ and $x_2$. At $a = 0$, we naturally recover the special case (136).

Now let us use these simple results to analyze the *double-barrier system* shown in Fig. 15. We could of course calculate its properties as before, writing down explicit expressions for all five traveling waves symbolized by arrows in Fig. 15, then using the boundary conditions (124) and (125) at each of the points $x_{1,2}$ to get a system of four linear equations, and finally, solving it for four amplitude ratios.

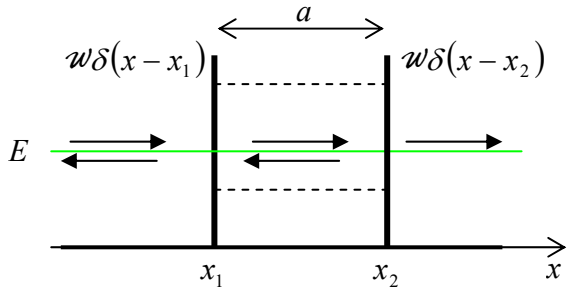


Fig. 2.15. The double-barrier system. The dashed lines show (schematically) the quasi-levels of the metastable-state energies.

However, the transfer matrix approach simplifies the calculations, because we may immediately use Eqs. (132), (135), and (138) to write

$$\mathrm{T} = \mathrm{T}_\alpha \mathrm{T}_a \mathrm{T}_\alpha = \begin{pmatrix} 1-i\alpha & -i\alpha \\ i\alpha & 1+i\alpha \end{pmatrix} \begin{pmatrix} e^{ika} & 0 \\ 0 & e^{-ika} \end{pmatrix} \begin{pmatrix} 1-i\alpha & -i\alpha \\ i\alpha & 1+i\alpha \end{pmatrix}. \tag{2.139}$$

Let me hope that the reader remembers the "row by column" rule of the multiplication of square matrices;[30] using it for the last two matrices, we may reduce Eq. (139) to

$$\mathrm{T} = \begin{pmatrix} 1-i\alpha & -i\alpha \\ i\alpha & 1+i\alpha \end{pmatrix} \begin{pmatrix} (1-i\alpha)e^{ika} & -i\alpha e^{ika} \\ i\alpha e^{-ika} & (1+i\alpha)e^{-ika} \end{pmatrix}. \tag{2.140}$$

Now there is no need to calculate all elements of the full product T, because, according to Eq. (128), for the calculation of the barrier's transparency $T$ we need only one of its elements, $T_{11}$:

$$\mathscr{T} = \frac{1}{|T_{11}|^2} = \frac{1}{\left|\alpha^2 e^{-ika} + (1-i\alpha)^2 e^{ika}\right|^2}. \tag{2.141}$$

Double barrier: transparency

This result describes oscillations of the transparency: at a fixed parameter $\alpha$, $\mathscr{T}$ is a $\pi$-periodic function of the product $ka$, reaching its maximum ($\mathscr{T} = 1$) at some point of each period – see Fig. 16a. Indeed, the denominator in Eq. (141) may be interpreted as the squared length of the difference between two 2D vectors, one of length $\alpha^2$ and another of length $|(1 - i\alpha)^2| = 1 + \alpha^2$, with the angle $\theta = 2ka +$ const between them – see Fig. 16b. At the resonance, the vectors are aligned, and their difference is smallest (equal to 1) so $\mathscr{T}_{\max} = 1$. (This result is exact only if the two barriers are exactly equal.) This means that, rather counter-intuitively, the maximum transparency of the system is *perfect* even at $\alpha >> 1$, i.e. in the case of a very low transparency of each of the component barriers. This is the famous *resonant tunneling* effect.[31]

[30] In the analytical form: $(\mathrm{AB})_{jj'} = \sum_{j''=1}^{N} A_{jj''} B_{j''j'}$, where $N$ is the square matrix rank (in our current case, $N = 2$).

[31] In older literature, it is sometimes called the *Townsend* (or "Ramsauer-Townsend") *effect*. However, nowadays it is more common to use the last term only for a similar effect at 3D scattering – to be discussed in Chapter 3.

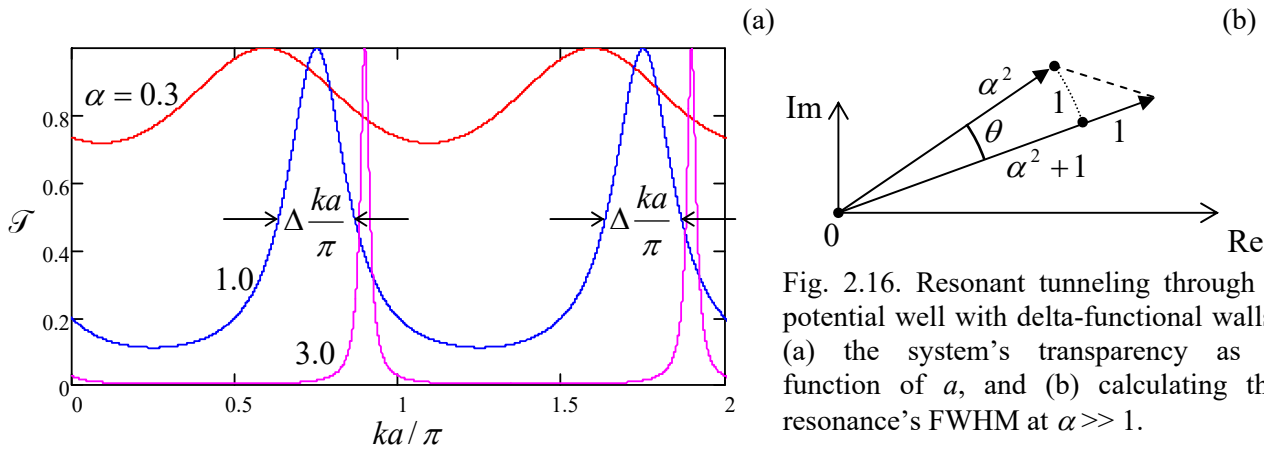


Fig. 2.16. Resonant tunneling through a potential well with delta-functional walls: (a) the system's transparency as a function of $a$, and (b) calculating the resonance's FWHM at $\alpha >> 1$.

Its physics is the *constructive interference* of de Broglie waves, similar to that of electromagnetic waves (for example, light) in a *Fabry-Perot resonator* formed by two parallel semi-transparent mirrors.[32] Namely, the incident de Broglie wave may be thought to undertake, on its way through the system, several sequential reflections from these semi-transparent walls. At $k = k_n$, i.e. at $2ka = 2k_n a = 2\pi n$, the phase differences between all these partial waves are multiples of $2\pi$, so they add up in phase – "constructively". (At large but finite $\alpha$, the resonance centers slightly deviate from the points $ka = \pi n$.) Note that the same constructive interference of numerous reflections from the walls may be used to interpret the standing-wave eigenfunctions (1.84), so the resonant tunneling at $\alpha >> 1$ in our current system may be also considered a result of the resonant induction of such a standing wave, with a very large amplitude, in the space between the barriers, with the transmitted wave's amplitude proportionately increased.

The resonance peaks of the transparency may be very narrow. Their so-called FWHM (the common acronym for the *Full Width at Half-Maximum*), for the most interesting case for $\alpha >> 1$, may readily calculated by using the same vector diagram shown in Fig. 16b. By definition, FWHM is the difference $\Delta k = k_+ - k_-$ between such two values of $k$, on the opposite slopes of the same resonance curve, at that $\mathscr{T} = \mathscr{T}_{max}/2$ – see the arrows in Fig. 16a.[33] Let the two vectors in Fig. 16b be misaligned by a small angle $\theta << 1$, so the length of the difference vector is much smaller than $\alpha^2$. To double its length squared, and hence to reduce $\mathscr{T}$ by a factor of two in comparison with its maximum value of 1, the arc between the vectors, equal to $|\alpha^2\theta|$, should also become equal to 1, i.e. $\alpha^2(2k_\pm a + \text{const})$ to become equal to $\pm 1$. Subtracting these two equalities from each other, we get

$$\Delta k \equiv k_+ - k_- = \frac{1}{a\alpha^2} << k_\pm . \qquad (2.142)$$

Now let us use the simple system shown in Fig. 15 to discuss an issue of large conceptual significance. For that, consider what would happen if at some initial moment (say, $t = 0$) we placed a 1D quantum particle inside the double-barrier well with $\alpha >> 1$, and left it there alone, without any incident wave. To simplify the analysis, let us assume that the initial state of the particle coincides with one of the stationary states of the infinite-wall well of the same size – see Eq. (1.84):

[32] See, e.g., EM Sec. 7.9. Note also that as Eqs. (2.71) and Fig. 7 show, similar resonant tunneling takes place on the top of the rectangular barrier of height $U_0 < E$, thanks to the step-down reflection from its borders.

[33] Per Eq. (78), $\alpha$ depends on $k$ but near a narrow resonance with $\Delta k << k_\pm$, that dependence is negligible.

$$\Psi(x,0)=\psi_n(x)=\left(\frac{2}{a}\right)^{1/2}\sin\left[k_n(x-x_1)\right],\qquad \text{where } k_n=\frac{\pi n}{a},\quad n=1,2,\ldots. \tag{2.143}$$

At $\alpha\to\infty$, this is just an eigenstate of the system, and from our analysis in Sec. 1.5 we know the time evolution of its wavefunction:

$$\Psi(x,t)=\psi_n(x)\exp\{-i\omega_n t\}=\left(\frac{2}{a}\right)^{1/2}\sin\left[k_n(x-x_1)\right]\exp\{-i\omega_n t\},\qquad \text{with } \omega_n=\frac{E_n}{\hbar}=\frac{\hbar k_n^2}{2m}, \tag{2.144}$$

telling us that the particle remains in the well at all times with a constant probability: $W(t) = W(0) = 1$.

However, if the parameter $\alpha$ is large but finite, the de Broglie wave would slowly "leak out" from the well, so $W(t)$ would slowly decrease. Such a state is called *metastable*. Let us derive the law of its time evolution, assuming that at the slow leakage, with a characteristic time $\tau >> 1/\omega_n$, does not affect the instant wave distribution inside the well, besides the gradual, slow reduction of $W$.[34] Then we can generalize Eq. (144) as

$$\Psi(x,t)=\left(\frac{2W}{a}\right)^{1/2}\sin\left[k_n(x-x_1)\right]\exp\{-i\omega_n t\}\equiv A\exp\{i(k_n x-\omega_n t)\}+B\exp\{-i(k_n x+\omega_n t)\}, \tag{2.145}$$

making the probability of finding the particle in the well equal to some $W \le 1$. As the last form of Eq. (145) shows, this is the sum of two traveling waves, with equal magnitudes of their amplitudes and hence equal but opposite probability currents (5):

$$|A|=|B|=\left(\frac{W}{2a}\right)^{1/2},\qquad I_A=\frac{\hbar}{m}|A|^2k_n=\frac{\hbar}{m}\frac{W}{2a}\frac{\pi n}{a},\qquad I_B=-I_A. \tag{2.146}$$

But we already know from Eq. (79) that at $\alpha >> 1$, the delta-functional wall's transparency $\mathscr{T}$ equals $1/\alpha^2$, so the wave carrying the current $I_A$, incident on the right wall from the inside, induces an outcoming wave outside of the well (Fig. 17) with the following probability current:

$$I_{\rm R}=\mathscr{T}I_A=\frac{1}{\alpha^2}I_A=\frac{1}{\alpha^2}\frac{\pi n\hbar W}{2ma^2}. \tag{2.147}$$

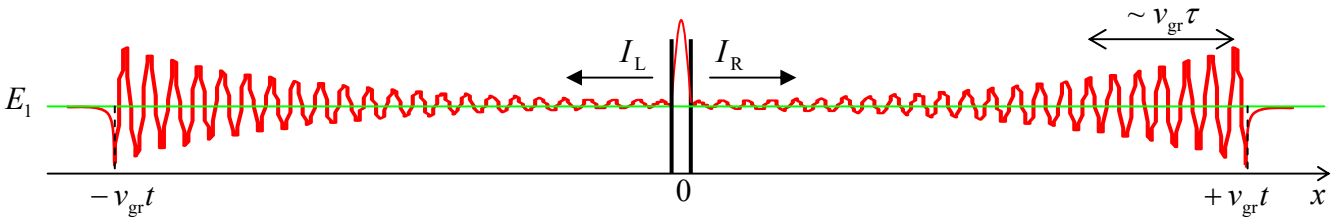


Fig. 2.17. A schematic snapshot of the wavefunction (say, $\mathrm{Re}\,\psi$) in the simple model shown in Fig. 15, at time $t > \tau >> 1/\omega_1$ after the particle's placement into the lowest metastable state with energy $E_1$.

Absolutely similarly,

$$I_{\rm L}=\frac{1}{\alpha^2}I_B=-I_{\rm R}. \tag{2.148}$$

[34] This (virtually evident) assumption finds its formal justification in the perturbation theory to be discussed in Chapter 6.

Now we may combine the 1D version (6) of the probability conservation law for the well's interior:

$$\frac{dW}{dt} + I_R - I_L = 0, \tag{2.149}$$

with Eqs. (147)-(148) to write

$$\frac{dW}{dt} = -\frac{1}{\alpha^2}\frac{\pi n\hbar}{ma^2}W. \tag{2.150}$$

This is just the standard differential equation,

Metastable state: decay law

$$\boxed{\frac{dW}{dt} = -\frac{1}{\tau}W}, \tag{2.151}$$

of an exponential decay, $W(t) = W(0)\exp\{-t/\tau\}$, where the constant $\tau$ is called the *metastable state's lifetime*. In our particular case,

$$\tau = \frac{ma^2}{\pi n\hbar}\alpha^2, \tag{2.152}$$

. Using Eq. (2.33b) for the de Broglie waves' group velocity, for our particular wave vector giving $v_{gr} = \hbar k_n/m = \pi n\hbar/ma$, Eq. (152) may be rewritten in a more general form,

Metastable state: lifetime

$$\boxed{\tau = \frac{t_a}{\mathscr{T}}}, \tag{2.153}$$

where the *attempt time* $t_a$ is equal to $a/v_{gr}$, and (in our particular case) $\mathscr{T} = 1/\alpha^2$. Eq. (153) is valid for a broad class of similar metastable systems;[35] it may be interpreted in the following semi-classical way. The particle travels back and forth between the confining potential barriers, with the time interval $t_a$ between the sequential moments of incidence, each time attempting to leak through the wall, with the success probability equal to $\mathscr{T}$, so the reduction of $W$ per each incidence is $\Delta W = -W\mathscr{T}$. In the limit $\mathscr{T} << 1$, this equality immediately leads to the decay equation (151) with the lifetime (153).

Another useful look at Eq. (152) may be taken by returning to the resonant tunneling problem in the same system, and expressing the resonance width (142) in terms of the incident particle's energy:

$$\Delta E = \Delta\left(\frac{\hbar^2k^2}{2m}\right) \approx \frac{\hbar^2k_n}{m}\Delta k = \frac{\hbar^2k_n}{m}\frac{1}{a\alpha^2} = \frac{\pi n\hbar^2}{ma^2\alpha^2}. \tag{2.154}$$

Comparing Eqs. (152) and (154), we get a remarkably simple, parameter-independent formula[36]

Energy-time uncertainty relation

$$\boxed{\Delta E\cdot\tau = \hbar}. \tag{2.155}$$

---

[35] Essentially the only requirement for the attempt time $t_a$ is to be much longer than the effective time (the so-called *instanton time*, see Sec. 5.3 below) of tunneling through the barrier. In the delta-functional approximation for the barrier, the latter time vanishes, so that this requirement is always fulfilled.

[36] Note that Eq. (2.151) may be formally obtained from the basic Schrödinger equation (1.61) by adding an imaginary part, equal to $(-\Delta E/2)$, to its eigenenergy $E_n$. Indeed, in this case Eq. (1.62) becomes $a_n(t) = \text{const}\times\exp\{-i(E_n - i\Delta E/2\}t/\hbar\} \equiv \text{const}\times\exp\{-iE_nt/\hbar\}\times\exp\{-\Delta Et/2\hbar\} = \text{const}\times\exp\{-iE_nt/\hbar\}\times\exp\{-t/2\tau\}$, so that $W(t) \propto |a_n(t)|^2 \propto \exp\{-t/\tau\}$. Such formalism, which hides the physical origin of the state's decay, may be convenient for some calculations, but misleading in other cases, and I will not use it in this course.

This *energy-time uncertainty relation* is certainly *more* general than our simple model; for example, it is valid for the lifetime and resonance tunneling width of any metastable state in the potential profile of any shape. This seems very natural since because of the energy identification with frequency, $E = \hbar\omega$, pertinent to quantum mechanics, Eq. (155) may be rewritten as $\Delta\omega\cdot\tau = 1$ and seems to follow directly from the Fourier transform in time, just as the Heisenberg's uncertainty relation (1.35) follows from the Fourier transform in space. In some cases, even those not involving any state decay, these two relations are indeed interchangeable. For example, Eq. (24) for the Gaussian wave packet width may be rewritten as $\delta E\cdot\Delta t = \hbar$, where $\delta E = \hbar(d\omega/dk)\delta k = \hbar v_{gr}\delta k$ is the r.m.s. spread of energies of monochromatic components of the packet, while $\Delta t \equiv \delta x/v_{gr}$ is the time scale of the packet's passage through a fixed observation point $x$.

However, Eq. (155) is much *less* general than Heisenberg's uncertainty relation (1.35). Indeed, the Cartesian coordinates of a particle, the Cartesian components of its momentum, and the energy $E$ are regular observables, represented by operators. In contrast, in the non-relativistic quantum mechanics we are studying now, time is treated as a $c$-number argument, and is *not* represented by an operator, so Eq. (155) cannot be derived in such general assumptions as Eq. (1.35). Thus the time-energy uncertainty relation should be used with caution. Unfortunately, not everybody is so careful. One can find, for example, claims that due to this relation, that the energy dissipated by any system performing an elementary (single-bit) calculation during a time interval $\Delta t$ has to be larger than $\hbar/\Delta t$.[37]

Now that we have a quantitative mathematical description of the metastable state's decay (valid, again, only at $\alpha >> 1$, i.e. at $\tau >> t_a$), we may use it to discuss two important conceptual issues of quantum mechanics. First, the decay is one of the simplest examples of systems that may be considered, from two different points of view, as either Hamiltonian (and hence *time-reversible*), or open (and hence *irreversible*). Indeed, from the former point of view, our particular system is certainly described by a time-independent Hamiltonian (1.41), with the potential energy

$$U(x) = \mathcal{W}\left[\delta(x - x_1) + \delta(x - x_2)\right] \tag{2.156}$$

– see Fig. 15 again. In this point of view, the total probability of finding the particle *somewhere* on the $x$-axis remains equal to 1, and the full system's energy, calculated from Eq. (1.23),

$$\langle E\rangle = \int_{-\infty}^{+\infty} \Psi^*(x,t)\hat{H}\,\Psi(x,t)d^3x\,, \tag{2.157}$$

remains constant. On the other hand, since the "emitted" wave packets would never return to the potential well,[38] it makes much sense to look at the well's region alone. For such a truncated, *open* system (for which the space beyond the interval $[x_1, x_2]$ serves as its *environment*), the probability $W$ of finding the particle inside this interval, and hence its energy $\langle E\rangle = WE_n$, decay exponentially per Eq.

[37] Here I dare to refer to my own old work K. Likharev, *Int. J. Theor. Phys*. **21**, 311 (1982), which provided a constructive proof (for a particular system) that at *reversible computations*, whose idea had been put forward in 1973 by C. Bennett (see, e.g., SM Sec. 2.3), energy dissipation may be lower than this apparent "quantum limit".

[38] For more realistic 2D and 3D systems, this statement is true even if the system as a whole is confined inside some closed volume, much larger than the potential well housing the metastable states. Indeed, if the walls providing such confinement are even slightly uneven, the emitted plane-wave packets will be reflected from them, but would never return to the well intact. (See SM Sec. 2.1 for a more detailed discussion of this issue.)

(151) – the decay equation typical for irreversible systems. We will return to the discussion of the dynamics of such open quantum systems in Chapter 7.

Second, the same model enables a preliminary discussion of one important aspect of quantum measurements. As Eq. (151) and Fig. 17 show, at $t >> \tau$, the well becomes virtually empty ($W \approx 0$), and the whole probability is localized in two clearly separated wave packets with equal amplitudes, moving from each other with speed $v_{gr}$, each "carrying the particle away" with a probability of 50%. Now assume that an experiment has detected the particle on the left side of the well. Though the formalisms suitable for quantitative analysis of the detection process will not be discussed until Chapter 7, due to the wide separation $\Delta x = 2v_{gr}t >> 2v_{gr}\tau$ of the packets, we may safely assume that such detection may be done without any actual physical effect on the counterpart wave packet.[39] But if we know that the particle has been found on the left side, there is no chance of finding it on the right side. If we attributed the full wavefunction to all stages of this particular experiment, this situation might be rather confusing. Indeed, that would mean that the wavefunction at the right packet's location should instantly turn into zero – the so-called *wave packet reduction* (or "collapse") – a hypothetical irreversible process that cannot be described by the Schrödinger equation for this system, even including the particle detectors.

However, if (as was already discussed in Sec. 1.3) we attribute the wavefunction to a certain statistical ensemble of similar experiments, there is no need to involve such artificial notions. The two-wave-packet picture we have calculated (Fig. 17) describes the full ensemble of experiments with all systems prepared in the initial state (143), i.e. does not depend on the particle detection results. On the other hand, the "reduced packet" picture (with no wave packet on the right of the well) describes only a sub-ensemble of such experiments, in which the particles have been detected on the left side. As was discussed in classical examples in Sec. 1.3, for such a redefined ensemble, the probability distribution may be rather different. So, the "wave packet reduction" is just a result of a purely accounting decision of the observer.[40] I will return to this important issue in Sec. 10.1 – on the basis of the forthcoming discussion of open systems in Chapters 7 and 8.

## 2.6. Localized state coupling, and quantum oscillations

Now let us discuss one more effect specific to quantum mechanics. Its mathematical description may be simplified using a model potential consisting of two very short and deep potential wells. For that, let us first analyze the properties of a single well of this type (Fig. 18), which may be modeled similarly to the short and high potential barrier – see Eq. (74), but with a negative "weight":

$$U(x) = -\mathcal{W}\delta(x), \qquad \text{with } \mathcal{W} > 0. \tag{2.158}$$

In contrast to its tunnel-barrier counterpart (74), such potential sustains a stationary state with a negative eigenenergy $E < 0$, and a *localized* eigenfunction $\psi$, with $|\psi| \to 0$ at $x \to \pm\infty$.

[39] This argument is especially convincing if the particle's detection time is much shorter than the time $t_c = 2v_{gr}t/c$, where $c$ is the speed of light in vacuum, i.e. the maximum velocity of any information transfer.

[40] "The collapse of the wavefunction after measurement represents nothing more than the updating of that scientist's expectations." N. D. Mermin, *Phys. Today*, **72**, 53 (Jan. 2013).

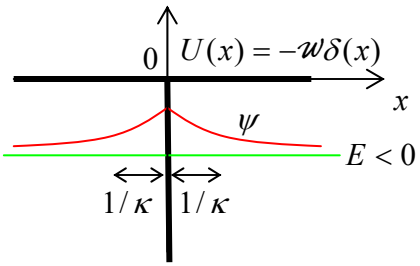


Fig. 2.18. Delta-functional potential well and its localized eigenstate (schematically).

Indeed, at $x \neq 0$, $U(x) = 0$, so the 1D Schrödinger equation is reduced to the Helmholtz equation (1.83), whose localized solutions with $E < 0$ are single exponents vanishing at large distances:[41]

$$\psi(x) = \psi_0(x) \equiv \begin{cases} Ae^{-\kappa x}, & \text{for } x > 0, \\ Ae^{+\kappa x}, & \text{for } x < 0, \end{cases} \qquad \text{with } \frac{\hbar^2\kappa^2}{2m} = -E, \quad \kappa > 0. \tag{2.159}$$

Here the pre-exponential coefficients are taken equal to satisfy the boundary condition (76) of the wavefunction's continuity at $x = 0$. Plugging Eq. (159) into the second boundary condition, given by Eq. (75) but now with the negative sign before $\mathcal{W}$, we get

$$(-\kappa A) - (+\kappa A) = -\frac{2m\mathcal{W}}{\hbar^2} A, \tag{2.160}$$

in which the common factor $A \neq 0$ may be canceled. This equation[42] has one solution for any $\mathcal{W} > 0$:

$$\kappa = \kappa_0 \equiv \frac{m\mathcal{W}}{\hbar^2}, \tag{2.161}$$

and hence the system has only one localized state, with the following eigenenergy:[43]

$$E = E_0 \equiv -\frac{\hbar^2\kappa_0^2}{2m} = -\frac{m\mathcal{W}^2}{2\hbar^2}. \tag{2.162}$$

Now we are ready to analyze the localized states of the two-well potential shown in Fig. 19:

$$U(x) = -\mathcal{W}\left[\delta\left(x - \frac{a}{2}\right) + \delta\left(x + \frac{a}{2}\right)\right], \qquad \text{with } \mathcal{W} > 0. \tag{2.163}$$

Here we may still use the single-exponent solutions similar to Eq. (159), for the wavefunction outside the interval $[-a/2, +a/2]$, but inside the interval, we need to take into account both possible exponents:

$$\psi = C_+ e^{\kappa x} + C_- e^{-\kappa x} \equiv C_A \sinh \kappa x + C_S \cosh \kappa x, \qquad \text{for } -\frac{a}{2} \le x \le +\frac{a}{2}, \tag{2.164}$$

with the parameter $\kappa$ defined as in Eq. (159). The latter of these two equivalent expressions is more convenient because due to the symmetry of the potential (163) with respect to the central point $x = 0$, the system's eigenfunctions should be either symmetric (even) or antisymmetric (odd) functions of $x$ (see

[41] See Eqs. (56)-(58), with $U_0 = 0$.

[42] Such algebraic equations are frequently called *characteristic*.

[43] Note that this $E_0$ is equal, by magnitude, to the constant $E_0$ that participates in Eq. (79). Note also that this result was actually already obtained, "backward", in the solution of Problem 1.12(ii), but that solution did not address the issue of whether the calculated potential (158) could sustain any other localized eigenstates.

Fig. 19), so they may be analyzed separately, only for one half of the system, say $x \geq 0$, and using just one of the hyperbolic functions (164) in each case.

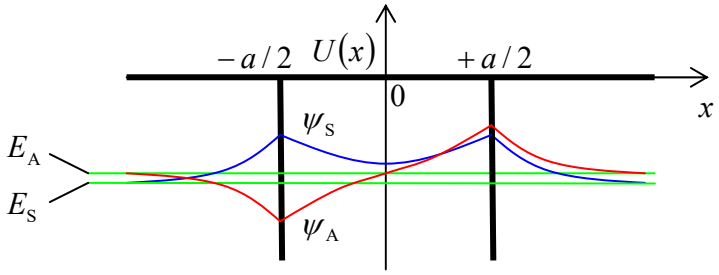


Fig. 2.19. A system of two coupled potential wells, and its localized eigenstates (schematically).

For the *antisymmetric* eigenfunction, Eqs. (159) and (164) yield

$$\psi_A \equiv C_A \times \begin{cases} \sinh \kappa x, & \text{for } 0 \leq x \leq \dfrac{a}{2}, \\ \sinh \dfrac{\kappa a}{2} \exp\left\{-\kappa\left(x - \dfrac{a}{2}\right)\right\}, & \text{for } \dfrac{a}{2} \leq x, \end{cases} \tag{2.165}$$

where the front coefficient in the lower line is adjusted to satisfy the condition (76) of the wavefunction's continuity at $x = +a/2$ – and hence at $x = -a/2$. What remains is to satisfy the condition (75), with a negative sign before $\mathcal{W}$, for the derivative's jump at that point. This condition yields the following characteristic equation:

$$\sinh \frac{\kappa a}{2} + \cosh \frac{\kappa a}{2} = \frac{2m\mathcal{W}}{\hbar^2 \kappa} \sinh \frac{\kappa a}{2}, \qquad \text{i.e. } 1 + \coth \frac{\kappa a}{2} = 2 \frac{(\kappa_0 a)}{(\kappa a)}, \tag{2.166}$$

where the $\kappa_0$, given by Eq. (161), is the value of $\kappa$ for a single well, i.e. the reciprocal spatial width of its localized eigenfunction – see Fig. 18.

Figure 20a shows both sides of Eq. (166) as functions of the dimensionless product $\kappa a$, for several values of the parameter $\kappa_0 a$, i.e. of the normalized distance between the two wells. The plots show, first of all, that as the parameter $\kappa_0 a$ is decreased, the left-hand side and right-hand side plots cross (i.e. Eq. (166) has a solution) at lower and lower values of $\kappa a$. At $\kappa a << 1$, the left-hand side of the last form of this equation may be approximated as $2/\kappa a$. Comparing this expression with the right-hand side, we see that this transcendental characteristic equation has a solution (i.e. the system has an antisymmetric localized state) only if $\kappa_0 a > 1$, i.e. if the distance $a$ between the two narrow potential wells is larger than the following value,

$$a_{\min} = \frac{1}{\kappa_0} \equiv \frac{\hbar^2}{m\mathcal{W}}, \tag{2.167}$$

which is equal to the characteristic spread of the wavefunction in a single well – see Fig. 18. (At $a \to a_{\min}$, $\kappa a \to 0$, meaning that the state's localization becomes weaker and weaker.)

In the opposite limit of large distances between the potential wells, i.e. $\kappa_0 a >> 1$, Eq. (166) shows that $\kappa a >> 1$ as well, so its left-hand side may be approximated as $2(1 + \exp\{-\kappa a\})$, and the equation yields

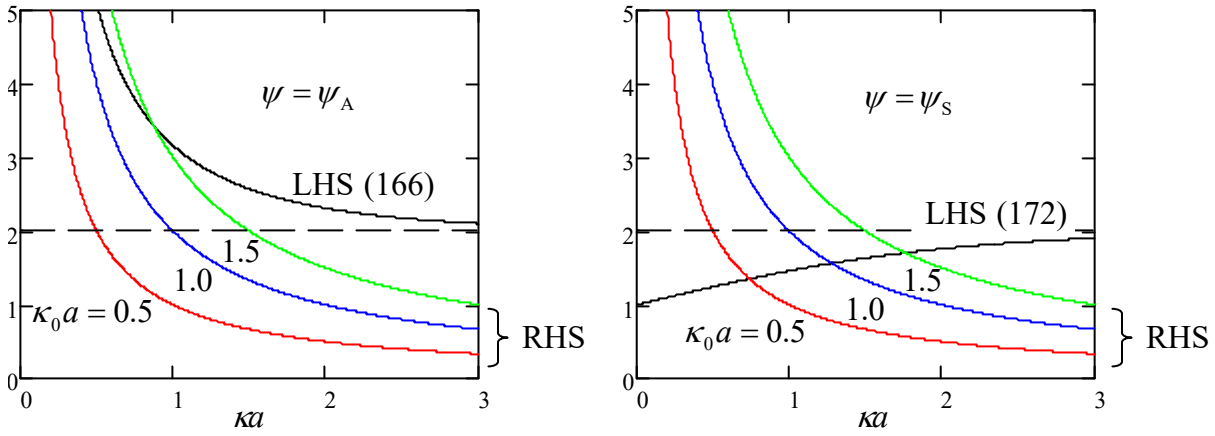


Fig. 2.20. Graphical solutions of the characteristic equations of the two-well system, for: (a) the antisymmetric eigenstate (165), and (b) the symmetric eigenstate (171).

$$\kappa \approx \kappa_0 \left(1 - \exp\{-\kappa_0 a\}\right) \approx \kappa_0 \ . \tag{2.168}$$

This result means that the eigenfunction is an antisymmetric superposition of two virtually unperturbed wavefunctions (159) of each partial potential well:

$$\psi_A(x) \approx \frac{1}{\sqrt{2}}\left[\psi_R(x) - \psi_L(x)\right], \qquad \text{with } \psi_R(x) \equiv \psi_0\left(x - \frac{a}{2}\right), \quad \psi_L(x) \equiv \psi_0\left(x + \frac{a}{2}\right), \tag{2.169}$$

where the front coefficient is selected in such a way that if the eigenfunction $\psi_0$ of each well is normalized, so is $\psi_A$. Plugging the middle (more exact) form of Eq. (168) into the last of Eqs. (159), we can see that in this limit the antisymmetric state's energy is slightly higher than the eigenenergy $E_0$ of a single well, given by Eq. (162):

$$E_A \approx E_0\left(1 - 2\exp\{-\kappa_0 a\}\right) \equiv E_0 + \delta, \qquad \text{where } \delta \equiv \frac{2m\mathcal{W}^2}{\hbar^2}\exp\{-\kappa_0 a\} > 0\,. \tag{2.170}$$

The s*ymmetric* eigenfunction has a form similar to Eq. (165), but is still different from it:

$$\psi = \psi_S \equiv C_S \times \begin{cases} \cosh \kappa x, & \text{for } 0 \le x \le \dfrac{a}{2}, \\ \cosh\dfrac{\kappa a}{2}\exp\left\{-\kappa\left(x - \dfrac{a}{2}\right)\right\}, & \text{for } \dfrac{a}{2} \le x, \end{cases} \tag{2.171}$$

giving a characteristic equation similar in structure to Eq. (166), but with a different left-hand side:

$$1 + \tanh\frac{\kappa a}{2} = 2\frac{(\kappa_0 a)}{(\kappa a)}\,. \tag{2.172}$$

Figure 20b shows both sides of this equation for several values of the parameter $\kappa_0 a$. It is evident that in contrast to Eq. (166), Eq. (172) has a unique solution (and hence the system has a localized symmetric eigenstate) for *any* value of the parameter $\kappa_0 a$, i.e. for any distance between the partial wells. In the limit of very close wells (i.e. their strong coupling), $\kappa_0 a << 1$, we get $\kappa a << 1$, $\tanh(\kappa a/2) \to 0$, and Eq. (172) yields $\kappa \to 2\kappa_0$, leading to a four-fold increase of the eigenenergy's magnitude in comparison with that of the single well:

$$E_S \approx 4E_0 \equiv -\frac{m(2\mathcal{W})^2}{2\hbar^2}, \qquad \text{for } \kappa_0 a << 1. \tag{2.173}$$

The physical meaning of this result is very simple: two very close potential wells act (on the symmetric eigenfunction only!) together, so their "weights" $\mathcal{W} \equiv \int U(x)dx$ just add up.

In the opposite, weak coupling limit, i.e. for $\kappa_0 a >> 1$, Eq. (172) shows that $\kappa a >> 1$ as well, so its left-hand side may be approximated as $2(1 - \exp\{-\kappa a\})$, and the equation yields

$$\kappa \approx \kappa_0 \left(1 + \exp\{-\kappa_0 a\}\right) \approx \kappa_0 . \tag{2.174}$$

In this limit, the eigenfunction is a symmetric superposition of two virtually unperturbed wavefunctions (159) of each partial potential well:

$$\psi_S(x) \approx \frac{1}{\sqrt{2}}\left[\psi_R(x) + \psi_L(x)\right], \tag{2.175}$$

and the eigenenergy is also close to the energy $E_0$ of each partial well, but is slightly lower than it:

$$E_S \approx E_0\left(1 + 2\exp\{-\kappa_0 a\}\right) \equiv E_0 - \delta, \qquad \text{so that } E_A - E_S = 2\delta , \tag{2.176}$$

where $\delta$ is again given by the last of Eqs. (170).

So, the eigenenergy of the symmetric state is always lower than that of the antisymmetric state. The physics of this effect (which remains qualitatively the same in more complex two-component systems, most importantly in diatomic molecules such as $H_2$) is evident from the sketch of the wavefunctions $\psi_A$ and $\psi_S$, given by Eqs. (165) and (171), in Fig. 19. In the antisymmetric mode, the wavefunction has to vanish at the center of the system, so each its half is squeezed into one half of the system's spatial extension. Such a squeeze increases the function's gradient, and hence its kinetic energy (1.27), and hence its total energy. On the contrary, in the symmetric mode, the wavefunction effectively spreads into the counterpart well. As a result, it changes in space slower, and hence its kinetic energy is also lower.

Even more importantly, the symmetric state's energy level goes down as the distance $a$ is decreased, corresponding to the effective attraction of the partial wells. This is a good toy model of the strongest (and most important) type of atomic cohesion – the *covalent* (or "chemical") *bonding*.[44] In the simplest case of the $H_2$ molecule, each of two electrons of the system, in its ground state,[45] reduces its kinetic energy by spreading its wavefunction around both hydrogen nuclei (protons), rather than being confined near one of them – as it had to be in a single atom. The resulting bonding is very strong: in chemical units, it is close to 430 kJ/mol, i.e. to 4.5 eV per molecule. Perhaps counter-intuitively, this quantum-mechanical bonding may be even stronger than the strongest classical (*ionic*) bonding due to electron transfer between atoms, leading to the Coulomb attraction of the resulting ions. (For example, the atomic cohesion in the NaCl molecule is 4.25 eV.)

[44] Historically, the development of the quantum theory of such bonding in the $H_2$ molecule (by Walter Heinrich Heitler and Fritz Wolfgang London in 1927) was the breakthrough decisive for the acceptance of the then-emerging quantum mechanics by the community of chemists.

[45] Due to the opposite spins of these electrons, the Pauli principle allows them to be in the same orbital ground state – see Chapter 8.

Now let us analyze the dynamic properties of our model system (Fig. 19) carefully because such a pair of weakly coupled potential wells is our first example of the very important class of *two-level systems*.[46] It is easiest to do in the weak-coupling limit $\kappa_0 a >> 1$, when the simple results (168)-(170) and (174)-(176) are quantitatively valid. In particular, Eqs. (169) and (175) enable us to represent the quasi-localized states of the particle in each partial well as linear combinations of its two eigenstates:

$$\psi_R(x) = \frac{1}{\sqrt{2}}[\psi_S(x) + \psi_A(x)], \qquad \psi_L(x) = \frac{1}{\sqrt{2}}[\psi_S(x) - \psi_A(x)]. \tag{2.177}$$

Let us perform the following thought ("gedanken") experiment: place a particle, at $t = 0$, into one of these quasi-localized states, say $\psi_R(x)$, and leave the system alone to evolve, so

$$\Psi(x,0) = \psi_R(x) = \frac{1}{\sqrt{2}}[\psi_S(x) + \psi_A(x)]. \tag{2.178}$$

According to the general solution (1.69) of the Schrödinger equation, the time dynamics of this wavefunction may be obtained simply by multiplying each eigenfunction by the corresponding complex-exponential time factor:

$$\Psi(x,t) = \frac{1}{\sqrt{2}}\left[\psi_S(x)\exp\left\{-i\frac{E_S}{\hbar}t\right\} + \psi_A(x)\exp\left\{-i\frac{E_A}{\hbar}t\right\}\right]. \tag{2.179}$$

From here, using Eqs. (170) and (176), and then Eqs. (169) and (175) again, we get

$$\begin{aligned}\Psi(x,t) &= \frac{1}{\sqrt{2}}\left(\psi_S(x)\exp\left\{\frac{i\delta t}{\hbar}\right\} + \psi_A(x)\exp\left\{-\frac{i\delta t}{\hbar}\right\}\right)\exp\left\{-\frac{iE_0 t}{\hbar}\right\} \\ &\equiv \left(\psi_R(x)\cos\frac{\delta t}{\hbar} + i\psi_L(x)\sin\frac{\delta t}{\hbar}\right)\exp\left\{-i\frac{E_0 t}{\hbar}\right\}.\end{aligned} \tag{2.180}$$

This result implies, in particular, that the probabilities $W_R$ and $W_L$ to find the particle, respectively, in the right and left wells change with time as

$$\boxed{W_R = \cos^2\frac{\delta t}{\hbar}, \qquad W_L = \sin^2\frac{\delta t}{\hbar},} \tag{2.181}$$

Quantum oscillations

mercifully leaving the total probability constant: $W_R + W_L = 1$. (If our calculation had not passed this sanity check, we would be in big trouble.)

This is the famous effect of *quantum oscillations*[47] of the particle's wavefunction between two coupled localized states, with the frequency

$$\omega = \frac{2\delta}{\hbar} \equiv \frac{E_A - E_S}{\hbar}. \tag{2.182}$$

In its last form, this result does not depend on the assumption of weak coupling, though the simple form (181) of the oscillations, with its 100% probability variations, does. (Indeed, at a strong coupling of two

[46] As we will see later in Chapter 4, these properties are similar to those of spin-½ particles; hence two-level systems are sometimes called *spin-½-like* systems.

[47] Sometimes they are called the *Bloch oscillations*, but more commonly the last term is reserved for a related but different effect in spatially-periodic systems – to be discussed in Sec. 8 below.

subsystems, the very notion of the quasi-localized states $\psi_R$ and $\psi_L$ is ambiguous.) Qualitatively, this effect may be interpreted as follows: the particle placed into one of the potential wells tries to escape from it via tunneling through the potential barrier separating the wells. (In our particular system shown in Fig. 19, the barrier is formed by the spatial segment of length $a$, which has the potential energy, $U = 0$, higher than the eigenstate energy $-E_0$.) However, in the two-well system, the particle can only escape into the adjacent well. After the tunneling into that counterpart well, the particle tries to escape from it, and hence comes back, etc. – very much as a classical 1D oscillator, initially deflected from its equilibrium position, at negligible damping.

Some care is required in using such interpretation for quantitative conclusions. In particular, let us compare the period $\mathcal{T} \equiv 2\pi/\omega$ of the oscillations (181) with the metastable state's lifetime discussed in the previous section. For our particular model, we may use the second of Eqs. (170) to write

$$\omega = \frac{4|E_0|}{\hbar}\exp\{-\kappa_0 a\}, \quad \text{i.e. } \mathcal{T} = \frac{\pi\hbar}{\delta} = \frac{\pi\hbar}{2|E_0|}\exp\{\kappa_0 a\} \equiv \frac{t_a}{2}\exp\{\kappa_0 a\}, \qquad \text{for } \kappa_0 a >> 1, \quad (2.183)$$

where $t_a \equiv 2\pi/\omega_0 \equiv 2\pi\hbar/|E_0|$ is the effective attempt time. On the other hand, according to Eq. (80), the transparency $\mathcal{T}$ of our potential barrier, in this limit, scales as $\exp\{-2\kappa_0 a\}$,[48] so according to the general relation (153), the lifetime $\tau$ is of the order of $t_a\exp\{2\kappa_0 a\} >> \mathcal{T}$. This is a rather counter-intuitive result: the speed of particle tunneling into a similar adjacent well is much higher than that, through a similar barrier, to the free space!

In order to show that this important result is not an artifact of our simple delta-functional model of the potential wells, and also compare $\mathcal{T}$ and $\tau$ more directly, let us analyze the quantum oscillations between two weakly coupled wells, now assuming that the (symmetric) potential profile $U(x)$ is sufficiently soft (Fig. 21), so all its eigenfunctions $\psi_S$ and $\psi_A$ are at least differentiable at all points.[49]

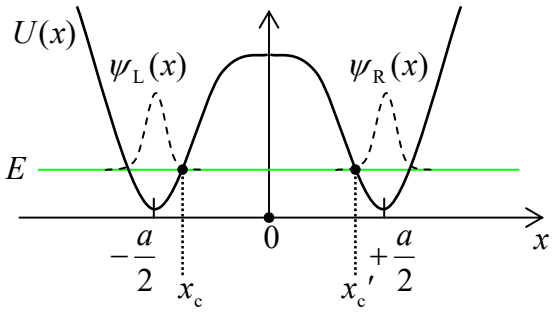


Fig. 2.21. Weak coupling between two similar soft potential wells.

If the barrier's transparency is low, the quasi-localized wavefunctions $\psi_R(x)$ and $\psi_L(x) = \psi_R(-x)$ and their eigenenergies may be found approximately by solving the Schrödinger equations in one of the wells, neglecting the tunneling through the barrier, but the calculation of $\delta$ requires a little bit more care. Let us write the stationary Schrödinger equations for the symmetric and antisymmetric solutions as

[48] It is hard to use Eq. (80) for a more exact evaluation of $\mathcal{T}$ in our current system, with its infinitely deep potential wells because the meaning of the wave number $k$ is not quite clear. However, this is not too important, because, in the limit $\kappa_0 a >> 1$, the tunneling exponent makes the dominant contribution to the transparency – see, again, Fig. 2.7b.

[49] Such smooth wells may have more than one localized eigenstate, so the proper state (and energy) index $n$ is implied in all remaining formulas of this section.

$$\left[E_{\rm A}-U(x)\right]\psi_{\rm A}=-\frac{\hbar^2}{2m}\frac{d^2\psi_{\rm A}}{dx^2},\qquad \left[E_{\rm S}-U(x)\right]\psi_{\rm S}=-\frac{\hbar^2}{2m}\frac{d^2\psi_{\rm S}}{dx^2},\tag{2.184}$$

multiply the former equation by $\psi_{\rm S}$ and the latter one by $\psi_{\rm A}$, subtract them from each other, and then integrate the result from 0 to ∞. The result is

$$(E_{\rm A}-E_{\rm S})\int_0^\infty \psi_{\rm S}\psi_{\rm A}\,dx=\frac{\hbar^2}{2m}\int_0^\infty\left(\frac{d^2\psi_{\rm S}}{dx^2}\psi_{\rm A}-\frac{d^2\psi_{\rm A}}{dx^2}\psi_{\rm S}\right)dx.\tag{2.185}$$

If $U(x)$, and hence $d^2\psi_{\rm A,S}/dx^2$, are finite for all $x$, we may integrate the right-hand side by parts to get

$$(E_{\rm A}-E_{\rm S})\int_0^\infty \psi_{\rm S}\psi_{\rm A}\,dx=\frac{\hbar^2}{2m}\left(\frac{d\psi_{\rm S}}{dx}\psi_{\rm A}-\frac{d\psi_{\rm A}}{dx}\psi_{\rm S}\right)_0^\infty.\tag{2.186}$$

So far, this result is exact (provided that the derivatives participating in it are finite at each point); for *weakly* coupled wells, it may be further simplified. Indeed, in this case, the left-hand side of Eq. (186) may be approximated as

$$(E_{\rm A}-E_{\rm S})\int_0^\infty \psi_{\rm S}\psi_{\rm A}\,dx\approx\frac{E_{\rm A}-E_{\rm S}}{2}\equiv\delta\,,\tag{2.187}$$

because this integral is dominated by the vicinity of point $x = a/2$, where the second terms in each of Eqs. (169) and (175) are negligible, so assuming the proper normalization of the function $\psi_{\rm R}(x)$, the integral is equal to ½. On the right-hand side of Eq. (186), the substitution at $x = \infty$ vanishes (due to the wavefunction's decay in the classically forbidden region), and so does the first term at $x = 0$, because for the antisymmetric solution, $\psi_{\rm A}(0) = 0$. As a result, the energy half-split $\delta$ may be expressed in any of the following (equivalent) forms:

$$\delta=\frac{\hbar^2}{2m}\psi_{\rm S}(0)\frac{d\psi_{\rm A}}{dx}(0)=\frac{\hbar^2}{m}\psi_{\rm R}(0)\frac{d\psi_{\rm R}}{dx}(0)=-\frac{\hbar^2}{m}\psi_{\rm L}(0)\frac{d\psi_{\rm L}}{dx}(0).\tag{2.188}$$

It is straightforward (and hence left for the reader's exercise) to show that within the limits of the WKB approximation's validity, Eq. (188) may be reduced to

$$\delta=\frac{\hbar}{t_{\rm a}}\exp\left\{-\int_{x_{\rm c}}^{x_{\rm c}'}\kappa(x')dx'\right\},\qquad \text{so that }\ \mathcal{T}\equiv\frac{\pi\hbar}{\delta}=\frac{t_{\rm a}}{2}\exp\left\{\int_{x_{\rm c}}^{x_{\rm c}'}\kappa(x')dx'\right\},\tag{2.189}$$

where $t_{\rm a}$ is the time period of the classical motion of the particle, with the energy $E \approx E_{\rm A} \approx E_{\rm S}$, inside each well, the function $\kappa(x)$ is defined by Eq. (82), and $x_{\rm c}$ and $x_{\rm c}'$ are the classical turning points limiting the potential barrier at the level $E$ of the particle's eigenenergy – see Fig. 21. The result (189) is evidently a natural generalization of Eq. (183), so the strong relationship between the times of particle tunneling into the continuum of states and into a discrete eigenstate, is indeed not specific for the delta-functional model. We will return to this fact, in its more general form, at the end of Chapter 6.

## 2.7. Periodic systems: Energy bands and gaps

Let us now proceed to the discussion of one of the most consequential issues of wave mechanics: particle motion through a periodic system. As a precursor to this discussion, let us calculate the transparency of the potential profile shown in Fig. 22 (frequently called the *Dirac comb*): a sequence of $N$ similar, equidistant delta-functional potential barriers separated by $(N – 1)$ potential-free intervals $a$.

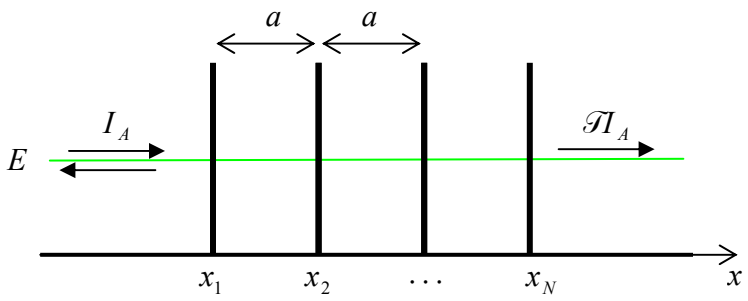


Fig. 2.22. Tunneling through a Dirac comb: a system of $N$ similar, equidistant barriers, i.e. $(N-1)$ similar coupled potential wells.

According to Eq. (132), its transfer matrix is the following product

$$\mathrm{T} = \underbrace{\mathrm{T}_\alpha \mathrm{T}_a \mathrm{T}_\alpha \ldots \mathrm{T}_a \mathrm{T}_\alpha}_{N+(N-1)\ \text{operands}}, \tag{2.190}$$

with the component matrices given by Eqs. (135) and (138), and the barrier height parameter $\alpha$ defined by the last of Eqs. (78). Remarkably, this multiplication may be carried out analytically for arbitrary $N$,[50] giving

$$\mathcal{T} \equiv \left|T_{11}\right|^{-2} = \left[(\cos Nqa)^2 + \left(\frac{\sin ka - \alpha \cos ka}{\sin qa}\sin Nqa\right)^2\right]^{-1}, \tag{2.191a}$$

where $q$ is a new parameter, with the wave number dimensionality, defined by the following relation:

$$\cos qa \equiv \cos ka + \alpha \sin ka. \tag{2.191b}$$

For $N = 1$, Eqs. (191) immediately yield our old result (79), while for $N = 2$ they may be readily reduced to Eq. (141) – see Fig. 16a. Fig. 23 shows their predictions for two larger numbers $N$, and several values of the dimensionless parameter $\alpha$.

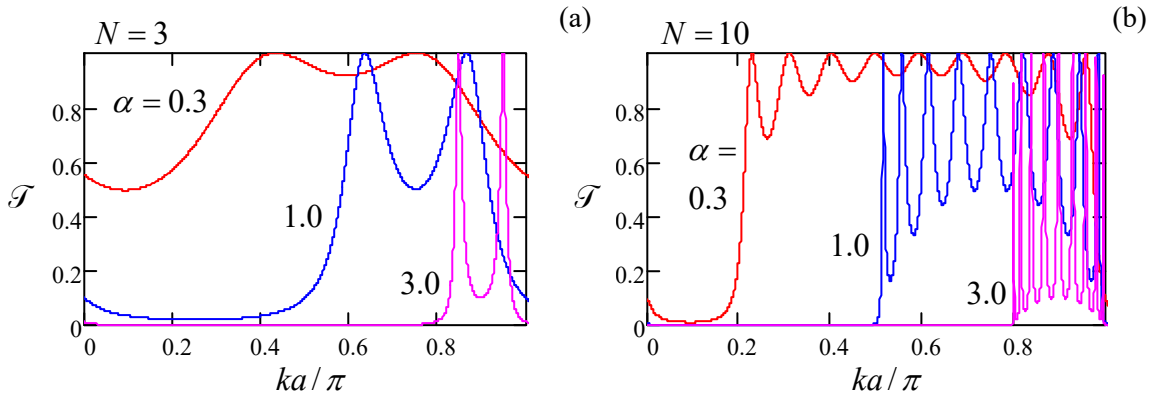


Fig. 2.23. The Dirac comb's transparency as a function of the product $ka$ for three values of $\alpha$. Since the function $\mathcal{T}(ka)$ is $\pi$-periodic (just like it is for $N = 2$, see Fig. 16a), only one period is shown.

Let us start the discussion of the plots from the case $N = 3$ when three barriers limit two coupled potential wells between them. Comparison of Fig. 23a and Fig. 16a shows that the transmission patterns,

[50] This formula will be easier to prove after we have discussed the properties of Pauli matrices in Chapter 4.

and their dependence on the parameter $\alpha$, are very similar, besides that in the coupled-well system, each resonant tunneling peak splits into two, with the $ka$-difference between them scaling as $1/\alpha$. From the discussion in the last section, we may now readily interpret this result: each pair of resonance peaks of transparency corresponds to the alignment of the incident particle's energy $E$ with the pair of energy levels of the symmetric ($E_S$) and antisymmetric ($E_A$) states of the system. However, in contrast to the system shown in Fig. 19, these states are metastable, because the particle may leak out from these states just as it could in the system studied in Sec. 5 – see Fig. 15 and its discussion. As a result, each of the resonant peaks has a non-zero energy width $\Delta E$, obeying Eq. (155).

A further increase of $N$ (see Fig. 23b) results in the increase of the number of resonant peaks per period to $(N - 1)$, and at $N \to \infty$ the peaks merge into the so-called *allowed energy bands* (frequently called just the "energy bands") with average transparency $\mathscr{T} \sim 1$, separated from similar bands in the adjacent periods of the function $\mathscr{T}(ka)$ by *energy gaps*[51] where $\mathscr{T} \to 0$. Notice the following important features of the pattern:

(i) at $N \to \infty$, the band/gap edges become sharp for any $\alpha$, and tend to fixed positions (determined by $\alpha$ but independent of $N$);

(ii) the larger the well coupling (the smaller is $\alpha$), the broader the allowed energy bands and the narrower the gaps between them.

Our previous discussion of the resonant tunneling gives us a clue for a semi-quantitative interpretation of these features: if $(N - 1)$ potential wells are weakly coupled by tunneling through the potential barriers separating them, the system's energy spectrum consists of groups of $(N - 1)$ metastable energy levels, each group being close to one of the unperturbed eigenenergies of the well. (According to Eq. (1.84), for our current example shown in Fig. 22, with its rectangular potential wells, these eigenenergies correspond to $k_n a = \pi n$.)

Now let us recall that in the case $N = 2$ analyzed in the previous section, the eigenfunctions (169) and (175) differed only by the phase shift $\Delta\varphi$ between their localized components $\psi_R(x)$ and $\psi_L(x)$, with $\Delta\varphi = 0$ for one of them ($\psi_S$) and $\Delta\varphi = \pi$ for its counterpart. Hence it is natural to expect that for other $N$ as well, each metastable energy level corresponds to an eigenfunction that is a superposition of similar localized functions in each potential well, but with certain phase shifts $\Delta\varphi$ between them.

Moreover, we may expect that at $N \to \infty$, i.e. for *periodic structures*,[52] with

$$U(x + a) = U(x), \tag{2.192}$$

when the system does not have the ends that could affect its properties, the phase shifts $\Delta\varphi$ between the localized wavefunctions in all couples of adjacent potential wells should be equal, i.e.

$$\psi(x + a) = \psi(x) e^{i\Delta\varphi} \tag{2.193a}$$

for all $x$.[53] This equality is the much-celebrated *Bloch theorem*,[54] or rather its 1D version. Mathematical rigor aside,[55] it is a virtually evident fact because the particle's density $w(x) = \psi^*(x)\psi(x)$, which has to

[51] In solid-state (especially semiconductor) physics and electronics, the term *bandgaps* is more common.

[52] This is a reasonable 1D model, for example, for solid-state crystals, whose samples may feature up to ~$10^9$ similar atoms or molecules in each direction of the crystal lattice.

be periodic in this $a$-periodic system, may be so only $\Delta\varphi$ is constant. For what follows, it is more convenient to represent the real constant $\Delta\varphi$ in the form $qa$, so that the Bloch theorem takes the form

Bloch theorem: 1D version

$$\psi(x+a)=\psi(x)e^{iqa}. \tag{2.193b}$$

The physical sense of the parameter $q$ will be discussed in detail below, but we may immediately notice that according to Eq. (193b), an addition of $(2\pi/a)$ to this parameter yields the same wavefunction; hence all observables have to be $(2\pi/a)$-periodic functions of $q$.[56]

Now let us use the Bloch theorem to calculate the eigenfunctions and eigenenergies for the infinite version of the system shown in Fig. 22, i.e. for an infinite set of delta-functional potential barriers – see Fig. 24.

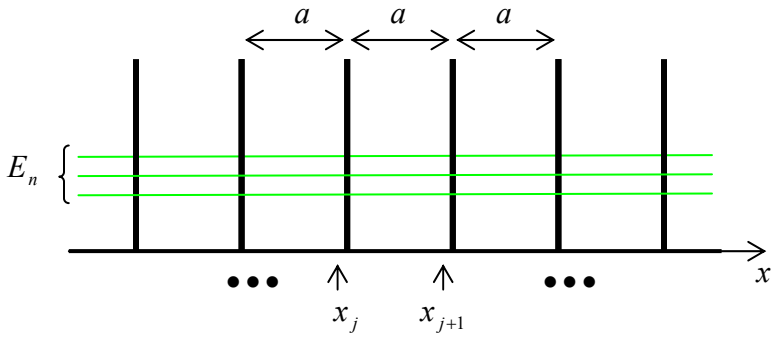


Fig. 2.24. The simplest periodic potential: an infinite Dirac comb.

To start, let us consider two points separated by one period $a$: one of them, $x_j$, just left of one of the barriers, and another one, $x_{j+1}$, just left of the following barrier – see Fig. 24 again. The eigenfunctions at each of the points may be represented as linear superpositions of two simple waves $\exp\{\pm ikx\}$, and the amplitudes of their components should be related by a 2×2 transfer matrix T of the potential fragment separating them. According to Eq. (132), this matrix may be found as the product of the matrix (135) of one delta-functional barrier by the matrix (138) of one zero-potential interval $a$:

$$\begin{pmatrix} A_{j+1} \\ B_{j+1} \end{pmatrix} = \mathrm{T}_a \mathrm{T}_\alpha \begin{pmatrix} A_j \\ B_j \end{pmatrix} = \begin{pmatrix} e^{ika} & 0 \\ 0 & e^{-ika} \end{pmatrix} \begin{pmatrix} 1-i\alpha & -i\alpha \\ i\alpha & 1+i\alpha \end{pmatrix} \begin{pmatrix} A_j \\ B_j \end{pmatrix}. \tag{2.194}$$

However, according to the Bloch theorem (193b), the component amplitudes should be also related as

---

[53] A reasonably fair classical image of $\Delta\varphi$ is the geometric angle between similar objects – e.g., similar paper clips – attached at equal distances to a long, uniform rubber band. If the band's ends are twisted, the twist is equally distributed between the structure's periods, representing the constancy of $\Delta\varphi$.

[54] Named after F. Bloch who applied this concept to wave mechanics in 1929, i.e. very soon after its formulation. Note, however, that an equivalent statement in mathematics, called the *Floquet theorem*, has been known since at least 1883.

[55] I will recover this rigor in two steps. Later in this section, we will see that the function obeying Eq. (193) is indeed *a* solution to the Schrödinger equation. However, to save time/space, it will be better for us to postpone until Chapter 4 the proof that *any* eigenfunction of the equation, with periodic boundary conditions, obeys the Bloch theorem. As a partial reward for this delay, that proof will be valid for an arbitrary spatial dimensionality.

[56] The product $\hbar q$, which has the linear momentum's dimensionality, is called either the *quasimomentum* or (especially in solid-state physics) the "crystal momentum" of the particle. Informally, it is very convenient (and common) to use the name "quasimomentum" for the bare $q$ as well, despite its evidently different dimensionality.

$$\begin{pmatrix} A_{j+1} \\ B_{j+1} \end{pmatrix} = e^{iqa} \begin{pmatrix} A_j \\ B_j \end{pmatrix} \equiv \begin{pmatrix} e^{iqa} & 0 \\ 0 & e^{iqa} \end{pmatrix} \begin{pmatrix} A_j \\ B_j \end{pmatrix}. \tag{2.195}$$

The condition of self-consistency of these two equations gives the following characteristic equation:

$$\left| \begin{pmatrix} e^{ika} & 0 \\ 0 & e^{-ika} \end{pmatrix} \begin{pmatrix} 1-i\alpha & -i\alpha \\ i\alpha & 1+i\alpha \end{pmatrix} - \begin{pmatrix} e^{iqa} & 0 \\ 0 & e^{iqa} \end{pmatrix} \right| = 0. \tag{2.196}$$

In Sec. 5, we have already calculated the matrix product participating in this equation – see the second operand in Eq. (140). Using it, we see that Eq. (196) is reduced to the same simple Eq. (191b) that has jumped at us from the solution of the somewhat different (resonant tunneling) problem. Let us explore that simple result in detail. First of all, the left-hand side of Eq. (191b) is a sinusoidal function of the product $qa$ with unit amplitude, while its right-hand side is a sinusoidal function of the product $ka$, with amplitude $(1 + \alpha^2)^{1/2} > 1$ – see Fig. 25.

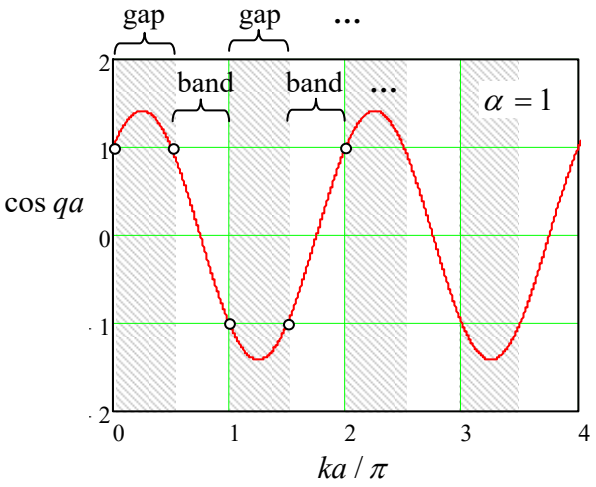


Fig. 2.25. The graphical representation of the characteristic equation (191b) for a fixed value of the parameter $\alpha$. The ranges of $ka$ that yield $|\cos qa| < 1$, correspond to allowed energy bands, while those with $|\cos qa| > 1$, correspond to energy gaps between them.

As a result, within each half-period $\Delta(ka) = \pi$ of the right-hand side, there is an interval where the magnitude of the right-hand side is larger than 1, so the characteristic equation does not have a real solution for $q$. These intervals correspond to the energy gaps (see Fig. 23 again) while the complementary intervals of $ka$, where a real solution for $q$ exists, correspond to the allowed energy bands. In contrast, the parameter $q$ can take *any* real values, so it is more convenient to plot the eigenenergy $E = \hbar^2k^2/2m$ as the function of the quasimomentum $\hbar q$ (or, even more conveniently, of the dimensionless parameter $qa$) rather than $ka$.[57] Before doing that, we need to recall that the parameter $\alpha$, defined by the last of Eqs. (78), depends on the wave vector $k$ as well, so if we vary $q$ (and hence $k$), it is better to characterize the structure by another, $k$-independent dimensionless parameter, for example

$$\beta \equiv (ka)\alpha \equiv \frac{\mathcal{W}}{\hbar^2/ma}, \tag{2.197}$$

so our characteristic equation (191b) becomes

[57] A more important reason for taking $q$ as the argument is that for a general periodic potential $U(x)$, the particle's momentum $\hbar k$ is not uniquely related to $E$, while (according to the Bloch theorem) the quasimomentum $\hbar q$ is.

Dirac comb: $q$ vs $k$

$$\cos qa \equiv \cos ka + \beta \frac{\sin ka}{ka}. \tag{2.198}$$

Fig. 26 shows the plots of $k$ and $E$, following from Eq. (198), as functions of $qa$, for a particular, moderate value of the parameter $\beta$. The first evident feature of the pattern is its $2\pi$-periodicity in argument $qa$, which we have already predicted from the general Bloch theorem arguments. Due to this periodicity, the complete band/gap pattern may be studied, for example, on just one interval $-\pi \le qa \le +\pi$, called the *1st Brillouin zone* – the so-called *reduced zone picture*. For some applications, however, it is more convenient to use the *extended zone picture* with $-\infty \le qa \le +\infty$ – see, e.g., the next section.

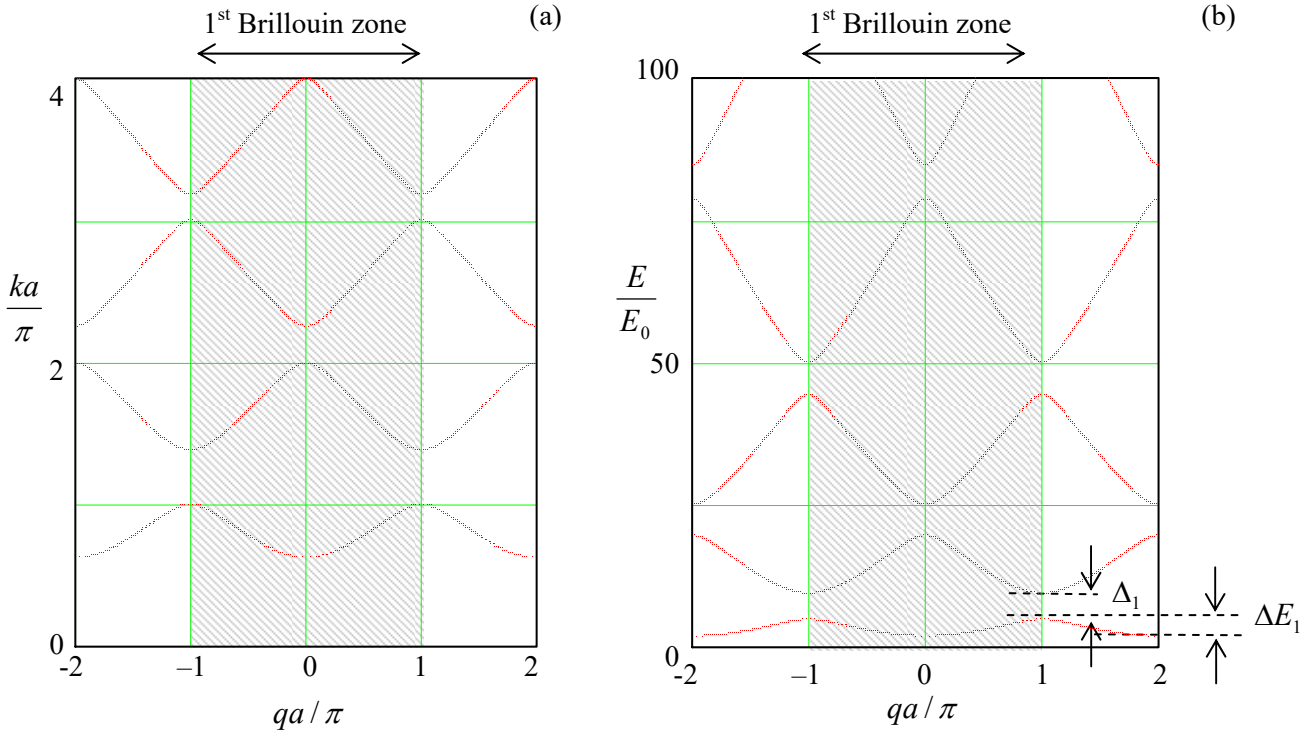


Fig. 2.26. (a) The "genuine" momentum $k$ of a particle in an infinite Dirac comb (Fig. 24), and (b) its energy $E = \hbar^2k^2/2m$ (in the units of $E_0 \equiv \hbar^2/2ma^2$), as functions of the normalized quasimomentum, for a particular value ($\beta = 3$) of the dimensionless parameter defined by Eq. (197). Arrows in the lower right corner of panel b illustrate the definitions of the energy band ($\Delta E_n$) and energy gap ($\Delta_n$) widths.

However, maybe the most important fact, clearly visible in Fig. 26, is that there is an infinite number of energy bands, with different energies $E_n(q)$ for the same value of $q$. Mathematically, it is evident from Eq. (198) – or alternatively, from Fig. 25. Indeed, for each value of $qa$, there is a solution $ka$ of this equation on each half-period $\Delta(ka) = \pi$. Each of such solutions (see Fig. 26a) gives a specific value of the particle's energy $E = \hbar^2k^2/2m$. A continuous set of similar solutions for various $qa$ forms a particular energy band.

Since the energy band picture is one of the most practically important results of quantum mechanics, it is imperative to understand its physics. It is natural to describe this physics, in two opposite potential strength limits, in different ways. In parallel, we will use this discussion to obtain simpler expressions for the energy band/gap structure in each limit. An important advantage of this

approach is that both analyses may be carried out for an arbitrary periodic potential $U(x)$ rather than for the particular Dirac comb model shown in Fig. 24.

(i) *Tight-binding approximation*. This approximation works well when the eigenenergy $E_n$ of the states quasi-localized at the energy profile minima is much lower than the height of the potential barriers separating them – see Fig. 27. As should be clear from our discussion in Sec. 6, essentially the only role of coupling between these states (via tunneling through the potential barriers separating the minima) is to establish a certain phase shift $\Delta\varphi \equiv qa$ between the adjacent quasi-localized wavefunctions $u_n(x - x_j)$ and $u_n(x - x_{j+1})$.

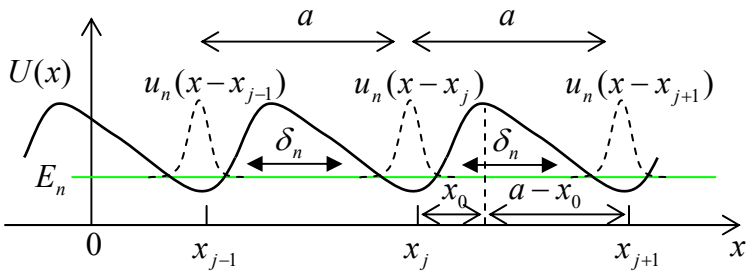


Fig. 2. 27. The tight-binding approximation (schematically).

To describe this effect quantitatively, let us first return to the problem of two coupled wells considered in Sec. 6, and recast the result (180), with the restored eigenstate index $n$, as

$$\Psi_n(x,t) = \left[a_{\mathrm{R}}(t)\psi_{\mathrm{R}}(x) + a_{\mathrm{L}}(t)\psi_{\mathrm{L}}(x)\right]\exp\left\{-i\frac{E_n}{\hbar}t\right\}, \tag{2.199}$$

where the probability amplitudes $a_{\mathrm{R}}$ and $a_{\mathrm{L}}$ oscillate sinusoidally in time:

$$a_{\mathrm{R}}(t) = \cos\frac{\delta_n}{\hbar}t, \qquad a_{\mathrm{L}}(t) = i\sin\frac{\delta_n}{\hbar}t. \tag{2.200}$$

This evolution satisfies the following system of two equations whose structure is similar to Eq. (1.61a):

$$i\hbar\dot{a}_{\mathrm{R}} = -\delta_n a_{\mathrm{L}}, \qquad i\hbar\dot{a}_{\mathrm{L}} = -\delta_n a_{\mathrm{R}}. \tag{2.201}$$

Eq. (199) may be readily generalized to the case of many similar coupled wells:

$$\Psi_n(x,t) = \left[\sum_j a_j(t)u_n(x-x_j)\right]\exp\left\{-i\frac{E_n}{\hbar}t\right\}, \tag{2.202}$$

where $E_n$ are the eigenenergies and $u_n$ the eigenfunctions of each well. In the tight-binding limit, only the adjacent wells are coupled, so instead of Eq. (201) we should write an infinite system of similar equations

$$i\hbar\dot{a}_j = -\delta_n a_{j-1} - \delta_n a_{j+1}, \tag{2.203}$$

for each well number $j$, where parameters $\delta_n$ describe the coupling between two adjacent potential wells. Repeating the calculation outlined at the end of the last section for our new situation, for a smooth potential we may get an expression essentially similar to the last form of Eq. (188):

$$\boxed{\delta_n = \frac{\hbar^2}{m}u_n(x_0)\frac{du_n}{dx}(a - x_0),} \tag{2.204}$$

Tight-binding limit: coupling energy

where $x_0$ is the distance between the well bottom and the middle of the potential barrier on the right of it – see Fig. 27. The only substantial new feature of this expression in comparison with Eq. (188) is that the sign of $\delta_n$ alternates with the level number $n$: $\delta_1 > 0$, $\delta_2 < 0$, $\delta_3 > 0$, etc. Indeed, the number of zeros (and hence, "wiggles") of the eigenfunctions $u_n(x)$ of any potential well increases as $n$ – see, e.g., Fig. 1.8,[58] so the difference of the exponential tails of the functions, sneaking under the left and right barriers limiting the well also alternates with $n$.

The infinite system of ordinary differential equations (203) enables solutions of many important problems (such as the spread of the wavefunction that was initially localized in one well, etc.), but our task right now is just to find its stationary states, i.e. the solutions proportional to $\exp\{-i(\varepsilon_n/\hbar)t\}$, where $\varepsilon_n$ is a still unknown, $q$-dependent addition to the background energy $E_n$ of the $n^{\text{th}}$ energy level. To satisfy the Bloch theorem (193) as well, such a solution should have the following form:

$$a_j(t) = a\exp\left\{iqx_j - i\frac{\varepsilon_n}{\hbar}t + \text{const}\right\}. \tag{2.205}$$

Plugging this solution into Eq. (203) and canceling the common exponent, we get

Tight-binding limit: energy bands

$$E = E_n + \varepsilon_n = E_n - \delta_n\left(e^{-iqa} + e^{iqa}\right) \equiv E_n - 2\delta_n\cos qa\,, \tag{2.206}$$

so in this approximation, the energy band width $\Delta E_n$ (see Fig. 26b) equals $4|\delta_n|$.

The relation (206), whose validity is restricted to $|\delta_n| << E_n$, describes the lowest energy bands plotted in Fig. 26b reasonably well. (For larger $\beta$, the agreement would be even better.) So, this calculation explains what the energy bands really are: in the tight-binding limit, they are best interpreted as isolated well's energy levels $E_n$ broadened into bands by the interwell interaction. Also, this result gives clear proof that the energy band extremes correspond to $qa = 2\pi l$ and $qa = 2\pi(l + ½)$, with integer $l$. Finally, the sign alteration of the coupling coefficient $\delta_n$ (204) explains why the energy maxima of one band are aligned, on the $qa$ axis, with energy minima of the adjacent bands – see Fig. 26.

(ii) *Weak-potential limit*. Amazingly, the energy-band structure is also compatible with a completely different physical picture that may be developed in the opposite limit. Let the particle's energy $E$ be so high that the periodic potential $U(x)$ may be treated as a small perturbation. Naively, in this limit, we could expect a slightly and smoothly deformed parabolic dispersion relation $E = \hbar^2k^2/2m$. However, if we are plotting the stationary-state energy as a function of $q$ rather than $k$, we need to add $2\pi l/a$, with an arbitrary integer $l$, to the argument. Let us show this by expanding all variables into the 1D-spatial Fourier series. For the potential energy $U(x)$ that obeys Eq. (192), such an expansion is straightforward:[59]

$$U(x) = \sum_{l''} U_{l''}\exp\left\{-i\frac{2\pi x}{a}l''\right\}, \tag{2.207}$$

where the summation is over all integers $l''$, from $-\infty$ to $+\infty$. However, for the wavefunction we should show due respect to the Bloch theorem (193), which shows that strictly speaking, $\psi(x)$ is *not* periodic.

[58] Below, we will see several other examples of this behavior. This alternation rule is also described by the Wilson-Sommerfeld quantization condition (110).

[59] The benefits of such an unusual notation of the summation index ($l''$ instead of, say, $l$) will be clear in a few lines.

To overcome this difficulty, let us define another function:

$$u(x) \equiv \psi(x) e^{-iqx}, \tag{2.208}$$

and study its periodicity:

$$u(x+a) = \psi(x+a) e^{-iq(x+a)} = \psi(x) e^{-iqx} = u(x). \tag{2.209}$$

We see that the new function is $a$-periodic, and hence we can use Eqs. (208)-(209) to rewrite the Bloch theorem in a different form:

1D Bloch theorem: alternative form

$$\boxed{\psi(x) = u(x) e^{iqx}, \quad \text{with} \quad u(x+a) = u(x).} \tag{2.210}$$

Now it is safe to expand the periodic function $u(x)$ exactly as $U(x)$:

$$u(x) = \sum_{l'} u_{l'} \exp\left\{-i \frac{2\pi x}{a} l'\right\}, \tag{2.211}$$

so, according to Eq. (210),

$$\psi(x) = e^{iqx} \sum_{l'} u_{l'} \exp\left\{-i \frac{2\pi x}{a} l'\right\} = \sum_{l'} u_{l'} \exp\left\{i\left(q - \frac{2\pi}{a} l'\right)x\right\}. \tag{2.212}$$

The only nontrivial part of using Eqs. (207) and (212) in the stationary Schrödinger equation (53) is how to handle the product term,

$$U(x)\psi = \sum_{l',l''} U_{l''} u_{l'} \exp\left\{i\left[q - \frac{2\pi}{a}(l' + l'')\right]x\right\}. \tag{2.213}$$

At fixed $l'$, we may change the summation over $l''$ to that over $l \equiv l' + l''$ (so that $l'' \equiv l - l'$), and write:

$$U(x)\psi = \sum_{l} \exp\left\{i\left(q - \frac{2\pi}{a} l\right)x\right\} \sum_{l'} u_{l'} U_{l-l'}. \tag{2.214}$$

Now plugging Eq. (212) (with the summation index $l'$ replaced with $l$) and Eq. (214) into the stationary Schrödinger equation (53), and requiring the coefficients of each spatial exponent to match, we get an infinite system of linear equations for $u_l$:

$$\sum_{l'} U_{l-l'} u_{l'} = \left[E - \frac{\hbar^2}{2m}\left(q - \frac{2\pi}{a} l\right)^2\right] u_l. \tag{2.215}$$

(Note that by this calculation we have essentially proved that the Bloch wavefunction (210) is indeed a solution of the Schrödinger equation, provided that the quasimomentum $q$ is selected in a way to make the system of linear equation (215) compatible, i.e. is a solution of its characteristic equation.)

So far, the system of equations (215) is an equivalent alternative to the initial Schrödinger equation, for any potential's strength.[60] In the weak-potential limit, i.e. if all Fourier coefficients $U_n$ are

[60] By the way, the system is very efficient for a fast numerical solution of the stationary Schrödinger equation for any periodic profile $U(x)$, even though to describe potentials with large $U_n$, this approach may require taking into account a correspondingly large number of Fourier amplitudes $u_l$.

small,[61] we can complete all the calculations analytically.[62] Indeed, in the so-called 0th approximation we can ignore *all* $U_n$, so in order to have at least one $u_l$ different from 0, Eq. (215) requires that

$$E \to E_l \equiv \frac{\hbar^2}{2m}\left(q - \frac{2\pi l}{a}\right)^2 . \tag{2.216}$$

($u_l$ itself should be obtained from the normalization condition). This result means that in this approximation, the dispersion relation $E(q)$ has an infinite number of similar quadratic branches numbered by integer $l$ – see Fig. 28.

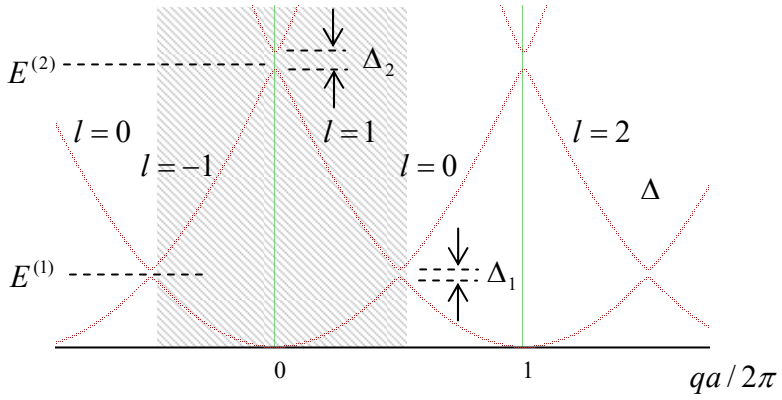


Fig. 2.28. A typical energy band/gap pattern in the weak-potential case, with the shading showing the 1st Brillouin zone.

On every branch, such eigenfunction has just one Fourier coefficient, i.e. is a monochromatic traveling wave

$$\psi_l \to u_l e^{ikx} = u_l \exp\left\{i\left(q - \frac{2\pi l}{a}\right)x\right\}. \tag{2.217}$$

Next, the above definition of $E_l$ allows us to rewrite Eq. (215) in a more transparent form

$$\sum_{l' \neq l} U_{l-l'} u_{l'} = \left(E - E_l\right) u_l , \tag{2.218}$$

which may be formally solved for $u_l$:

$$u_l = \frac{1}{E - E_l} \sum_{l' \neq l} U_{l-l'} u_{l'} . \tag{2.219}$$

This formula shows that if the Fourier coefficients $U_n$ are non-zero but small, the wavefunctions do acquire other Fourier components (besides the main one, with the index corresponding to the branch number), but these additions are all small, besides narrow regions near the points $E_l = E_{l'}$ where two branches (216) of the dispersion relation $E(q)$, with some specific numbers $l$ and $l'$, cross. According to Eq. (216), this happens when

[61] Besides, possibly, the average potential $U_0$, which, as was discussed in Chapter 1, may be always taken for the energy reference. In the following calculations, I will take $U_0 = 0$ to simplify the formulas.

[62] This method is so powerful that its multi-dimensional version is not much more complex than the 1D version described here – see, e.g., Sec. 3.2 in the classical textbook by J. Ziman, *Principles of the Theory of Solids*, 2nd ed., Cambridge U. Press, 1979.

$$\left(q-\frac{2\pi}{a}l\right)\approx-\left(q-\frac{2\pi}{a}l'\right), \tag{2.220}$$

i.e. at $q \approx q_m \equiv \pi m/a$ (with the integer $m \equiv l + l'$) [63] corresponding to

$$E_l \approx E_{l'} \approx \frac{\hbar^2}{2ma^2}\left[\pi(l+l')-2\pi l\right]^2 = \frac{\pi^2\hbar^2}{2ma^2}n^2 \equiv E^{(n)}, \tag{2.221}$$

Weak-potential limit: energy gap positions

with integer $n \equiv l - l'$. (According to their definitions, the index $n$ is just the number of the branch crossing on the energy scale, while the index $m$ numbers the position of the crossing points on the $q$-axis – see Fig. 28.) In such a region, $E$ has to be close to both $E_l$ and $E_{l'}$, so the denominator in just one of the infinite number of terms in Eq. (219) is very small, making the term substantial despite the smallness of $U_n$. Hence we can take into account only one term in each of the sums (written for $l$ and $l'$):

$$\begin{aligned} U_n u_{l'} &= (E-E_l)u_l, \\ U_{-n}u_l &= (E-E_{l'})u_{l'}. \end{aligned} \tag{2.222}$$

Taking into account that for any real function $U(x)$, the Fourier coefficients in its Fourier expansion (207) have to be related as $U_{-n} = U_n^*$, Eq. (222) yields the following simple characteristic equation

$$\begin{vmatrix} E-E_l & -U_n \\ -U_n^* & E-E_{l'} \end{vmatrix} = 0, \tag{2.223}$$

with the following solution:

$$E_\pm = E_{\text{ave}} \pm \left[\left(\frac{E_l-E_{l'}}{2}\right)^2 + U_n U_n^*\right]^{1/2}, \qquad \text{with } E_{\text{ave}} \equiv \frac{E_l+E_{l'}}{2} = E^{(n)}. \tag{2.224}$$

Weak-potential limit: level anticrossing

According to Eq. (216), close to the branch crossing point $q_m = \pi(l + l')/a$, the fraction participating in this result may be approximated as[64]

$$\frac{E_l-E_{l'}}{2} \approx \gamma\tilde{q}, \qquad \text{with } \gamma \equiv \left.\frac{dE_l}{dq}\right|_{q=q_m} = \frac{\pi\hbar^2 n}{ma} = \frac{2aE^{(n)}}{\pi n}, \quad \text{and } \tilde{q} \equiv q-q_m, \tag{2.225}$$

while the parameters $E_{\text{ave}} = E^{(n)}$ and $U_n U_n^* = |U_n|^2$ do not depend on $\tilde{q}$, i.e. on the distance from the central point $q_m$. This is why Eq. (224) may be plotted as the famous *level anticrossing* (also called "avoided crossing", or "intended crossing", or "non-crossing") *diagram* (Fig. 29), with the energy gap width $\Delta_n$ equal to $2|U_n|$, i.e. just twice the magnitude of the $n$-th Fourier harmonic of the periodic potential $U(x)$. Such anticrossings are also clearly visible in Fig. 28, which shows the result of the exact solution of Eq. (198) for the particular case $\beta = 0.5$.[65]

[63] Let me hope that the difference between this new integer and the particle's mass, both called $m$, is absolutely clear from the context.

[64] Physically, $\gamma/\hbar \equiv \hbar(\pi n/a)/m = \hbar k^{(n)}/m$ is just the velocity of a free classical particle with energy $E^{(n)}$.

[65] From that figure, it is also clear that in the weak potential limit, the width $\Delta E_n$ of the $n^{\text{th}}$ energy band is just $E^{(n)} - E^{(n-1)}$ – see Eq. (221). Note that this is exactly the distance between the adjacent energy levels of the simplest 1D potential well of infinite depth – cf. Eq. (1.85).

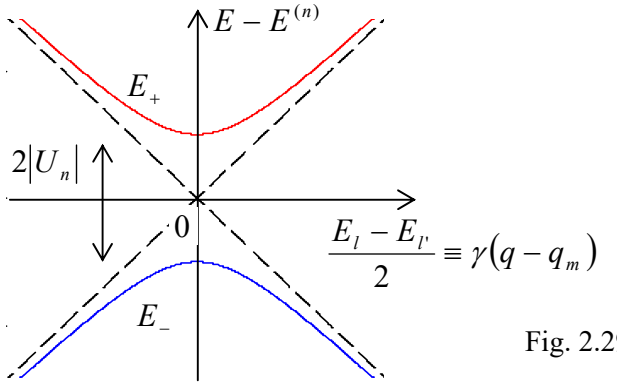


Fig. 2.29. The level anticrossing diagram.

We will run into the anticrossing diagram again and again in the course, notably at the discussion of spin-½ and other two-level systems. It is also repeatedly met in classical mechanics, for example at the calculation of frequencies of coupled oscillators.[66,67] In our current case of the weak potential limit of the band theory, the diagram describes the interaction of two traveling de Broglie waves (217), with oppositely directed wave vectors, $l$ and $-l'$, via the $(l - l')^{th}$ (i.e. the $n^{th}$) Fourier harmonic of the potential profile $U(x)$.[68] This effect exists also in the classical wave theory and is known as the *Bragg reflection*, describing, for example, a 1D model of the X-wave reflection by a crystal lattice (see, e.g. Fig. 1.5) in the limit of weak interaction between the incident wave and each atom.

The anticrossing diagram shows that rather counter-intuitively, even a weak periodic potential changes the topology of the initially parabolic dispersion relation radically, connecting its different branches, and thus creating the energy gaps. Let me hope that the reader has enjoyed the elegant description of this effect, discussed above, as well as one more illustration of the wonderful ability of physics to give completely different interpretations (and different approximate approaches) to the same effect in opposite limits.

So, we have explained analytically (though only in two limits) the particular band structure shown in Fig. 26. Now one may wonder how general this structure is, i.e. how much of it is independent of the Dirac comb model (Fig. 24). For that, let us represent the band pattern, such as that shown in Fig. 26b (plotted for a particular value of the parameter $\beta$, characterizing the potential barrier strength) in a more condensed form, which would allow us to place the results for a range of $\beta$ values on a single comprehensible plot. The way to do this should be clear from Fig. 26b: since the dependence of energy on the quasimomentum in each energy band is not too eventful, we may plot just the highest and the smallest values of the particle's energy $E = \hbar^2k^2/2m$ as functions of $\beta \equiv ma\mathcal{W}/\hbar^2$ – see Fig. 30, which may be obtained from Eq. (198) with $qa = 0$ and $qa = \pi$.

[66] See, e.g., CM Sec. 6.1 and in particular Fig. 6.2.

[67] Actually, we could readily obtain this diagram in the previous section, for the system of two weakly coupled potential wells (Fig. 21), if we assumed the wells to be slightly dissimilar.

[68] In the language of the de Broglie wave scattering, to be discussed in Sec. 3.3, Eq. (220) may be interpreted as the condition that each of these waves, scattered on the $n^{th}$ Fourier harmonic of the potential profile, constructively interferes with its counterpart, leading to a strong enhancement of their interaction.

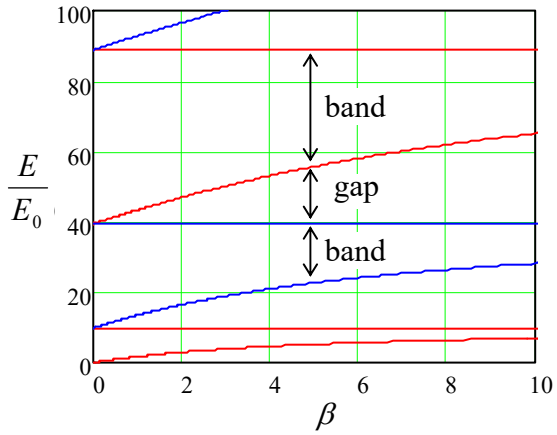


Fig. 2.30. Characteristic curves of the Schrödinger equation for the infinite Dirac comb (Fig. 24).

These plots (in mathematics, commonly called *characteristic curves*, while in applied physics and electronic engineering, *band-edge diagrams*) show, first of all, that at small $\beta$, all energy gap widths are equal and proportional to this parameter, and hence to $\mathcal{W}$. This feature is in a full agreement with the main conclusion (224) of our general analysis of the weak-potential limit, because for the Dirac comb potential (Fig. 24),

$$U(x) = \mathcal{W} \sum_{j=-\infty}^{+\infty} \delta(x - ja + \text{const}), \tag{2.226}$$

all Fourier harmonic amplitudes defined by Eq. (207), are equal by magnitude: $|U_l| = \mathcal{W}/a$. As $\beta$ is further increased, the gaps grow and the allowed energy bands shrink, but rather slowly. This is also natural, because, as Eq. (79) shows, the transparency $\mathcal{T}$ of the delta-functional barriers separating the quasi-localized states (and hence the coupling parameters $\delta_n \propto \mathcal{T}^{1/2}$ participating in the general tight-binding limit's theory) decrease with $\mathcal{W} \propto \beta$ very gradually.

These features may be compared with those for more realistic and relatively simple periodic functions $U(x)$, for example, the sinusoidal potential $U(x) = A\cos(2\pi x/a)$ – see Fig. 31a.

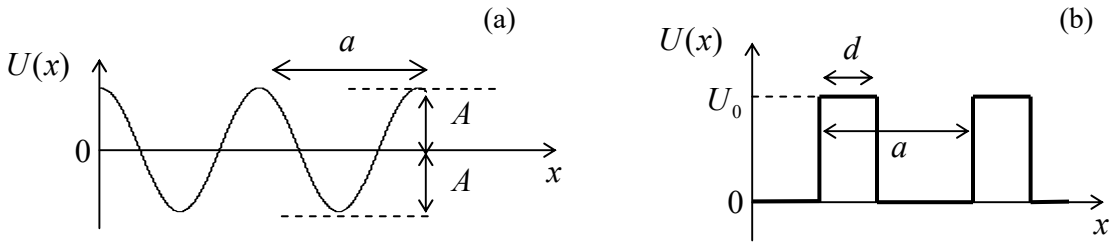


Fig. 2.31. Two other simple periodic potential profiles: (a) the sinusoidal ("Mathieu") potential and (b) the Kronig-Penney potential.

For this potential, the stationary Schrödinger equation (53) takes the following form:

$$-\frac{\hbar^2}{2m}\frac{d^2\psi}{dx^2} + A\cos\frac{2\pi x}{a}\psi = E\psi\,. \tag{2.227}$$

By the introduction of dimensionless variables

$$\xi \equiv \frac{\pi x}{a}, \quad \alpha \equiv \frac{E}{E^{(1)}}, \quad 2\beta \equiv \frac{A}{E^{(1)}}, \tag{2.228}$$

where $E^{(1)}$ is defined by Eq. (221) with $n = 1$,[69] Eq. (227) is reduced to the canonical form of the well-studied *Mathieu equation*[70]

Mathieu equation

$$\boxed{\frac{d^2\psi}{d\xi^2} + (\alpha - 2\beta\cos 2\xi)\psi = 0.} \tag{2.229}$$

Figure 32 shows the characteristic curves of this equation. We see that now at small $\beta$ the first energy gap grows much faster than the higher ones: $\Delta_n \propto \beta^n$. This feature is in accord with the weak-coupling result $\Delta_1 = 2|U_1|$, which is valid only in the linear approximation in $U_n$, because for the Mathieu potential, $U_l = A(\delta_{l,+1} + \delta_{l,-1})/2$. Another clearly visible feature is the exponentially fast shrinkage of the allowed energy bands at $2\beta > \alpha$ (in Fig. 32, on the right from the dashed line), i.e. at $E < A$. It may be readily explained by our tight-binding approximation result (206): as soon as the eigenenergy drops significantly below the potential maximum $U_{max} = A$ (see Fig. 31a), the quantum states in the adjacent potential wells are connected only by tunneling through relatively high potential barriers separating these wells, so the coupling amplitudes $\delta_n$ become exponentially small – see, e.g., Eq. (189).

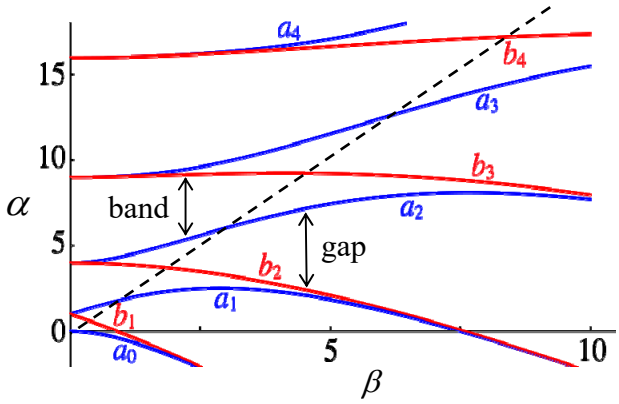


Fig. 2.32. Characteristic curves of the Mathieu equation. The dashed line corresponds to the equality $\alpha = 2\beta$, i.e. $E = A \equiv U_{max}$, separating the regions of under-barrier tunneling and over-barrier motion. Adapted from Fig. 28.2.1 at http://dlmf.nist.gov as a contribution by the US Government (not subject to copyright).

Another simple periodic profile is the *Kronig-Penney potential* shown in Fig. 31b, which gives relatively simple analytical expressions for the band/gap patterns (though transcendent equations for the characteristic curves). Its advantage over the Dirac comb (226) is a more realistic law of the decrease of the Fourier harmonics $U_l$ at $l >> 1$, and hence of the energy gaps in the weak-potential limit:

$$\Delta_n \approx 2|U_n| \propto \frac{U_0}{n}, \quad \text{at } E \sim E^{(n)} >> U_0. \tag{2.230}$$

Leaving a detailed analysis of the Kronig-Penney potential for the reader's exercise, let me conclude this section by addressing the effect of potential modulation on the number of eigenstates in 1D systems of a large but finite length $l >> a, k^{-1}$. Perhaps surprisingly, the Bloch theorem makes the

[69] Note that this definition of $\beta$ is quantitatively different from that for the Dirac comb (226), but in both cases, this parameter is proportional to the amplitude of the potential's periodic modulation.

[70] This equation, first studied in the 1860s by É. Mathieu in the context of a rather practical problem of vibrating elliptical drumheads (!), has many other important applications in physics and engineering, notably including the parametric excitation of oscillations – see, e.g., CM Sec. 5.5.

analysis of this problem elementary, for arbitrary $U(x)$. Indeed, let us assume that $l$ is comprised of an integer number of periods $a$, and its ends are described by similar boundary conditions – both assumptions evidently inconsequential for $l >> a$. Then, according to Eq. (210), the boundary conditions impose, on the quasimomentum $q$, exactly the same quantization condition as we had for $k$ for a free 1D motion. Hence, instead of Eq. (1.93), we can write

$$dN = \frac{l}{2\pi} dq \,, \tag{2.231}$$

1D number of states

with the corresponding change of the summation rule:

$$\sum_q f(q) \to \frac{l}{2\pi} \int f(q) dk \,. \tag{2.232}$$

As a result, the density of states in the 1D *q-space,* $dN/dq = l/2\pi$, does not depend on the potential profile at all! Note, however, that the profile does affect the density of states on the *energy* scale, $dN/dE$. As an extreme example, on the bottom and at the top of each energy band we have $dE/dq \to 0$, and hence

$$\frac{dN}{dE} = \frac{dN}{dq} \Big/ \frac{dE}{dq} = \frac{l}{2\pi} \Big/ \frac{dE}{dq} \to \infty \,. \tag{2.233}$$

This effect of state concentration at the band/gap edges (which survives in higher spatial dimensionalities as well) has important implications for the operation of several important electronic and optical devices, in particular semiconductor lasers and light-emitting diodes.

## 2.8. Periodic systems: Particle dynamics

The band structure of the energy spectrum of a particle moving in a periodic potential has profound implications not only for its density of states but also for its dynamics. Indeed, let us consider the simplest case of a wave packet composed of the Bloch functions (210), all belonging to the same (say, $n^{th}$) energy band. Similarly to Eq. (27) for a free particle, we can describe such a packet as

$$\Psi(x,t) = \int a_q u_q(x) e^{i[qx - \omega(q)t]} dq \,, \tag{2.234}$$

where the $a$-periodic functions $u(x)$, defined by Eq. (208), are now indexed to emphasize their dependence on the quasimomentum, and $\omega(q) \equiv E_n(q)/\hbar$ is the function of $q$ describing the shape of the corresponding energy band – see, e.g., Fig. 26b or Fig. 28. If the packet is narrow in the $q$-space, i.e. if the width $\delta q$ of the distribution $a_q$ is much smaller than all the characteristic $q$-scales of the dispersion relation $\omega(q)$, in particular than $\pi/a$, we may simplify Eq. (234) exactly as it was done in Sec. 2 for a free particle, despite the presence of the periodic factors $u_q(x)$ under the integral. In the linear approximation of the Taylor expansion, we get a full analog of Eq. (32), but now with $q$ rather than $k$, and

$$v_{gr} = \left. \frac{d\omega}{dq} \right|_{q=q_0} , \quad \text{and} \quad v_{ph} = \left. \frac{\omega}{q} \right|_{q=q_0} , \tag{2.235}$$

where $q_0$ is the central point of the quasimomentum's distribution. Despite the formal similarity with Eqs. (33) for the free particle, this result is much more eventful. For example, as evident from the dispersion relation's topology (see Figs. 26b, 28), the group velocity vanishes not only at $q = 0$, but at all

values of $q$ that are multiples of $(\pi/a)$, i.e. at the bottom and on the top of each energy band. Even more intriguing, the group velocity's sign changes periodically with $q$.

This group velocity alternation leads to fascinating, counter-intuitive phenomena if a particle placed in a periodic potential is the subject of an additional external force $F(t)$. (For an electron, this may be, for example, the force exerted by the applied electric field.) Let the force be relatively weak so that the product $Fa$ (i.e. the scale of the energy increment from the additional force per one lattice period) is much smaller than both relevant energy scales of the dispersion relation $E(q)$ – see Fig. 26b:

$$Fa << \Delta E_n, \Delta_n . \tag{2.236}$$

This strong relation enables us to neglect the force-induced interband transitions, so the wave packet (234) includes the Bloch eigenfunctions belonging to only one (initial) energy band at all times. The time evolution of its center $q_0$ obeys an extremely simple equation of motion:[71]

Time evolution of quasi-momentum

$$\boxed{\dot{q}_0 = \frac{1}{\hbar} F(t) .} \tag{2.237}$$

This equation is physically very transparent: it is essentially the 2nd Newton law for the time evolution of the quasimomentum $\hbar q$ under the effect of the additional force $F(t)$ only, excluding the periodic force $-\partial U(x)/\partial x$ of the background potential $U(x)$. This is very natural, because as Eq. (210) implies, $\hbar q$ is essentially the particle's momentum $\hbar k$ averaged over the potential's period, and the periodic force effect drops out at such an averaging.

Despite the simplicity of Eq. (237), the results of its solution may be highly nontrivial. First, let us use Eqs. (235) and (237) to find the instant *group acceleration* of the particle (i.e. the acceleration of its wave packet's envelope):

$$a_{\rm gr} \equiv \frac{dv_{\rm gr}}{dt} \equiv \frac{d}{dt}\frac{d\omega(q_0)}{dq_0} \equiv \frac{d}{dq_0}\frac{d\omega(q_0)}{dq_0}\frac{dq_0}{dt} = \frac{d^2\omega(q_0)}{dq_0^2}\frac{dq_0}{dt} = \frac{1}{\hbar}\frac{d^2\omega}{dq^2}\Big|_{q=q_0} F(t) . \tag{2.238}$$

This means that the second derivative of the dispersion relation $\omega(q)$ (specific for each energy band) plays the role of the effective reciprocal mass of the particle at this particular value of $q_0$:

Effective mass

$$\boxed{m_{\rm ef} = \frac{\hbar}{d^2\omega/dq^2} \equiv \frac{\hbar^2}{d^2E_n/dq^2} .} \tag{2.239}$$

For the particular case of a free particle, for which Eq. (216) is exact, this expression is reduced to the original (and constant) mass $m$, but generally, the effective mass depends on the wave packet's momentum. According to Eq. (239), at the bottom of any energy band, $m_{\rm ef}$ is always positive but depends on the strength of the particle's interaction with the periodic potential. In particular, according to Eq. (206), in the tight-binding limit, the effective mass is very large:

$$\left|m_{\rm ef}\right|_{q=(\pi/a)n} = \frac{\hbar^2}{2\delta_n a^2} \equiv m\frac{E^{(1)}}{\pi^2\delta_n} >> m . \tag{2.240}$$

[71] The proof of Eq. (237) is not difficult but is more compact in the bra-ket formalism to be discussed in Chapter 4. This is why I recommend to the reader its proof as an exercise after reading that chapter.

On the contrary, in the weak-potential limit, the effective mass is close to $m$ at most points of each energy band, but at the edges of the (narrow) bandgaps, it is much smaller. Indeed, expanding Eq. (224) in the Taylor series near point $q = q_m$, we get

$$E_{\pm}\Big|_{E\approx E^{(n)}} - E_{\text{ave}} \approx \pm|U_n| \pm \frac{1}{2|U_n|}\left(\frac{dE_1}{dq}\right)^2_{q=q_m} \tilde{q}^2 = \pm|U_n| \pm \frac{\gamma^2}{2|U_n|}\tilde{q}^2, \tag{2.241}$$

where $\gamma$ and $\tilde{q}$ are defined by Eq. (225), and hence

$$|m_{\text{ef}}|_{q=q_m} = |U_n|\frac{\hbar^2}{\gamma^2} \equiv m\frac{|U_n|}{2E^{(n)}} << m\,. \tag{2.242}$$

The effective mass effects in real atomic crystals may be very significant. For example, the charge carriers in silicon have $m_{\text{ef}} \approx 0.19\ m_{\text{e}}$ in the lowest, normally-empty energy band (traditionally called the *conduction band*), and $m_{\text{ef}} \approx 0.98\ m_{\text{e}}$ in the adjacent lower, normally-filled *valence band*. In some semiconducting compounds, the conduction-band mass may be even smaller – down to $0.0145\ m_{\text{e}}$ in InSb!

However, the effective mass magnitude is not the most surprising effect. A more fascinating corollary of Eq. (239) is that on the top of each energy band, the effective mass is *negative* – please revisit Figs. 26b, 28, and 29 again. This means that the particle (or more strictly, its wave packet's envelope) is accelerated in the direction *opposite* to the applied force. This is exactly what electronic engineers, working with electrons in semiconductors, call *holes*, characterizing them by a *positive mass* $|m_{\text{ef}}|$, but compensating this sign change by taking their charge $e$ positive. If the particle stays in close vicinity of the energy band's top (say, due to frequent scattering effects, typical for the semiconductors used in engineering practice), such double sign flip does not lead to an error in calculations of hole's dynamics, because the electric field's force is proportional to the particle's charge, so the particle's acceleration $a_{\text{gr}}$ is proportional to the charge-to-mass ratio.[72]

However, in some phenomena such simple representation is unacceptable.[73] For example, let us form a narrow wave packet at the bottom of the lowest energy band,[74] and then exert on it a constant force $F > 0$ – say, due to a constant external electric field directed along the $x$-axis. According to Eq. (237), this force would lead to linear growth of $q_0$ in time, so in the quasimomentum space, the packet's center would slide, with a constant speed, along the $q$ axis – see Fig. 33a. Close to the energy band's bottom, this motion would correspond to a positive effective mass (possibly, somewhat different than the genuine particle's mass $m$), and hence be close to the free particle's acceleration. However, as soon as $q_0$ has reached the inflection point where $d^2E_1/dq^2 = 0$, the effective mass, and hence its acceleration (238) change signs to negative, i.e. the packet starts to slow down (in the direct space), while still moving ahead with the same velocity in the quasimomentum space. Finally, at the energy band's top, the particle stops at a certain $x_{\text{max}}$, while continuing to move forward in the $q$-space.

[72] More discussion of this issue may be found in SM Sec. 6.4.

[73] The balance of this section describes effects that are not discussed in most quantum mechanics textbooks. Though, in my opinion, every educated physicist should be aware of them, some readers may skip them at the first reading, jumping directly to the next Sec. 9.

[74] Physical intuition tells us (and the theory of open systems, to be discussed in Chapter 7, confirms) that this may be readily done, for example, by weakly coupling the system to a relatively low-temperature environment, and letting it relax to the lowest possible energy.

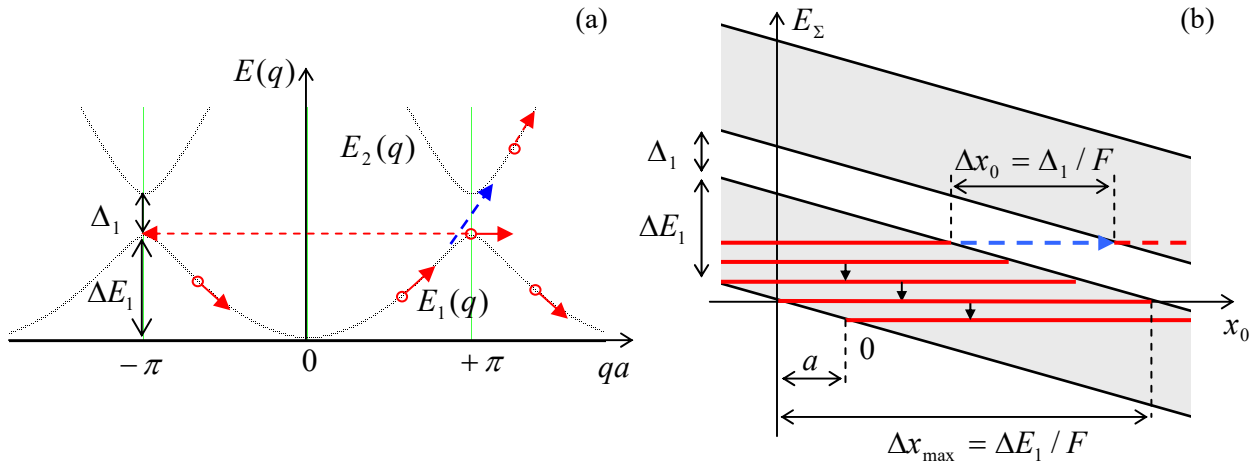


Fig. 2.33. The Bloch oscillations (red lines) and the Landau-Zener tunneling (blue arrows) represented in: (a) the reciprocal space of $q$, and (b) the direct space. On panel (b), the tilted gray strips show the allowed energy bands, while the bold red lines, the Wannier-Stark ladder's steps.

Now we have two alternative ways to look at the further time evolution of the wave packet along the quasimomentum's axis. From the extended zone picture (which is the simplest for this analysis, see Fig. 33a),[75] we may say that the particle crosses the 1st Brillouin zone's boundary and continues to go forward in $q$-space, i.e. down the lowest energy band. According to Eq. (235), this region (up to the next energy minimum at $qa = 2\pi$) corresponds to a negative group velocity. After $q_0$ has reached that minimum, the whole process repeats again – and again, and again.

These are the famous *Bloch oscillations* – the effect which had been predicted, by the same F. Bloch, as early as 1929 but evaded experimental observation until the 1980s (see below) due to the strong scattering effects in real solid-state crystals. The time period of the oscillations may be readily found from Eq. (237):

$$\Delta t_B = \frac{\Delta q}{dq/dt} = \frac{2\pi/a}{F/\hbar} = \frac{2\pi\hbar}{Fa}, \tag{2.243}$$

so their frequency may be expressed by a very simple formula

Bloch oscillations: frequency

$$\boxed{\omega_B \equiv \frac{2\pi}{\Delta t_B} = \frac{Fa}{\hbar}}, \tag{2.244}$$

and hence is independent of any peculiarities of the energy band/gap structure.

The direct-space motion of the wave packet's center $x_0(t)$ during the Bloch oscillation process may be analyzed by integrating the first of Eqs. (235) over some time interval $\Delta t$, and using Eq. (237):

[75] This phenomenon may be also discussed from the point of view of the reduced zone picture, but then it requires the introduction of instant jumps between the Brillouin zone boundary points (see the dashed red line in Fig. 33) that correspond to physically equivalent states of the particle. Evidently, for the description of this particular phenomenon, this language is more artificial.

$$\Delta x_0(t) \equiv \int_0^{\Delta t} v_{gr}\,dt = \int_0^{\Delta t} \frac{d\omega(q_0)}{dq_0}\,dt \equiv \int_0^{\Delta t} \frac{d\omega(q_0)}{dq_0/dt} = \frac{\hbar}{F}\int_{t=0}^{t=\Delta t} d\omega = \frac{\hbar}{F}\Delta\omega(q_0). \tag{2.245}$$

If the interval $\Delta t$ is equal to the Bloch oscillation period $\Delta t_B$ (243), the initial and final values of $E(q_0) = \hbar\omega(q_0)$ are equal, giving $\Delta x_0 = 0$: in the end of the period, the wave packet returns to its initial position in space. However, if we carry out this integration only from the smallest to the largest values of $\omega(q_0)$, i.e. the adjacent points where the group velocity vanishes, we get the following Bloch oscillation swing:

Bloch oscillations: spatial swing

$$\boxed{\Delta x_{max} = \frac{\hbar}{F}(\omega_{max} - \omega_{min}) \equiv \frac{\Delta E_1}{F}.} \tag{2.246}$$

This simple result may be interpreted using an alternative energy diagram (Fig. 33b), which results from the following arguments. The additional force $F$ may be described not only via the 2nd Newton law's version (237), but, alternatively, by its contribution $-Fx$ to the Gibbs potential energy[76]

$$U_\Sigma(x) = U(x) - Fx \tag{2.247}$$

The exact solution of the Schrödinger equation (61) with such a potential may be hard to find directly, but if the force $F$ is sufficiently weak, as we are assuming throughout this discussion, the second term in Eq. (247) may be considered as a constant on the scale of $a << \Delta x_{max}$. In this case, our quantum-mechanical treatment of the periodic potential $U(x)$ is still virtually correct, but with an energy shift depending on the "global" position $x_0$ of the packet's center. In this approximation, the total energy of the wave packet is

$$E_\Sigma = E(q_0) - Fx_0. \tag{2.248}$$

In a plot of such energy as a function of $x_0$ (Fig. 33b), the energy dependence on $q_0$ is hidden, but as was discussed above, it is rather uneventful and may be well characterized by the position of band-gap edges on the energy axis.[77] In this representation, the Bloch oscillations keep the full energy $E_\Sigma$ of the particle constant, i.e. follow a horizontal line in Fig. 33b, limited by the classical turning points corresponding to the bottom and the top of the allowed energy band. The distance $\Delta x_{max}$ between these points is evidently given by Eq. (246).

Besides this alternative look at the Bloch oscillation swing, the total energy diagram shown in Fig. 33b enables one more remarkable result. Let a wave packet be so narrow in the momentum space that $\delta x \sim 1/\delta q >> \Delta x_{max}$; then it may be well represented by a definite energy, i.e. by a horizontal line in Fig. 33b. But Eq. (247) is exactly invariant with respect to the following simultaneous translation of the coordinate and the energy:

$$x \to x + a, \quad E \to E - Fa. \tag{2.249}$$

[76] Physically, this is just the relevant part of the potential energy of the total system comprised of our particle (in the periodic potential) and the source of the force $F$ – see, e.g., CM Sec. 1.4.

[77] In semiconductor physics and engineering, such spatial *band-edge diagrams* are virtually unavoidable components of almost every discussion/publication. In this series, a few more examples of such diagrams may be found in SM Sec. 6.4.

This means that it is satisfied by an infinite set of similar solutions, each corresponding to one of the horizontal red lines shown in Fig. 33b. This is the famous *Wannier-Stark ladder*,[78] with the step height

Wannier-Stark ladder

$$\Delta E_{\rm WS} = Fa\,. \tag{2.250}$$

The importance of this alternative representation of the Bloch oscillations is due to the following fact. In most experimental realizations, the power of electromagnetic radiation with frequency (244), which may be extracted from the oscillations of a charged particle, is very low, so their direct detection represents a hard problem.[79] However, let us apply to a Bloch oscillator an additional ac field at frequency $\omega \approx \omega_{\rm B}$. As these frequencies are brought close together, the external signal should synchronize ("phase-lock") the Bloch oscillations,[80] resulting in certain changes of time-independent observables – for example, a resonant change of absorption of the external radiation. Now let us notice that the combination of Eqs. (244) and (250) yield the following simple relation:

$$\Delta E_{\rm WS} = \hbar\omega_{\rm B}\,. \tag{2.251}$$

This means that the phase-locking at $\omega \approx \omega_{\rm B}$ allows for an alternative (but equivalent) interpretation – as the result of ac-field-induced quantum transitions[81] between the steps of the Wannier-Stark ladder. (Again, such occasions when two very different languages may be used for alternative interpretations of the same effect is one of the most beautiful features of physics.)

This phase-locking effect has been used for the first experimental confirmations of the Bloch oscillation theory.[82] For this purpose, the natural periodic structures, solid-state crystals, are inconvenient due to their very small period $a \sim 10^{-10}$ m. Indeed, according to Eq. (244), such structures require very high forces $F$ (and hence very high electric fields $\mathscr{E} = F/e$) to bring $\omega_{\rm B}$ to an experimentally convenient range. This problem has been overcome using artificial periodic structures (*superlattices*) of certain semiconductor compounds, such as $Ga_{1-x}Al_xAs$ with various degrees $x$ of the gallium-to-aluminum atom replacement, whose layers may be grown over each other epitaxially, i.e., with very few crystal structure violations. Such superlattices, with periods $a \sim 10$ nm, have enabled a clear observation of the resonance at $\omega \approx \omega_{\rm B}$, and hence a measurement of the Bloch oscillation frequency, in particular its proportionality to the applied dc electric field, predicted by Eq. (244).

Very soon after this discovery, the Bloch oscillations were observed[83] in small Josephson junctions, where they result from the quantum dynamics of the Josephson phase difference $\varphi$ in a $2\pi$-periodic potential profile, created by the junction. A straightforward translation of Eq. (244) to this case (left for the reader's exercise) shows that the frequency of such Bloch oscillations is

---

[78] This effect was first discussed in detail by G. Wannier in his 1959 monograph on solid-state physics, while the name of J. Stark is traditionally associated with virtually any electric field effect on atomic systems after he had discovered the first of such effects in 1913 – see its discussion in Sec. 6.2 below.

[79] In systems with many independent particles (such as electrons in semiconductors), the detection problem is exacerbated by the phase incoherence of the Bloch oscillations performed by each particle. This drawback is absent in atomic Bose-Einstein condensates whose Bloch oscillations (in a periodic potential created by standing optical waves) were eventually observed by M. Ben Dahan *et al.*, *Phys. Rev. Lett.* **76**, 4508 (1996).

[80] A simple analysis of the phase locking of a classical oscillator may be found, e.g., in CM Sec. 5.4. (See also the brief discussion of the phase locking of the Josephson oscillations at the end of Sec. 1.6 of this course.)

[81] A quantitative theory of such transitions will be discussed in Sec. 6.6 and then in Chapter 7.

[82] E. Mendez *et al.*, *Phys. Lev. Lett.* **60**, 2426 (1988).

[83] D. Haviland *et al.*, *Z. Phys. B* **85**, 339 (1991).

$$\omega_{\rm B} = \frac{\pi \bar{I}}{2e}, \qquad \text{i.e. } f_{\rm B} \equiv \frac{\omega_{\rm B}}{2\pi} = \frac{\bar{I}}{2e}, \tag{2.252}$$

where $\bar{I}$ is the dc current passed through the junction – the effect not to be confused with the "classical" Josephson oscillations with frequency (1.75). It is curious that Eq. (252) may be legitimately interpreted as a result of a periodic transfer, through the Josephson junction, of discrete Cooper pairs (with electric charge $-2e$ each), between two coherent Bose-Einstein condensates in the superconducting electrodes of the junction.[84]

So far, our discussion of the Bloch oscillations was based on the premise that the wave packet of the particle stays within one (say, the lowest) energy band. However, just one look at Fig. 28 shows that this assumption becomes unrealistic if the energy gap separating this band from the next one becomes very small, $\Delta_1 \to 0$. Indeed, in the weak-potential approximation, which is adequate in this limit, $|U_1| \to 0$, the two dispersion curve branches (216) cross without any interaction, so if our particle (meaning its the wave packet) is driven to approach that point, it should continue to move up in energy – see the dashed blue arrow in Fig. 33a. Similarly, in the real-space representation shown in Fig. 33b, it is intuitively clear that at $\Delta_1 \to 0$, the particle residing at one of the steps of the Wannier-Stark ladder should be able to somehow overcome the vanishing spatial gap $\Delta x_0 = \Delta_1/F$ and to "leak" into the next band – see the horizontal dashed blue arrow on that panel.

This process, called the *Landau-Zener* (or "interband", or "band-to-band") *tunneling*,[85] is indeed possible. To analyze it, let us first take $F = 0$, and consider what happens if a quantum particle, described by an $x$-long (and hence $E$-narrow) wave packet, is incident from free space upon a periodic structure of a large but finite length $l = Na >> a$ – see, e.g., Fig. 22. If the packet's energy $E$ is within one of the energy bands, it may evidently propagate through the structure (though may be partly reflected from its ends). The corresponding quasimomentum may be found by solving the dispersion relation for $q$; for example, in the weak-potential limit, Eq. (224) (which is valid near the gap) yields

$$q = q_m + \tilde{q}, \quad \text{with} \quad \tilde{q} = \pm \frac{1}{\gamma}\left[\tilde{E}^2 - |U_n|^2\right]^{1/2}, \quad \text{for } |U_n|^2 \le \tilde{E}^2, \tag{2.253}$$

where $\tilde{E} \equiv E_{\pm} - E^{(n)}$ and $\gamma = 2aE^{(n)}/\pi n$ – see the second of Eqs. (225).

Now, if the energy $E$ is inside one of the energy gaps $\Delta_n$, the wave packet's propagation in an infinite periodic lattice is impossible, so it is completely reflected from it. However, our analysis of the potential step problem in Sec. 3 implies that the packet's wavefunction should still have an exponential tail protruding into the structure and decaying on some length $\delta$ – see Eq. (58) and Fig. 2.4. Indeed, a straightforward review of the calculations leading to Eq. (253) shows that it remains valid for energies within the gap as well, if the quasimomentum is understood as a purely imaginary number:

$$\tilde{q} \to \pm i\kappa, \quad \text{where } \kappa \equiv \frac{1}{\gamma}\left[|U_n|^2 - \tilde{E}^2\right]^{1/2}, \qquad \text{for } \tilde{E}^2 \le |U_n|^2. \tag{2.254}$$

[84] See, e.g., D. Averin *et al.*, *Sov. Phys. – JETP* **61**, 407 (1985). This effect is qualitatively similar to the transfer of single electrons, with a similar frequency $f = \bar{I}/e$, in tunnel junctions between "normal" (non-superconducting) metals – see, e.g., EM Sec. 2.9 and references therein.

[85] It was predicted, apparently independently, by L. Landau, C. Zener, E. Stueckelberg, and E. Majorana in 1932.

With this replacement, the Bloch solution (193b) indeed describes an exponential decay of the wavefunction at length $\delta \sim 1/\kappa$.

Returning to the effects of weak force $F$, in the real-space approach described by Eq. (248) and illustrated in Fig. 33b, we may recast Eq. (254) as

$$\kappa \to \kappa(x) = \frac{1}{\gamma}\left[|U_n|^2 - (F\widetilde{x})^2\right]^{1/2}, \tag{2.255}$$

where $\widetilde{x}$ is the particle's (i.e. its wave packet center's) deviation from the midgap point. Thus the gap creates a potential barrier of a finite width $\Delta x_0 = 2|U_n|/F$, through which the wave packet may tunnel with a non-zero probability. As we already know, in the WKB approximation (in our case requiring $\kappa\Delta x_0 >> 1$) this probability is just the potential barrier's transparency $\mathscr{T}$, which may be calculated from Eq. (117):

$$-\ln \mathscr{T} = 2\int_{\kappa(x)^2>0} \kappa(x)dx = \frac{2}{\gamma}\int_{-x_c}^{x_c}\left[|U_n|^2 - (F\widetilde{x})^2\right]^{1/2} d\widetilde{x} = \frac{2|U_n|}{\gamma} 2x_c \int_0^1 \left(1-\xi^2\right)^{1/2} d\xi\,. \tag{2.256}$$

where $\pm x_c \equiv \pm\Delta x_0/2 = \pm|U_n|/F$ are the classical turning points. Working out this simple integral (or just noticing that it is a quarter of the unit circle's area, and hence is equal to $\pi/4$), we get

Landau-Zener tunneling probability

$$\boxed{\mathscr{T} = \exp\left\{-\frac{\pi|U_n|^2}{\gamma F}\right\}}. \tag{2.257}$$

This famous result may be also obtained in a more complex way, whose advantage is a constructive proof that Eq. (257) is valid for an arbitrary relation between $\gamma F$ and $|U_n|^2$, i.e. arbitrary $\mathscr{T}$, while our simple derivation was limited to the WKB approximation, valid only at $\mathscr{T} << 1$.[86] Using Eq. (225), we may rewrite the product $\gamma F$ participating in Eq. (257), as

$$\gamma F = \frac{1}{2}\left|\frac{d(E_l - E_{l'})}{dq_0}\right|_{E_l = E_{l'} = E^{(n)}} \hbar\frac{dq_0}{dt} = \frac{\hbar}{2}\left|\frac{d(E_l - E_{l'})}{dt}\right|_{E_l = E_{l'} = E^{(n)}} \equiv \frac{\hbar u}{2}, \tag{2.258}$$

where $u$ has the meaning of the "speed" of the energy level crossing in the absence of the gap. Hence, Eq. (257) may be rewritten in the form

$$\mathscr{T} = \exp\left\{-\frac{2\pi|U_n|^2}{\hbar u}\right\}, \tag{2.259}$$

which is more transparent physically. Indeed, the fraction $2|U_n|/u = \Delta_n/u$ gives the time scale $\Delta t$ of the energy's crossing the gap region, and according to the Fourier transform, its reciprocal, $\omega_{max} \sim 1/\Delta t$ gives the upper cutoff of the frequencies essentially involved in the Bloch oscillation process. Hence Eq. (259) means that

$$-\ln \mathscr{T} \approx \frac{\Delta_n}{\hbar\omega_{max}}. \tag{2.260}$$

[86] In Chapter 6 below, Eq. (257) will be derived using a different method, based on the so-called *Golden Rule* of quantum mechanics, but also in the weak-potential limit, i.e. for hyperbolic dispersion law (253).

This formula allows us to interpret the Landau-Zener tunneling as the system's excitation across the energy gap $\Delta_n$ by the highest-energy quantum $\hbar\omega_{max}$ available from the Bloch oscillation process. This interpretation remains valid even in the opposite, tight-binding limit, in which, according to Eqs. (206) and (237), the Bloch oscillations are purely sinusoidal, so the Landau-Zener tunneling is completely suppressed at $\hbar\omega_B < \Delta_1$.

Such interband tunneling is an important ingredient of several physical phenomena and even some practical electron devices, for example, the *tunneling* (or "Esaki") *diodes*. This simple device is just a junction of two semiconductor electrodes, one of them so strongly *n*-doped by electron donors that some electrons form a degenerate Fermi gas at the bottom of the conduction band. [87] Similarly, the counterpart semiconductor electrode is *p*-doped so strongly that the Fermi level in the valence band is shifted below the band edge – see Fig. 34.

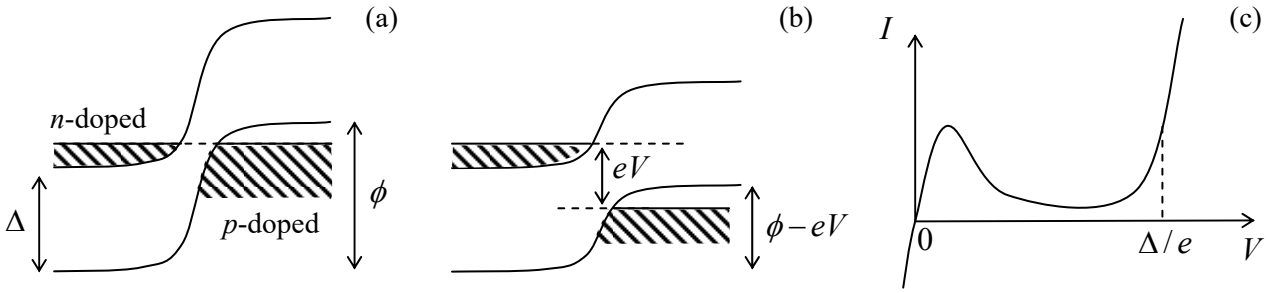


Fig. 2.34. The tunneling ("Esaki") diode: (a) the band-edge diagram of the device at zero bias; (b) the same diagram at a modest positive bias $eV \sim \Delta/2$, and (c) the *I-V* curve of the device (schematically). Dashed lines on panels (a) and (b) show the Fermi-level positions.

In thermal equilibrium, and in the absence of external voltage bias, the Fermi levels of the two electrodes self-align, leading to the build-up of the *contact potential difference* $\phi/e$, with $\phi$ a bit larger than the energy bandgap $\Delta$ – see Fig. 34a. This potential difference creates an internal electric field that tilts the energy bands (just as the external field did in Fig. 33b), and leads to the formation of the so-called *depletion layer*, in which the Fermi level is located within the energy gap and hence there are no charge carriers ready to move. In the usual *p-n* junctions, this layer is broad and prevents any current at applied voltages *V* lower than $\sim\Delta/e$. In contrast, in a tunneling diode the depletion layer is so thin (below ~10 nm) that the interband tunneling is possible and provides a substantial Ohmic current at small applied voltages – see Fig. 34c. However, at larger positive biases, with $eV \sim \Delta/2$, the conduction band is aligned with the middle of the energy gap in the *p*-doped electrode, and electrons cannot tunnel there. Similarly, there are no electrons in the *n*-doped semiconductor to tunnel into the available states just above the Fermi level in the *p*-doped electrode – see Fig. 34b. As a result, at such voltages the current drops significantly, to grow again only when *eV* exceeds $\sim\Delta$, enabling electron motion within each energy band. Thus the junction's *I-V* curve has a part with *negative differential resistance* ($dV/dI < 0$) – see Fig. 34c. This phenomenon, equivalent in its effect to negative kinematic friction in mechanics, may

[87] Here I have to rely on the reader's background knowledge of basic semiconductor physics; this picture will be discussed in more detail in SM Sec. 6.4.

be used for amplification of weak analog signals, for self-excitation of electronic oscillators[88] (i.e. an ac signal generation), and for signal swing restoration in digital electronics.

## 2.9. Harmonic oscillator: Brute force approach

To complete our review of the basic 1D wave mechanics, we have to consider the famous harmonic oscillator, i.e. a 1D particle moving in the quadratic-parabolic potential (111). For it, the stationary Schrödinger equation (53) reads

$$-\frac{\hbar^2}{2m}\frac{d^2\psi}{dx^2}+\frac{m\omega_0^2x^2}{2}\psi=E\psi\,. \tag{2.261}$$

Conceptually, on the background of the fascinating quantum effects discussed in the previous sections, this is not a very interesting system: Eq. (261) is just a standard 1D eigenproblem, resulting in a discrete energy spectrum $E_n$, with smooth eigenfunctions $\psi_n(x)$ vanishing at $x \to \pm\infty$ (because the potential energy tends to infinity there).[89] However, as we will repeatedly see later in the course, this problem's solutions have an enormous range of applications, so we have to know their basic properties.

The direct analytical solution of the problem is not very simple (see below), so let us start by trying some indirect approaches to it. First, as was discussed in Sec. 4, the WKB-approximation-based Wilson-Sommerfeld quantization rule (110), applied to this potential, yields the eigenenergy spectrum (114). With the common quantum number convention, this result is

Harmonic oscillator: energy levels

$$E_n=\hbar\omega_0\left(n+\frac{1}{2}\right),\quad \text{with } n=0,1,2,\ldots, \tag{2.262}$$

so (in contrast to the 1D rectangular potential well) the ground-state energy corresponds to $n = 0$. However, as was discussed in the end of Sec. 4, for the quadratic potential (111) the WKB approximation's conditions are strictly satisfied only at $E_n >> \hbar\omega_0$, so at this point, we can only trust Eq. (262) for high levels, with $n >> 1$, rather than for the (most important) ground state.

This is why let me use Eq. (261) to demonstrate another approximate approach, called the *variational method*, whose simplest form is aimed at finding ground states. The method is based on the following observation. (Here I am presenting its 1D wave mechanics form, though the method is much more general.) Let $\psi_n$ be the exact, full, and orthonormal set of stationary wavefunctions of the system under study, and $E_n$ the set of the corresponding energy levels, satisfying Eq. (1.60):

$$\hat{H}\psi_n=E_n\psi_n\,. \tag{2.263}$$

Then we may use this set for the unique expansion of an arbitrary *trial wavefunction*:

$$\psi_{\text{trial}}=\sum_n\alpha_n\psi_n,\qquad \text{so that } \psi^*_{\text{trial}}=\sum_n\alpha_n^*\psi_n^*, \tag{2.264}$$

[88] See, e.g., CM Sec. 5.4.

[89] The stationary state of the harmonic oscillator (which, as will be discussed in Secs. 5.4 and 7.1, may be considered as the state with a definite number of identical bosonic excitations) is sometimes called its *Fock state* – after V. A. Fock. (This term is also used in a more general sense, for definite-particle-number states of systems with indistinguishable bosons of any kind – see Sec. 8.3.)

where $\alpha_n$ are some (generally, complex) coefficients. Let us require the trial function to be normalized, using the condition (1.66) of orthonormality of the eigenfunctions $\psi_n$:

$$\int \psi_{\text{trial}}^* \psi_{\text{trial}} d^3x \equiv \sum_{n,n'} \int \alpha_n^* \psi_n^* \alpha_{n'} \psi_{n'} d^3x \equiv \sum_{n,n'} \alpha_{n'} \alpha_n^* \int \psi_n^* \psi_{n'} d^3x \equiv \sum_{n,n'} \alpha_{n'} \alpha_n^* \delta_{n,n'} \equiv \sum_n W_n = 1, \quad (2.265)$$

where each of the coefficients $W_n$, defined as

$$W_n \equiv \alpha_n^* \alpha_n \equiv |\alpha_n|^2 \geq 0, \quad (2.266)$$

may be interpreted as the probability for the particle, in the trial state, to be found in the $n^{\text{th}}$ genuine stationary state. Now let us use Eq. (1.23) for a similar calculation of the expectation value of the system's Hamiltonian in the trial state:

$$\begin{aligned} \langle H \rangle_{\text{trial}} &= \int \psi_{\text{trial}}^* \hat{H} \psi_{\text{trial}} d^3x \equiv \sum_{n,n'} \int \alpha_n^* \psi_n^* \hat{H} \alpha_{n'} \psi_{n'} d^3x \equiv \sum_{n,n'} \alpha_{n'} \alpha_n^* E_{n'} \int \psi_n^* \psi_{n'} d^3x \\ &\equiv \sum_{n,n'} \alpha_{n'} \alpha_n^* E_{n'} \delta_{n,n'} \equiv \sum_n W_n E_n . \end{aligned} \quad (2.267)$$

Since the exact ground state energy $E_g$ is, by definition, the lowest one of the set $E_n$, i.e. $E_n \geq E_g$, Eqs. (265) and (267) yield the following inequality:

$$\langle H \rangle_{\text{trial}} \geq \sum_n W_n E_g \equiv E_g \sum_n W_n = E_g . \quad (2.268)$$

Variational method's justification

Thus, the genuine ground state energy of the system is always lower than (or equal to) its energy in any trial state. Hence, if we make several attempts with reasonably selected trial wavefunctions, we may expect the lowest of the results to approximate the genuine ground state energy reasonably well. Even more conveniently, if we select some reasonable class of trial wavefunctions dependent on a free parameter $\lambda$, then we may use the necessary condition of the minimum of $\langle H \rangle_{\text{trial}}$,

$$\frac{\partial \langle H \rangle_{\text{trial}}}{\partial \lambda} = 0, \quad (2.269)$$

to find the closest of them to the genuine ground state. Sometimes, even better results may be obtained using trial wavefunctions dependent on several parameters. Note, however, that the variational method does not tell us how exactly the trial function should be selected, or how close its final result is to the genuine ground-state function. In this sense, this method has "uncontrollable accuracy", and differs from both the WKB approximation and the perturbation methods (to be discussed in Chapter 6), for which we have certain accuracy criteria. Because of this drawback, the variational method is typically used as the last resort – though sometimes (as in the example that follows) it works remarkably well.[90]

Let us apply this method to the harmonic oscillator. Since the potential (111) is symmetric with respect to point $x = 0$, and continuous at all points (so, according to Eq. (261), $d^2\psi/dx^2$ has to be continuous as well), the most natural selection of the ground-state trial function is the Gaussian function

[90] The variational method may be used also to estimate the first excited state (or even a few lowest excited states) of the system, by requiring the new trial function to be orthogonal to the previously calculated eigenfunctions of the lower-energy states. However, the method's error typically grows with the state number.

$$\psi_{\text{trial}}(x) = C\exp\{-\lambda x^2\}, \tag{2.270}$$

with some real $\lambda > 0$. The normalization coefficient $C$ may be immediately found either from the standard Gaussian integration of $|\psi_{\text{trial}}|^2$, or just from the comparison of this expression with Eq. (16), in which $\lambda = 1/(2\delta x)^2$, i.e. $\delta x = 1/2\lambda^{1/2}$, giving $|C|^2 = (2\lambda/\pi)^{1/2}$. Now the expectation value of the particle's Hamiltonian,

$$\hat{H} = \frac{\hat{p}^2}{2m} + U(x) = -\frac{\hbar^2}{2m}\frac{d^2}{dx^2} + \frac{m\omega_0^2 x^2}{2}, \tag{2.271}$$

in the trial state, may be calculated as

$$\begin{aligned}\langle H\rangle_{\text{trial}} &\equiv \int_{-\infty}^{+\infty}\psi_{\text{trial}}^*\left(-\frac{\hbar^2}{2m}\frac{d^2}{dx^2} + \frac{m\omega_0^2 x^2}{2}\right)\psi_{\text{trial}}\,dx \\ &= \left(\frac{2\lambda}{\pi}\right)^{1/2}\left[\frac{\hbar^2\lambda}{m}\int_0^{\infty}\exp\{-2\lambda x^2\}dx + \left(\frac{m\omega_0^2}{2} - \frac{2\hbar^2\lambda^2}{m}\right)\int_0^{\infty} x^2\exp\{-2\lambda x^2\}dx\right].\end{aligned} \tag{2.272}$$

Both involved integrals are of the same well-known Gaussian type,[91] giving

$$\langle H\rangle_{\text{trial}} = \frac{\hbar^2}{2m}\lambda + \frac{m\omega_0^2}{8\lambda}. \tag{2.273}$$

As a function of $\lambda$, this expression has a single minimum at the value $\lambda_{\text{opt}}$ that may be found from the requirement (269), giving $\lambda_{\text{opt}} = m\omega_0/2\hbar$. The resulting minimum of $\langle H\rangle_{\text{trial}}$ is *exactly* equal to ground-state energy following from Eq. (262),

Harmonic oscillator: ground state energy

$$\boxed{E_0 = \frac{\hbar\omega_0}{2}}. \tag{2.274}$$

Such a coincidence of results of the WKB approximation and of the variational method is rather unusual and implies (though does not prove) that Eq. (274) is exact. As a minimum, this coincidence gives a strong motivation to verify the trial wavefunction (270), with $\lambda = \lambda_{\text{opt}}$, i.e.

Harmonic oscillator: ground state wavefunction

$$\boxed{\psi_0 = \left(\frac{m\omega_0}{\pi\hbar}\right)^{1/4}\exp\left\{-\frac{m\omega_0 x^2}{2\hbar}\right\}}, \tag{2.275}$$

and its energy (274), by plugging them into the Schrödinger equation (261). Such substitution[92] shows that the equation is indeed exactly satisfied.

According to Eq. (275), the characteristic scale of the wavefunction's spatial spread[93] is

Harmonic oscillator: spatial scale

$$\boxed{x_0 \equiv \left(\frac{\hbar}{m\omega_0}\right)^{1/2}}. \tag{2.276}$$

Due to the importance of this scale, let us give its crude estimates for several representative systems:[94]

[91] See, e.g., MA Eqs. (6.9b) and (6.9c).

[92] Actually, this is a twist on one of the tasks of Problem 1.13.

[93] Quantitatively, as was already mentioned in Sec. 2.1, $x_0 = \sqrt{2}\delta x = \langle 2x^2\rangle^{1/2}$.

(i) For atom-bound electrons in solids and fluids, $m \sim 10^{-30}$ kg, and $\omega_0 \sim 10^{15}$ s$^{-1}$, giving $x_0 \sim 0.3$ nm, of the order of the typical inter-atomic distances in condensed matter. As a result, classical mechanics is not valid at all for the analysis of their motion.

(ii) For atoms in solids, $m \approx 10^{-24}$-$10^{-26}$ kg, and $\omega_0 \sim 10^{13}$ s$^{-1}$, giving $x_0 \sim 0.01 - 0.1$ nm, i.e. somewhat smaller than inter-atomic distances. Because of that, the methods based on classical mechanics (e.g., molecular dynamics) are approximately valid for the analysis of atomic motion, though they may miss some effects exhibited by lighter atoms – e.g., the so-called *quantum diffusion* of hydrogen atoms, due to their tunneling through the energy barriers of the potential profiles created by other atoms.

(iii) Recently, the progress of patterning technologies has enabled the fabrication of high-quality *micromechanical* oscillators, still consisting of zillions of atoms. For example, the oscillator used in one of the pioneering experiments in this field[95] was a ~1-μm thick membrane with a 60-μm diameter, and had $m \sim 2\times10^{-14}$ kg and $\omega_0 \sim 3\times10^{10}$ s$^{-1}$, so $x_0 \sim 4\times10^{-16}$ m. It is remarkable that despite such extreme smallness of $x_0$ (much smaller than not only any atom but even any atomic nucleus!), quantum states of such oscillators may be manipulated and measured, using their coupling to electromagnetic (in particular, optical) resonant cavities.[96]

Returning to the Schrödinger equation (261), in order to analyze its higher eigenstates, we will need more help from mathematics. Let us recast this equation into a dimensionless form by introducing the natural dimensionless variable $\xi \equiv x/x_0$. This gives

$$-\frac{d^2\psi}{d\xi^2} + \xi^2\psi = \varepsilon\psi\,, \tag{2.277}$$

where $\varepsilon \equiv 2E/\hbar\omega_0 = E/E_0$. In this notation, the ground state's wavefunction (275) is proportional to $\exp\{-\xi^2/2\}$. Using this clue, let us look for solutions of Eq. (277) in the form

$$\psi = C\exp\left\{-\frac{\xi^2}{2}\right\}H(\xi)\,, \tag{2.278}$$

where $H(\xi)$ is a new function, and $C$ is the normalization constant. With this substitution, Eq. (277) yields

$$\frac{d^2H}{d\xi^2} - 2\xi\frac{dH}{d\xi} + (\varepsilon - 1)H = 0\,. \tag{2.279}$$

It is evident that $H$ = const and $\varepsilon = 1$ is one of its solutions, describing the ground-state eigenfunction (275) and energy (274), but what are the other eigenstates and eigenvalues? Fortunately, the linear differential equation (279) was studied in detail in the mid-1800s by C. Hermite who has shown that all its eigenvalues are given by the set

---

[94] By order of magnitude, such estimates are also valid for the systems whose dynamics is substantially different from that of harmonic oscillators, if a typical frequency of their quantum transitions is taken for $\omega_0$.

[95] A. O'Connell *et al*., *Nature* **464**, 697 (2010).

[96] See a review of such experiments by M. Aspelmeyer *et al*., *Rev. Mod. Phys*. **86**, 1391 (2014), and also more recent experiments with nanoparticles placed in much "softer" potential wells – e.g., by U. Delić *et al*., *Science* **367**, 892 (2020).

$$\varepsilon_n - 1 = 2n, \quad \text{with} \quad n = 0, 1, 2, \ldots, \tag{2.280}$$

so Eq. (262) is indeed exact for any $n$. The eigenfunction of Eq. (279), corresponding to the eigenvalue $\varepsilon_n$, is a polynomial (called the *Hermite polynomial*) of degree $n$, which may be most conveniently calculated using the following explicit formula:

Hermite polynomials

$$H_n = (-1)^n \exp\{\xi^2\} \frac{d^n}{d\xi^n} \exp\{-\xi^2\}. \tag{2.281}$$

It is easy to use this formula to spell out several lowest-degree polynomials – see Fig. 35a:

$$H_0 = 1, \quad H_1 = 2\xi, \quad H_2 = 4\xi^2 - 2, \quad H_3 = 8\xi^3 - 12\xi, \quad H_4 = 16\xi^4 - 48\xi^2 + 12, \ldots \tag{2.282}$$

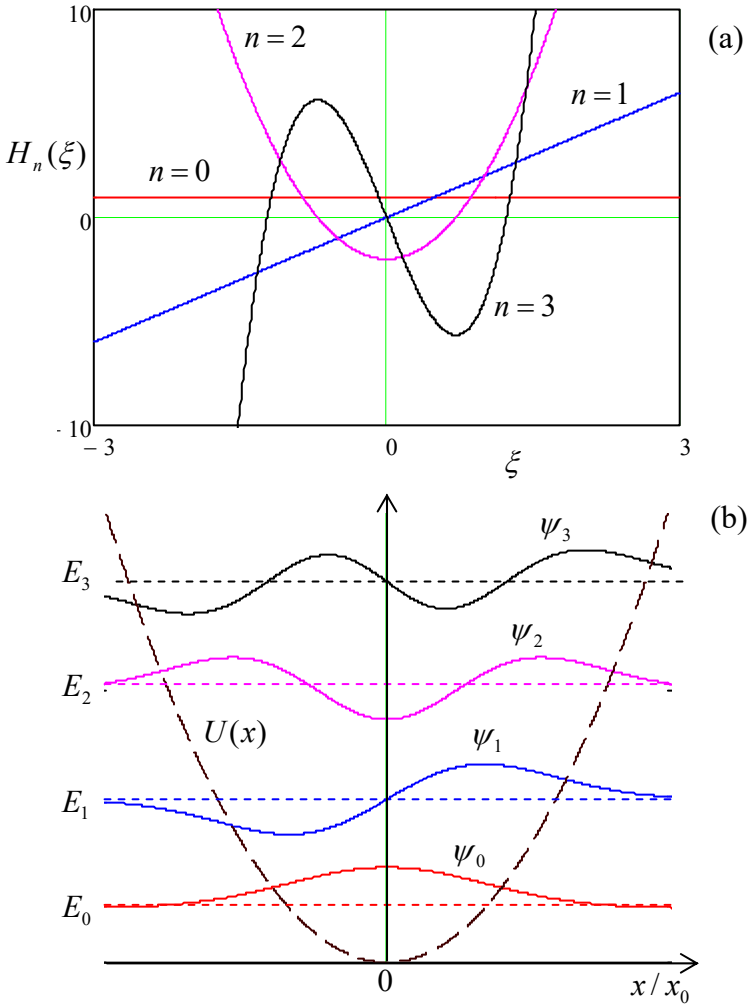


Fig. 2.35. (a) A few lowest Hermite polynomials and (b) the corresponding eigenenergies (horizontal dashed lines) and eigenfunctions (solid lines) of the harmonic oscillator. The dashed black curve shows the potential profile $U(x)$ drawn on the same scale as the energies $E_n$, so its crossings with the energy levels correspond to classical turning points.

The properties that are most important for applications are as follows:

(i) the function $H_n(\xi)$ has exactly $n$ zeros (i.e. its plot crosses the $\xi$-axis exactly $n$ times); as a result, the "parity" (odd-even) of these functions alternates with $n$, and

(ii) the polynomials are mutually orthonormal in the following sense:

$$\int_{-\infty}^{+\infty} H_n(\xi) H_{n'}(\xi) \exp\{-\xi^2\} d\xi = \pi^{1/2} 2^n n! \delta_{n,n'}. \quad (2.283)$$

Using the last property, we may readily calculate, from Eq. (278), the normalized eigenfunctions $\psi_n(x)$ of the harmonic oscillator – see Fig.35b:

$$\psi_n(x) = \frac{1}{\left(2^n n!\right)^{1/2} \pi^{1/4} x_0^{1/2}} \exp\left\{-\frac{x^2}{2x_0^2}\right\} H_n\left(\frac{x}{x_0}\right). \quad (2.284)$$

Harmonic oscillator: eigen-functions

At this point, it is instructive to compare these eigenfunctions with those of a 1D rectangular potential well, with its ultimately hard walls – see Fig. 1.8. Let us list their *common* features:

(i) The wavefunctions oscillate in the classically allowed regions with $E_n > U(x)$, while dropping exponentially beyond the boundaries of that region. (For the rectangular well with infinite walls, the latter regions are infinitesimally narrow.)

(ii) Each step up the energy level ladder increases the number of the oscillation half-waves (and hence the number of its zeros), by one.[97]

And here are the major features *specific* for a soft (e.g., quadratic-parabolic) confinement:

(i) The spatial spread of the wavefunction grows with $n$, following the gradual widening of the classically allowed region.

(ii) Correspondingly, $E_n$ exhibits a slower growth than the $E_n \propto n^2$ law given by Eq. (1.85), because the gradual reduction of spatial confinement moderates the kinetic energy's growth.

Unfortunately, the "brute-force" approach to the harmonic oscillator problem, discussed above, is not too appealing. First, the proof of Eq. (281) is rather longish – so I do not have time/space for it. More importantly, it is hard to use Eq. (284) for the calculation of the expectation values of observables including the so-called *matrix elements* of the system – as we will see in Chapter 4, virtually the only numbers important for most applications. Finally, it is also almost evident that there has to be some straightforward math leading to any formula as simple as Eq. (262) for $E_n$. Indeed, there is a much more efficient, operator-based approach to this problem; it will be described in Sec. 5.4.

## 2.10. Exercise problems

2.1. As was mentioned in Sec. 2.1 of the lecture notes, Eq. (2.1) may be incorrect if the particle's potential energy depends on just one spatial coordinate: $U = U(x, t)$, and is much more reliable for particles strongly but uniformly confined in the transverse directions $y$, $z$. Explain why.

2.2. Prove that the final form of Eq. (2.23) of the lecture notes is correct even though $x'$ has an ($x$-independent) imaginary part.

*Hint*: This is a good exercise in using the Cauchy theorem.[98]

[97] In mathematics, a slightly more general statement, valid for a broader class of ordinary linear differential equations, is frequently called the *Sturm oscillation theorem* and is a part of the *Sturm-Liouville theory* of such equations – see, e.g., Chapter 10 in the handbook by G. Arfken *et al*., cited in MA Sec. 16.

[98] See, e.g., MA Eq. (15.1).

2.3. The initial wave packet of a free 1D particle is described by Eq. (20): $\Psi(x,0) = \int a_k e^{ikx} dk$ .

(i) Obtain a compact expression for the expectation value $\langle p \rangle$ of the particle's momentum at an arbitrary moment $t > 0$.

(ii) Calculate $\langle p \rangle$ for the case when the function $|a_k|^2$ is symmetric with respect to some value $k_0$.

2.4. Calculate the function $a_k$ defined by Eq. (20), for the wave packet with a rectangular spatial envelope:

$$\Psi(x,0) = \begin{cases} C \exp\{ik_0 x\}, & \text{for } -a/2 \le x \le +a/2, \\ 0, & \text{otherwise.} \end{cases}$$

Analyze the result in the limit $k_0 a \to \infty$.

2.5. Prove Eq. (49) for the 1D propagator of a free quantum particle, by starting from Eq. (48).

2.6. Express the 1D propagator defined by Eq. (44) via the eigenfunctions and eigenenergies of a particle moving in an arbitrary stationary potential $U(x)$.

2.7. Calculate the change of a 1D particle's wavefunction, resulting from a short pulse of an external classical force that may be well approximated by a delta function: $F(t) = P\delta(t)$.

2.8. Calculate the transparency $\mathscr{T}$ of the rectangular potential barrier (68),

$$U(x) = \begin{cases} 0, & \text{for } x < -d/2, \\ U_0, & \text{for } -d/2 < x < +d/2, \\ 0, & \text{for } d/2 < x, \end{cases}$$

for a 1D particle of energy $E > U_0$. Analyze and interpret the result, taking into account that $U_0$ may be either positive or negative. (In the latter case, we are speaking about the particle's passage over a rectangular potential well of a finite depth $|U_0|$.)

2.9. Prove Eq. (117) for the case $\mathscr{T}_{\text{WKB}} << 1$, by using the connection formulas (105).

2.10. Spell out the stationary wavefunctions of a harmonic oscillator in the WKB approximation, and use them to calculate the expectation values $\langle x^2 \rangle$ and $\langle x^4 \rangle$ for an eigenstate number $n >> 1$.

2.11. Use the WKB approximation to express the expectation value of the kinetic energy of a 1D particle confined in a soft potential well, in its $n^{\text{th}}$ stationary state, via the derivative $dE_n/dn$, for $n >> 1$.

2.12. Use the WKB approximation to calculate the transparency $\mathscr{T}$ of the following triangular potential barrier:

$$U(x) = \begin{cases} 0, & \text{for } x < 0, \\ U_0 - Fx, & \text{for } x > 0, \end{cases}$$

with $F$, $U_0 > 0$, as a function of the incident particle's energy $E$.

*Hint*: Be careful treating the sharp potential step at $x = 0$.

2.13. Prove that Eq. (2.67) of the lecture notes is valid even if the potential $U(x)$ changes, sufficiently slowly, on both sides of the potential step, provided that $U(x) < E$ everywhere.

2.14.* Prove that the symmetry of the 1D scattering matrix S describing an arbitrary time-independent scatterer allows its representation in the form (127).

2.15. Prove the universal relations between elements of the 1D transfer matrix T of a stationary (but otherwise arbitrary) scatterer, mentioned in Sec. 5.

2.16.* A $k$-narrow wave packet is incident on a finite-length 1D scatterer. Obtain a general expression for the time of its delay caused by the scatterer, and evaluate the time for the case of a very short but high potential barrier.

2.17. A 1D particle had been localized in a very narrow and deep potential well, with the "weight" $\int U(x)dx$ equal to $-\mathcal{W}$, where $\mathcal{W} > 0$. Then (say, at $t = 0$) the well's bottom is suddenly lifted up, so that the particle becomes completely free. Calculate the probability density to find the particle in a state with a certain wave number $k$ at $t > 0$ and the total final energy of the system.

2.18. Calculate the lifetime of the metastable localized state of a 1D particle in the potential

$$U(x) = -\mathcal{W}\delta(x) - Fx, \qquad \text{with } \mathcal{W} > 0,$$

in the WKB approximation. Formulate the condition of validity of the result.

2.19. Calculate the energy levels and the corresponding eigenfunctions of a 1D particle placed into a flat-bottom potential well of width $2a$, with infinitely high hard walls and a narrow potential barrier in the middle – see the figure on the right. Discuss the particle's dynamics in the limit when $\mathcal{W}$ is very large but still finite.

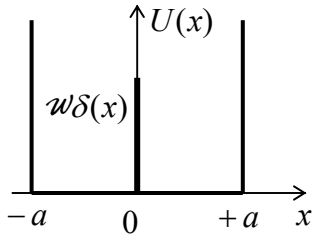


2.20.* Consider a symmetric system of two potential wells of the type shown in Fig. 21, but with $U(0) = U(\pm\infty) = 0$ – see the figure on the right. Derive a general expression for the well interaction force due to their sharing a quantum particle of mass $m$, and determine its sign for the cases when the particle is in:

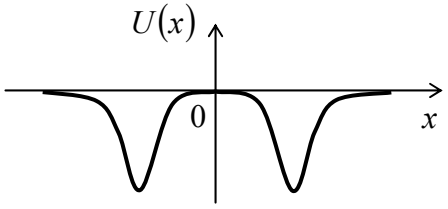


(i) a symmetric localized eigenstate: $\psi_S(-x) = \psi_S(x)$, and

(ii) an antisymmetric localized eigenstate: $\psi_A(-x) = -\psi_A(x)$.

Use a different approach to verify your conclusions for the particular case of delta-functional wells.

2.21. Derive and analyze the characteristic equation for localized eigenstates of a 1D particle in a rectangular potential well of a finite depth (see the figure on the right):

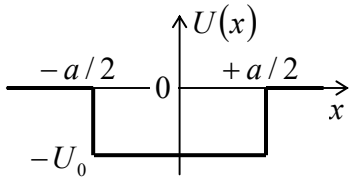


$$U(x) = \begin{cases} -U_0, & \text{for } |x| \le a/2, \\ 0, & \text{otherwise,} \end{cases} \qquad \text{with } U_0 > 0.$$

In particular, calculate the number of localized states as a function of the well's width $a$, and explore the limit $U_0 << \hbar^2/2ma^2$.

2.22. Calculate the energy of a 1D particle localized in a potential well of an arbitrary shape $U(x)$, provided that its width $a$ is finite, and the average depth is very small:

$$\left|\overline{U}\right| << \frac{\hbar^2}{2ma^2}, \qquad \text{where } \overline{U} \equiv \frac{1}{a}\int_{\text{well}} U(x)dx .$$

2.23. A particle of mass $m$ is moving in a field with the following potential:

$$U(x) = U_0(x) + \mathcal{W}\delta(x),$$

where $U_0(x)$ is a smooth symmetric function with $U_0(0) = 0$, growing monotonically at $x \to \pm\infty$. Use the WKB approximation to:

(i) derive the characteristic equation for the particle's energy spectrum, and

(ii) semi-quantitatively describe the spectrum's evolution at the increase of $|\mathcal{W}|$, for both signs of this parameter.

Spell out both results for the quadratic-parabolic potential (111): $U_0(x) = m\omega_0^2x^2/2$.

2.24. Prove Eq. (189).

2.25. For the problem discussed at the beginning of Sec. 7, i.e. the 1D particle's motion in an infinite Dirac comb potential (Fig. 24), write explicit expressions for the eigenfunctions at the very bottom and at the very top of the lowest energy band. Sketch both functions.

2.26. A 1D particle of mass $m$ moves in an infinite periodic system of very narrow and deep potential wells that may be described by delta functions:

$$U(x) = \mathcal{W}\sum_{j=-\infty}^{+\infty}\delta(x - ja), \qquad \text{with } \mathcal{W} < 0 .$$

(i) Sketch the energy band structure of the system for very small and very large values of the potential well's "weight" $|\mathcal{W}|$, and

(ii) calculate explicitly the ground-state energy of the system in these two limits.

2.27. For the system discussed in the previous problem, write explicit expressions for the eigenfunctions of the system, corresponding to:

(i) the bottom of the lowest energy band,

(ii) the top of that band, and

(iii) the bottom of each higher energy band.

Sketch these functions.

2.28.* The 1D "crystal" analyzed in the last two problems, now extends only to $x > 0$, with a sharp step to a flat potential plateau at $x < 0$:

$$U(x) = \begin{cases} \mathcal{W}\sum_{j=1}^{+\infty} \delta(x - ja), & \text{with } \mathcal{W} < 0, \quad \text{for } x > 0, \\ U_0 > 0, & \text{for } x < 0. \end{cases}$$

Prove that the system can have a set of the so-called *Tamm states* localized near the "surface" $x = 0$, and calculate their energies in the limit when $U_0$ is very large but finite. (Quantify this condition.) [99]

2.29. Calculate the transfer matrix of the rectangular potential barrier specified by Eq. (68), for particle energies both below and above $U_0$.

2.30. Use the results of the previous problem to calculate the transfer matrix of one period of the periodic Kronig-Penney potential shown in Fig. 31b.

2.31. Using the results of the previous problem, derive the characteristic equations for a particle's motion in the periodic Kronig-Penney potential, for both $E < U_0$ and $E > U_0$. Try to bring the equations to a form similar to that obtained in Sec. 7 for the delta-functional barriers – see Eq. (198). Use the equations to formulate the conditions of applicability of the tight-binding and weak-potential approximations, in terms of the system's parameters and the particle's energy $E$.

2.32. For the Kronig-Penney potential, use the tight-binding approximation to calculate the widths of the allowed energy bands. Compare the results with those of the previous problem (in the corresponding limit).

2.33. For the same Kronig-Penney potential, use the weak-potential limit formulas to calculate the energy gap widths. Again, compare the results with those of Problem 31, in the corresponding limit.

2.34. 1D periodic chains of atoms may exhibit what is called the *Peierls instability*, leading to the *Peierls transition* to a phase in which atoms are slightly displaced, from the exact periodicity, by equal but sign-alternating shifts $\Delta x_j = (-1)^j \Delta x$, with $\Delta x << a$, where $j$ is the atom's number in the chain, and $a$ is its initial period. These displacements lead to an alternation of the coupling amplitudes $\delta_n$ (see Eq. (204)) between close values $\delta_n^+$ and $\delta_n^-$. Use the tight-binding approximation to calculate the resulting change of the $n^{\text{th}}$ energy band, and discuss the result.

2.35.* Use Eqs. (1.73)-(1.74) to derive Eq. (252), and discuss the relation between these Bloch oscillations and the Josephson oscillations of frequency (1.75).

2.36. A 1D particle of mass $m$ is placed into the following triangular potential well:

$$U(x) = \begin{cases} +\infty, & \text{for } x < 0, \\ Fx, & \text{for } x > 0, \end{cases} \quad \text{with } F > 0.$$

(i) Calculate its energy spectrum using the WKB approximation.

[99] In applications to electrons in solid-state crystals, the delta-functional potential wells model the attractive potentials of atomic nuclei, while $U_0$ represents the workfunction, i.e. the energy necessary for the extraction of an electron from the crystal to the free space – see, e.g., Sec. 1.1(ii), and also EM Sec. 2.6 and SM Sec. 6.3.

(ii) Estimate the ground state energy using the variational method, with two different trial functions.

(iii) Calculate the three lowest energy levels, and also the $10^{th}$ level, with an accuracy better than 0.1%, from the exact solution of the problem.

(iv) Compare and discuss the results.

*Hint*: The values of the first few zeros of the Airy function, necessary for Task (iii), may be found in many math handbooks, for example, in Table 9.9.1 of the open-access online version of the collection edited by Abramowitz and Stegun.[100]

2.37. Use the variational method to estimate the ground state energy $E_g$ of a particle in the potential well

$$U(x) = -U_0 \exp\{-\alpha x^2\}, \qquad \text{with } \alpha > 0, \text{ and } U_0 > 0.$$

Spell out the results in the limits of small and large $U_0$, and give their interpretation.

2.38. For a 1D particle of mass $m$, in a potential well with the following profile,

$$U(x) = ax^{2s}, \quad \text{with } a > 0 \text{ and } s > 0,$$

(i) calculate its energy spectrum using the WKB approximation, and

(ii) estimate the ground state energy using the variational method.

Compare the ground-state energy results.

2.39. Use the variational method to estimate the lowest excited energy level of a 1D harmonic oscillator.

2.40. Assuming the quantum effects to be small, calculate the lower part of the energy spectrum of the following system: a small bead of mass $m$, free to move without friction along a ring of radius $R$, which is rotated about its vertical diameter with a constant angular velocity $\omega$ – see the figure on the right. Formulate a quantitative condition of validity of your results.

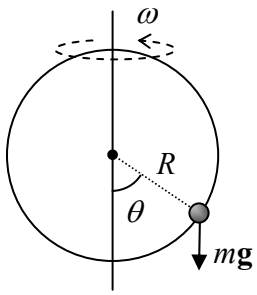


*Hint*: This system was used as the "testbed problem" in the CM part of this series, and the reader is welcome to use any relations derived there.

2.41. A 1D harmonic oscillator with mass $m$ and frequency $\omega_0$ was in its ground state. At $t = 0$, an additional force $F$ is suddenly exerted on it and then is kept constant. Calculate the probability of the oscillator staying in its ground state.

2.42. A 1D particle of mass $m$ was placed into a quadratic potential well (111),

$$U(x) = \frac{m\omega_0^2 x^2}{2},$$

[100] See https://dlmf.nist.gov/9.9.

and allowed to relax into the ground state. At $t = 0$, the well is fast accelerated to move with velocity $v$, without changing its profile, so that at $t \geq 0$ the above formula for $U$ is valid with the replacement $x \to x' \equiv x - vt$. Calculate the probability for the system to still be in the ground state at $t > 0$.

2.43. Initially, a 1D harmonic oscillator was in its ground state. At a certain moment of time, its spring constant $\kappa$ is abruptly increased so that its frequency $\omega_0 = (\kappa/m)^{1/2}$ is increased by a factor of $\alpha$, and then is kept constant at the new value. Calculate the probability that after the change, the oscillator is still in its ground state.

2.44. A 1D particle is in the following potential well:

$$U(x) = \begin{cases} +\infty, & \text{for } x < 0, \\ m\omega_0^2 x^2/2, & \text{for } x \geq 0. \end{cases}$$

(i) Find its eigenfunctions and eigenenergies.

(ii) The particle was let to relax into its ground state, and then the potential wall at $x < 0$ is rapidly removed so that the system is instantly turned into the usual harmonic oscillator (with the same $m$ and $\omega_0$). Find the probability for the particle to remain in the ground state.

2.45. Prove the following formula for the propagator of the 1D harmonic oscillator:

$$G(x,t;x_0,t_0) = \left\{\frac{m\omega_0}{2\pi i\hbar \sin[\omega_0(t-t_0)]}\right\}^{1/2} \exp\left\{\frac{im\omega_0}{2\hbar \sin[\omega_0(t-t_0)]}\left[\left(x^2 + x_0^2\right)\cos[\omega_0(t-t_0)] - 2xx_0\right]\right\}.$$

Discuss the relation between this formula and the propagator of a free 1D particle.

2.46. In the context of the Sturm oscillation theorem mentioned in Sec. 9, prove that the number of eigenfunction's zeros of a particle confined in an arbitrary but finite potential well always increases with the corresponding eigenenergy.

*Hint*: You may like to use the suitably modified Eq. (186).

2.47.* Use the WKB approximation to calculate the lifetime of the metastable ground state of a 1D particle of mass $m$ in the "pocket" of the potential profile

$$U(x) = \frac{m\omega_0^2}{2}x^2 - \alpha x^3.$$

Contemplate the significance of this problem.